Politecnico di Milano

School of Industrial and Information Engineering

Master of Science in Mathematical Engineering

A high-order discontinuous Galerkin approach to the poro-elasto-acoustic problem

Supervisors: Prof. Paola F. Antonietti, Dr. Ilario Mazzieri

Candidate:
Simone Nati Poltri Matr. 905751

Academic Year 2018-2019

Contents

List of Figures

List of Tables

Abstract

The aim of this thesis is to introduce a discretization of the physical phenomenon of propagation of acoustic waves through poroelastic materials, by exerting a finite element discontinuous Galerkin method on polygonal meshes. Wave propagation is modeled by acoustics equations in the acoustic domain and low-frequency Biot's equation in the poroelastic one. The coupling is introduced by considering interface conditions, imposed on the interface between the domains, of different nature: open and sealed pores. Existence and uniqueness is proven for the continuous problem. For the space discretization we introduce a discontinuous Galerkin method, which is then coupled with suitable time integration schemes, such as the leapfrog, the Newmark and the generalized α-method. A stability analysis both for the continuous problem and the semi-discrete one is presented and error estimates for the energy norm are derived. A numerical implementation is achieved through the software Matlab and a wide set of numerical results obtained on test cases with manufactured solutions are presented in order to validate the error analysis. Numerical experiments are also presented by dealing with different scenarios, meshes and interfaces.

Estratto

Lo scopo di questa tesi è quello di introdurre una discretizzazione del fenomeno fisico della propagazione di onde acustiche attraverso materiali poroelastici, tramite un metodo a elementi finiti di tipo discontinuous Galerkin su mesh poligonali. La propagazione delle onde è modellizzata da equazioni acustiche nel dominio acustico e dalle equazioni di Biot a bassa frequenza in quello poroelastico. L'accoppiamento viene introdotto considerando le condizioni di interfaccia, imposte all'interfaccia tra i due domini, di diversa natura: *open pores* e *sealed pores*. Viene dimostrata l'esistenza e unicità del problema continuo. Viene introdotto un metodo discontinuous Galerkin per la discretizzazione in spazio, che viene poi accoppiato tramite schemi di integrazione in tempo, e.g.: leapfrog, Newmark e generalized α-method. Un'analisi di stabilità è presentata sia per la formulazione debole del problema continuo, che per la formulazione del problema semi-discreto e vengono derivate stime dell'errore per la norma energia. Un'implementazione numerica è svolta attraverso il software Matlab e viene presentata una serie di risultati numerici, ottenuti da casi test con soluzioni costruite appositamente, al fine di confermare l'analisi sull'errore. Vengono inoltre presentate simulazioni numeriche trattando diversi scenari, mesh e interfacce.

Introduction

The *poro-elasto-acoustic coupling* is an important physical phenomenon that often occurs in nature and has different fields of applications. As intuitively suggested by the name, it happens whenever an acoustic/sound wave impacts a poroelastic medium and consequently propagates through it. As shown in Figure 1a[1], in acoustic engineering it has an important interest, as for example for the study of sound propagation through acoustic panels, whose main intent is to intercept and absorb acoustic waves, with the final goal of noise reduction [67, 68].

(a) Sound absorbing panels

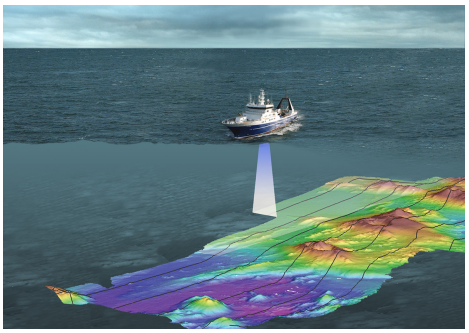

(b) Underwater wave propagation

Figure 1: Examples of applications in acoustic engineering (a) and underwater sound propagation (b)

As studied in [51], in civil engineering it plays a key role in passive control and vibroacoustics: plastic foams and fibrous or granular materials (see Figure 2a) are mainly used with this intent. In particular air-saturated porous materials find an interesting usage in aeronautical fields in the so called *inverse problem* [26, 36, 38]. With a totally different aim is the application in underwater sound propagation [28, 45, 49]: the coupling occurs when an acoustic wave moving in an acoustic domain, where a fluid (water) lives, reaches the seabed. Part of the wave is absorbed by sand, modeled as a poroelastic material, while a response given by the resulting reflection wave is studied in order to have information about depth (as shown in Figure 1b[2]). Many others are the fields of application, as for example the study of ultrasound propagation throughout bones [40, 44, 56, 58, 65], deeply studied in biomechanics, thanks to the

[1] https://www.soundproofcow.com
[2] https://ostiaedintorni.it/20-000-telefonate-sotto-i-mari

porous-sponge composition of cancellous bones (as shown in Figure 2b), in order to diagnose osteoporosis and study the evolution of the disease. Still in the medical field, the theory has been frequently used in order to solve soft tissues deformation, in particular heart tissue [46, 78], skin [59] and aortic tissue [48, 50] . The direct study of the interaction of soil with acoustic waves in geophysics [43, 77], seismology [52, 79], etc., also find a relevant application of Biot's theory.

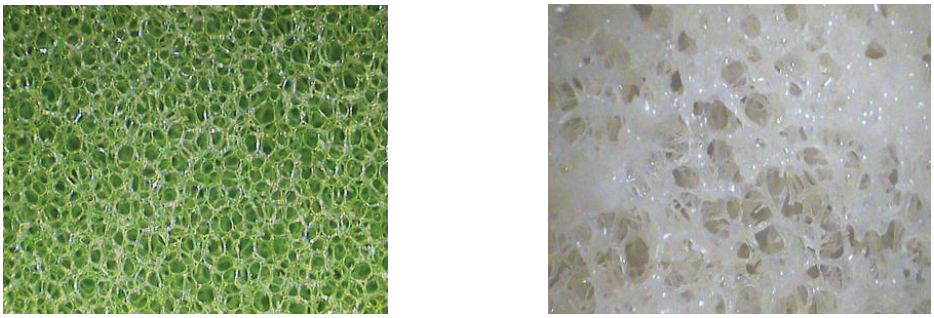

(a) Air-saturated material (b) Cancellous bone

Figure 2: Examples of porous materials[3]

Poroelastic waves study the combined propagation of pressure and elastic waves through a porous material. Pressure waves propagate through the saturating fluid inside pores, while acoustic ones through the porous skeleton. The theory of propagation of acoustic waves with application to poroelasticity has been developed mainly by Biot [16, 17, 18, 19, 20, 21] in 1956, by introducing general equations and proposing different ways to treat coupling between acoustic and poro-elastic domains. This theory has been mainly used in petroleum industries, in order to determine physical properties of reservoir rocks. Main discoverings of Biot's analysis concerned with slow compressional waves, whose study carried on the analysis on fast compressional waves, introduced in 1944 by Frenkel. Frenkel was in fact the first who pointed out the existence of two different compressional waves, dealing with the analysis of waves propagation in fluid saturated porous media [55, 69, 74], proposing a model of seismic waves in saturated soils. In particular, he distinguished in-phase (*fast*) movements between solid and fluid from out-phase (*slow*) ones.

As done in [6], it has been chosen to numerically address the problem through a high order discontinuous Galerkin (dG) method [25, 24, 61, 62]. The choice of this technique has been made in order to ensure adaptivity to unstructured meshes and to avoid numerical issues, even if imposing high computational requirements, possibly avoided through parallel computing. Moreover, recent studies (see [7]) have proven that this method supports *polytopic meshes*, a relevant aspect in dG-theory, not taken into account in this work, as discussed later on. Other methods certainly lend themselves to

[3]Images taken from reference [37]

polytopic meshes, such as the Virtual Element method [12, 13, 14], the Polygonal Finite Element method [71, 72], the Hybrid High-Order method [31, 32, 33] and the Mimetic Finite Difference method [3, 23]. On classical tetrahedral/hexahedral grids, standard continuous Galerkin [47], Finite Volume [15] and many other numerical methods could be equally considered. Lagrange Multipliers [11, 64] method could be adopted in order not to take into account a penalty term, ensuring convergence in non-matching grids and fitting perfectly with the coupled problem, due to its reduction to an interface problem (see [2] for a direct application to the Biot system).

As commonly found in literature, discretization adopted has been done in space, iterating then in time. As in [54] one could evenly consider a different approach, by discretizing firstly in time through a Fourier transform and adopting then a Finite Element method for the space.

As shown in Figure 3, poro-elastic materials could be very difficult to handle, since natural aspects impose many different scenarios. A first analysis on the poroelastic domain has been therefore introduced, in order to treat different cases of interest. In order to carry on the treatment of poroelastic domain, the definition of *pores* is necessary: bigger or smaller holes in (elastic) materials where a fluid is able to move. In particular pores can be easily subdivided into *open pores* and *sealed pores* (closed), widely simplifying previous concepts. Intuitively the first ones share a part with the outer surface of the material, while the latter ones are totally locked in. As shown in Figure 3, in-between these two definition, more rigorous ones can be given.

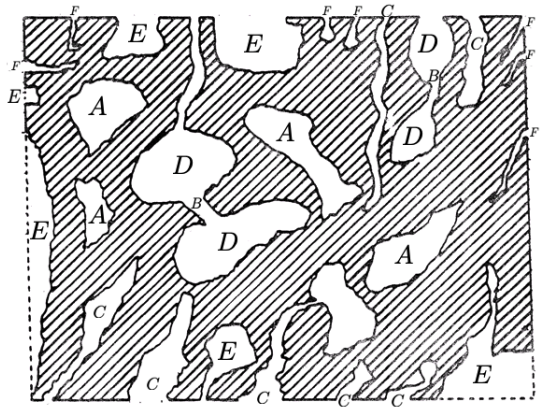

Figure 3: Pores subdivision in a poroelastic domain[4]: (A) *closed pores*, (B) *channel pores* which connect separate pores, (C) *blind alley pores*, (D) *loop pores*, (E) *pocket pores* and (F) *micro pores*.

In this study two different cases have been taken into account: *open* and *sealed pores*. From the modelling point of view, the difference between them is the way in which interface conditions between acoustic and poroelastic domains have been formulated, as described later on. Poroelastic theory has been therefore introduced through proper equations: numerical domains have been equally discretized, not taking into ac-

[4]Image taken from reference [1]

count possibly meshes with many small holes, to represent pores in poroelastic domain.

The remaining part of the thesis is structured as follows: in Chapter 1 we introduce the mathematical model equations to be solved, both for the acoustic and the poroelastic domains, and coupling conditions, in order to consider a well-posed problem, whose existence and uniqueness have been here proven. The weak formulation of the continuous problem has been presented and a stability estimate has been proven; in Chapter 2 dG theory has been taken into account, by introducing the discrete setting and trace operators, so that the problem has been discretized, both in space and in time, through suitable time integration methods. Moreover, a stability and an error estimate have been proven for the semi-discrete problem; in Chapter 3 it has been carried out a convergence analysis both in a monodomain and in a two-domains asset, in order to check the correct behaviour and the robustness of the implemented code. Moreover, some physical tests have been done, considering different domains and interfaces (linear, transversal, circular and sinusoidal), to represent various scenarios.

General notation

In this thesis lighteface letters are adopted to represent scalar fields, boldface roman letters are used for vector fields and boldface greek letters for second-order tensor fields. An open, bounded, polygonal and convex domain $\Omega \subset \mathbb{R}^d$ is introduced and shown in Figure 4, with $d \in \{2, 3\}$ and is decomposed as the union of two open, convex, polygonal and bounded subdomains: $\Omega = \Omega_p \cup \Omega_a$, representing respectively the poroelastic and the acoustic domain. The (Lipschitz) boundary of Ω is denoted by $\partial\Omega$. The two subdomains share part of their boundary, resulting in the interface $\Gamma_I = \partial\Omega_p \cap \partial\Omega_a$. Moreover, the following partions hold: $\partial\Omega_p = \Gamma_{pD} \cup \Gamma_I$ and $\partial\Omega_a = \Gamma_{aD} \cup \Gamma_I$, with

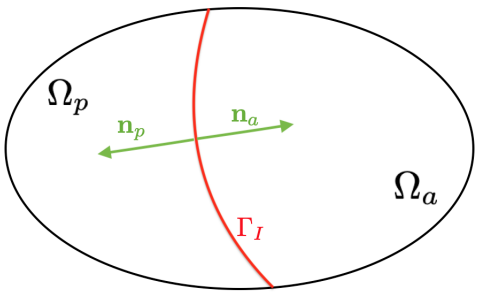

Figure 4: Domains and Interface

$\Gamma_{pD} \cap \Gamma_I = \emptyset$ and $\Gamma_{aD} \cap \Gamma_I = \emptyset$. Surface measures of $\partial\Omega$, $\partial\Omega_p$, $\partial\Omega_a$ and Γ_I are assumed to be strictly positive. Outer unit normal vectors to $\partial\Omega_p$ and $\partial\Omega_a$ are respectively denoted by $\boldsymbol{n}_p$ and $\boldsymbol{n}_a$, so that $\boldsymbol{n}_p = -\boldsymbol{n}_a$ on Γ_I.
By taking $X \subseteq \Omega$, the notation $\boldsymbol{L}^2(X)$ is adopted in place of $[L^2(X)]^d$, with $d \in \{2, 3\}$. The scalar product in X is denoted by $(\cdot, \cdot)_X$, with associated norm $\|\cdot\|_X$. Similarly

$\boldsymbol{H}^{\ell}(X)$ is defined as $[H^{\ell}(X)]^d$, with $\ell \geq 0$, equipped with the norm $\|\cdot\|_{\ell,X}$. Assuming conventionally that $\boldsymbol{H}^0(X) \equiv \boldsymbol{L}^2(X)$, we set: $\|\cdot\|_X \equiv \|\cdot\|_{0,X}$. Here $H^{\ell}(X) = \{v \in L^2(X) : D^{\alpha}v \in L^2(X), \forall \alpha : |\alpha| \leq \ell\}$, where the symbol D^{α} denotes the derivative in the sense of distributions of order $\alpha = (\alpha_1, \ldots, \alpha_d)$, such that $|\alpha| = \sum_{i=1}^{d} \alpha_i \leq \ell$, $d \in \{2, 3\}$.

The notation $x \lesssim y$ is introduced in place of $x \leq Cy$, with $C > 0$, independent of polynomial degree, meshsize, number of faces of mesh elements, but possibly dependent on physical properties of material.

Main differential operators used are gradient, divergence and Laplacian, denoted respectively by ∇, $\nabla\cdot$ and Δ (see [66]). $\dot{\Psi}(t)$ and $\ddot{\Psi}(t)$ stand for first and second time derivatives of a generic scalar or vector field $\Psi(t)$. A time interval $(0, T]$ is introduced by considering $T > 0$ as final time.

Chapter 1

The physical model and governing equations

1.1 The acoustic equations

Depending on cases of interest, different unknowns could be considered to represent an acoustic wave propagation phenomenon. In particular a pressure wave moving throughout a fluid can be simply modeled in terms of a pressure p, as done in [54]. In this work it has been chosen, as in [6, 41] to consider an *acoustic potential* φ. This notation allows moreover to rewrite acoustic equations in different ways: a velocity wave could be considered by defining $\boldsymbol{v}_a = -\nabla\varphi$; a pressure wave is written instead as $p_a = \rho_a\dot{\varphi}$. Those definitions will be useful to introduce interface equations later on.
An acoustic wave, moving with constant velocity c in a fluid domain Ω_a, with density ρ_a is considered. Acoustic equations depend on the acoustic potential φ and velocity $\boldsymbol{v}$ as follows:

$$\begin{cases} \rho_a\dot{\boldsymbol{v}} + \nabla\varphi = \mathbf{0} \\ \dot{\varphi} + \rho_a c^2 \nabla\cdot\boldsymbol{v} = f_a. \end{cases} \tag{1.1}$$

Here f_a indicates an external source term. In order to write equations (1.1) in terms of the acoustic potential φ, the second equation can be differentiated in time. By writing explicitly the time derivative of $\boldsymbol{v}$ and plugging it into the modified second equation, the system reduces to:

$$\ddot{\varphi} - c^2\Delta\varphi = f_a. \tag{1.2}$$

1.2 The poro-elastic equations

In this section we introduce the poroelastic equations, by considering a poroelastic domain Ω_p. As described in the introductive chapter, the domain could present different kind of pores, but for all of them the system of equation shortly introduced before holds true. Different cases will be treated as soon as the coupling equations with the

acoustic part will be introduced. Even for the poro-elastic model, different unknowns could be considered. In this thesis it has been chosen to consider a two-displacement formulation, as in [54], by considering solid and filtration displacements, indicated with $\boldsymbol{u}$ and $\boldsymbol{w}$, respectively. Other choices could consider velocities of the solid skeleton and filtration velocity [27], namely: $\dot{\boldsymbol{u}}$ and $\dot{\boldsymbol{w}}$ as unknowns. Eventually, a velocity-pressure $(\boldsymbol{u} - p)$ formulation is often used in literature, as in [2, 15, 61], where p denotes the pores pressure, in order to study the quasi-static Biot system. As in [27], we consider low-frequency Biot equations, that read:

$$\begin{cases} \rho\ddot{\boldsymbol{u}} + \rho_f\ddot{\boldsymbol{w}} - \nabla\cdot\boldsymbol{\sigma} = \boldsymbol{f}_p \\ \rho_f\ddot{\boldsymbol{u}} + \rho_w\ddot{\boldsymbol{w}} + \frac{\eta}{k}\dot{\boldsymbol{w}} + \nabla p = \boldsymbol{g}_p. \end{cases} \tag{1.3}$$

The three densities ρ, ρ_f and ρ_w that appear in the system are defined as: an average density $\rho = \phi\rho_f + (1-\phi)\rho_s$, with ρ_s solid density; ρ_f is the saturating fluid density, the same of the acoustic fluid density ρ_a; ρ_w is defined as $\rho_w = \frac{a}{\phi}\rho_f$, respectively. Here η is used to represent the dynamic *viscosity* of the fluid, a measure of internal resistance. Parameters of poro-elastic theory need to be introduced: $0 < \phi_0 \leq \phi \leq \phi_1 < 1$ indicates the *porosity* of the material, that is nothing but the percentual of void spaces; $a > 1$ is the *tortuosity* [70], a measure of the deviation of the pore fluid paths from straight streamlines in porous and saturated media. Here, k is the *permeability*, a measure of the ability of a material to host a fluid. The filtration displacement $\boldsymbol{w}$ has to be intended as a relative displacement with respect to the solid one, namely: $\boldsymbol{w} = \phi(\boldsymbol{u}_f - \boldsymbol{u})$. The term $\boldsymbol{u}_f$ denotes the fluid displacement, hidden in this analysis by the same filtration displacement. In (1.3) the forcing and boundary terms are denoted by $\boldsymbol{f}_p$ and $\boldsymbol{g}_p$, respectively.

Notice that the second equation of system (1.3) is valid under a constraint on frequencies. In particular, the spectrum of the waves has to lie in the low-frequency range, so that in this analysis will be considered only frequencies lower than:

$$f_c = \frac{\eta\phi}{2\pi a k \rho_f}.$$

System (1.3) counts as unknowns $\boldsymbol{u}, \boldsymbol{w}, \boldsymbol{\sigma}$ and p. In order to have two equations in two unknowns, constitutive laws for stress $\boldsymbol{\sigma}$ and pressure p are introduced:

$$\boldsymbol{\sigma}(\boldsymbol{u}, p) = \mathbb{C} : \boldsymbol{\epsilon}(\boldsymbol{u}) - \beta p \boldsymbol{I}, \tag{1.4}$$

$$p(\boldsymbol{u}, \boldsymbol{w}) = -m(\beta\nabla\cdot\boldsymbol{u} + \nabla\cdot\boldsymbol{w}). \tag{1.5}$$

Here the strain tensor is defined as $\boldsymbol{\epsilon}(\boldsymbol{u}) = \frac{1}{2}(\nabla \boldsymbol{u} + \nabla \boldsymbol{u}^T)$. Moreover, $\mathbb{C}$ stands for the fourth-order, symmetric and uniformly elliptic elasticity tensor, written as:

$$\mathbb{C} = \begin{pmatrix} \lambda + 2\mu & 0 & \lambda \\ 0 & \mu & 0 \\ \lambda & 0 & \lambda + 2\mu \end{pmatrix}.$$

It is important to stress the fact that the above tensor is a two-dimensional tensor. By the way it has been rewritten in such a way, in order to have an algebraic visualization of its action over the strain tensor. In particular $\mathbb{C} : \boldsymbol{\epsilon}(\boldsymbol{u})$ could be intended as a matrix-vector product $\mathbb{C}\ \boldsymbol{e}(\boldsymbol{u})$, where $\boldsymbol{e} = (\epsilon_{11},\ 2\ \epsilon_{12},\ \epsilon_{22})^T$, so that $\boldsymbol{\sigma} = (\sigma_{11},\ \sigma_{12},\ \sigma_{22})^T$ can be easily rebuilt as a matrix. The Lamé coefficients λ and μ of the elastic skeleton are introduced, as done in [6]. In (1.4)-(1.5) β and m are the Biot's coefficients of the isotropic matrix. It can be shown that Lamé coefficients of the saturated and dry matrices (respectively λ_f and λ) are linked, i.e.:

$$\lambda_f = \lambda + \beta^2 m.$$

Equation (1.4) plays a crucial role in theory of poroelasticity. In fact, it shows how stresses applied to a porous (saturated) medium are partly split into a solid skeleton contribute and partly into a pore fluid one. In literature this constitutive law is referred to the *principle of effective stress*, since responsible for solid deformations. This principle has been introduced in 1936 by Terzaghi [53, 74, 75], showing how stresses applied to rocks are opposed by fluid pressure of pores, constituting the rock itself. Beside main assumptions that need to be verified in order to state the principle, here not listed (see [74]), it is important to point out the need of a *fully saturated* asset for the soil, so that no air voids could be taken into account. Biot's coefficient β, has been set equal to 1 in Terzaghi's theory, in order to model soil and in general soft soil. We point out that this assumption fails to hold when dealing with rocks, so that in general $0 \leq \beta \leq 1$.

By plugging the constitutive laws (1.4) and (1.5) into (1.3), the poro-elastic system in two unknowns is the following:

$$\begin{cases} \rho \ddot{\boldsymbol{u}} + \rho_f \ddot{\boldsymbol{w}} - \nabla \cdot (\mathbb{C} : \boldsymbol{\epsilon}(\boldsymbol{u})) - \beta^2 m \nabla(\nabla \cdot \boldsymbol{u}) - \beta m \nabla(\nabla \cdot \boldsymbol{w}) = \boldsymbol{f}_p \\ \rho_f \ddot{\boldsymbol{u}} + \rho_w \ddot{\boldsymbol{w}} + \frac{\eta}{k} \dot{\boldsymbol{w}} - \beta m \nabla(\nabla \cdot \boldsymbol{u}) - m \nabla(\nabla \cdot \boldsymbol{w}) = \boldsymbol{g}_p. \end{cases} \tag{1.6}$$

1.3 The interface equations

So far, two different phenomena have been considered in two separate domains. The poro-elasto-acoustic coupling is now introduced by considering (physically consistent) interface conditions, a highly discussed topic in literature [22, 27, 39, 42, 54]. Interface conditions will be four for displacements in Ω_p and one for the acoustic potential in Ω_a.

In particular stress and velocities continuities are imposed in order to ensure respectively the continuity of normal stresses and the conservation of mass at the interface Γ_I. While a pressure continuity is imposed by rewriting the acoustic potential in terms of a pressure. This latter condition is nothing but a local Darcy's law, modelling the hydraulic contact between the fluid and the porous medium. From the above discussion we can write the interface conditions as:

$$\boldsymbol{\sigma} \cdot \boldsymbol{n}_p = -\rho_a \dot{\varphi} \boldsymbol{n}_p, \tag{1.7}$$

$$(\dot{\boldsymbol{u}} + \dot{\boldsymbol{w}}) \cdot \boldsymbol{n}_p = -\nabla\varphi \cdot \boldsymbol{n}_p, \tag{1.8}$$

$$[p] = -\frac{1}{\mathcal{K}} \dot{\boldsymbol{w}} \cdot \boldsymbol{n}_p, \tag{1.9}$$

where the operator $[\cdot]$ indicates the jump of the variable considered, from domain Ω_p to Ω_a over the interface Γ_I. The variable $\mathcal{K}$ is the hydraulic permeability at the interface and depending on it, different kind of pores can be considered in the analysis, as shown in Figure 3. In particular:

- If $\mathcal{K} \to +\infty$, equation (1.9) reduces to the continuity of pressure at the interface, that is: $p = \rho_a \dot{\varphi}$, where p is explicited in terms of $\boldsymbol{u}$ and $\boldsymbol{w}$ through constitutive law (1.5). Physically, this condition represents the *open pores* case.
- If $\mathcal{K} \to 0$, (1.9) simplifies to $\dot{\boldsymbol{w}} \cdot \boldsymbol{n}_p = 0$, that implies that (1.8) imposes a continuity only on the solid velocity, namely: $\dot{\boldsymbol{u}} \cdot \boldsymbol{n}_p = -\nabla\varphi \cdot \boldsymbol{n}_p$. This is the *sealed pores* case, in which the filtration velocity is imposed to be null at the interface.
- Following [27], intermediate scenarios between *open* and *sealed pores* could be considered. This is the case of *imperfect pores*, for which $0 < \mathcal{K} < +\infty$. This last condition will not be taken into account in this analysis.

In order to numerically treat those different cases, a variable k_{int} is introduced as follows:

$$k_{int} = \begin{cases} 1 & \text{if } \mathcal{K} \to +\infty \text{ } \textit{(open pores)} \\ 0 & \text{if } \mathcal{K} \to 0 \text{ } \textit{(sealed pores)}. \end{cases} \tag{1.10}$$

Interface equations impose therefore conditions mainly on time or space differentiated quantities. This aspect will be relevant in the postprocessing analysis of numerical tests, as having a graphical visualization of coupling conditions will not be trivial.

1.4 The fully-coupled poro-elasto-acoustic problem

Following the previous considerations on single domains, a coupled formulation can now be stated. As asserted before, unknowns are the solid displacement (of the skeleton) $\boldsymbol{u}$, the filtration displacement $\boldsymbol{w}$ and the acoustic potential φ. For simplicity, it has been chosen to set null boundary Dirichlet conditions on Γ_{pD} and Γ_{aD}, $\forall t > 0$. Second

order time derivatives require an initial condition on first time derivatives of unknowns, in addition to an initial condition on $\boldsymbol{u}$, $\boldsymbol{w}$ and φ. Therefore the *poro-elasto-acoustic problem* reads as:

for sufficiently smooth $\boldsymbol{f_p}$, $\boldsymbol{g_p}$, f_a *and initial conditions* $(\boldsymbol{u}_0, \boldsymbol{u}_1, \boldsymbol{w}_0, \boldsymbol{w}_1, \varphi_0, \varphi_1)$, *find* $\boldsymbol{u} : \Omega_p \times [0,T] \to \mathbb{R}^3$, $\boldsymbol{w} : \Omega_p \times [0,T] \to \mathbb{R}^3$ *and* $\varphi : \Omega_a \times [0,T] \to \mathbb{R}$ *s.t.:*

$$
\begin{cases}
\rho \ddot{\boldsymbol{u}} + \rho_f \ddot{\boldsymbol{w}} - \nabla \cdot \boldsymbol{\sigma} = \boldsymbol{f}_p & \text{in } \Omega_p \times (0,T], \\
\rho_f \ddot{\boldsymbol{u}} + \rho_w \ddot{\boldsymbol{w}} + \frac{\eta}{k} \dot{\boldsymbol{w}} + \nabla p = \boldsymbol{g}_p & \text{in } \Omega_p \times (0,T], \\
\rho_a c^{-2} \ddot{\varphi} - \rho_a \Delta \varphi = \rho_a f_a & \text{in } \Omega_a \times (0,T], \\
\boldsymbol{\sigma} \cdot \boldsymbol{n}_p = -\rho_a \dot{\varphi} \boldsymbol{n}_p & \text{in } \Gamma_I \times (0,T], \\
p + \frac{1}{\mathcal{K}} \dot{\boldsymbol{w}} \cdot \boldsymbol{n}_p = \rho_a \dot{\varphi} & \text{in } \Gamma_I \times (0,T], \\
\nabla \varphi \cdot \boldsymbol{n}_a = -(\dot{\boldsymbol{u}} + \dot{\boldsymbol{w}}) \cdot \boldsymbol{n}_a & \text{in } \Gamma_I \times (0,T], \\
\boldsymbol{u} = \boldsymbol{w} = \boldsymbol{0} & \text{in } \Gamma_{pD} \times (0,T], \\
\varphi = 0 & \text{in } \Gamma_{aD} \times (0,T], \\
\boldsymbol{u}(\cdot, 0) = \boldsymbol{u}_0 & \text{in } \Omega_p, \\
\boldsymbol{w}(\cdot, 0) = \boldsymbol{w}_0 & \text{in } \Omega_p, \\
\dot{\boldsymbol{u}}(\cdot, 0) = \boldsymbol{u}_1 & \text{in } \Omega_p, \\
\dot{\boldsymbol{w}}(\cdot, 0) = \boldsymbol{w}_1 & \text{in } \Omega_p, \\
\varphi(\cdot, 0) = \varphi_0 & \text{in } \Omega_a, \\
\dot{\varphi}(\cdot, 0) = \varphi_1 & \text{in } \Omega_a.
\end{cases}
\tag{1.11}
$$

The acoustic equation has been multiplied by ρ_a, in order to ensure (skew) symmetry of coupling bilinear forms introduced later on. Moreover, it has been chosen to split interface equations in order to be consistent with the integration by parts that will follow in the next chapter. Initial conditions will be differently taken into account from the numerical point of view, depending on the time integration schemes.

1.5 Existence and uniqueness of strong solution

The existence and uniqueness of a strong solution to (1.11) can be inferred in the framework of the Hille-Yosida theory. To this aim, suitable regularity assumptions are needed on source terms, as well as on initial and boundary data. Hilbertian Sobolev spaces are firstly introduced as follows:

$$
\begin{aligned}
\boldsymbol{H}^1_D(\Omega_p) &= \{\boldsymbol{v} \in \boldsymbol{H}^1(\Omega_p) : \boldsymbol{v} = \boldsymbol{0} \text{ on } \Gamma_{pD}\}, \\
H^1_D(\Omega_a) &= \{v \in H^1(\Omega_a) : v = 0 \text{ on } \Gamma_{aD}\},
\end{aligned}
$$

$$
\begin{aligned}
\boldsymbol{H}^{\Delta}_{\mathbb{C}}(\Omega_p) &= \{\boldsymbol{v} \in \boldsymbol{L}^2(\Omega_p) \ : \nabla \cdot (\mathbb{C} : \boldsymbol{\epsilon}(\boldsymbol{v})) \in \boldsymbol{L}^2(\Omega_p)\},\\
\boldsymbol{H}^{2}_{*}(\Omega_p) &= \{\boldsymbol{v} \in \boldsymbol{L}^2(\Omega_p) \ : D^2\boldsymbol{v} \in \boldsymbol{L}^2(\Omega_p)\},\\
H^{\Delta}(\Omega_a) &= \{v \in L^2(\Omega_a) \ : \Delta v \in L^2(\Omega_a)\}.
\end{aligned}
$$

For any integer $k \geq 0$ and a generic Hilbert space $\mathbb{H}$, the usual notation $C^k([0,T];\mathbb{H})$ has been adopted for the space of functions k-times differentiable in $[0,T]$, belonging to $\mathbb{H}$.
For the sake of presentation, it will be considered in the following problem (1.11) equipped with homogeneous Dirichlet boundary conditions.

Theorem 1 (Existence and uniqueness)**.** *Assume that the initial data have the following regularity:*

$$
\begin{aligned}
&\boldsymbol{u}_0 \in \boldsymbol{H}^{\Delta}_{\mathbb{C}}(\Omega_p) \cap \boldsymbol{H}^1_D(\Omega_p) \cap \boldsymbol{H}^2_*(\Omega_p), && \boldsymbol{u}_1 \in \boldsymbol{H}^1_D(\Omega_p),\\
&\boldsymbol{w}_0 \in \boldsymbol{H}^1_D(\Omega_p) \cap \boldsymbol{H}^2_*(\Omega_p), && \boldsymbol{w}_1 \in \boldsymbol{H}^1_D(\Omega_p),\\
&\varphi_0 \in H^{\Delta}(\Omega_a) \cap H^1_D(\Omega_a), && \varphi_1 \in H^1_D(\Omega_a),
\end{aligned}
$$

and that the source terms are such that $\boldsymbol{f}_p \in C^1([0,T];\boldsymbol{L}^2(\Omega_p))$, $\boldsymbol{g}_p \in C^1([0,T];\boldsymbol{L}^2(\Omega_p))$ *and* $f_a \in C^1([0,T];L^2(\Omega_a))$. *Then, problem (1.11) admits a unique strong solution* $(\boldsymbol{u},\boldsymbol{w},\varphi)$ *s.t.*

$$
\begin{aligned}
\boldsymbol{u} &\in C^2([0,T];\boldsymbol{L}^2(\Omega_p)) \cap C^1([0,T];\boldsymbol{H}^1_D(\Omega_p)) \cap C^0([0,T];\boldsymbol{H}^{\Delta}_{\mathbb{C}}(\Omega_p) \cap \boldsymbol{H}^2_*(\Omega_p) \cap \boldsymbol{H}^1_D(\Omega_p)),\\
\boldsymbol{w} &\in C^2([0,T];\boldsymbol{L}^2(\Omega_p)) \cap C^1([0,T];\boldsymbol{H}^1_D(\Omega_p)) \cap C^0([0,T];\boldsymbol{H}^2_*(\Omega_p) \cap \boldsymbol{H}^1_D(\Omega_p)),\\
\varphi &\in C^2([0,T];L^2(\Omega_a)) \cap C^1([0,T];H^1_D(\Omega_a)) \cap C^0([0,T];H^{\Delta}(\Omega_a) \cap H^1_D(\Omega_a)).
\end{aligned}
$$

Proof. Let $\boldsymbol{v} = \dot{\boldsymbol{u}}$, $\boldsymbol{z} = \dot{\boldsymbol{w}}$, $\lambda = \dot{\varphi}$ and let $\mathcal{U} = (\boldsymbol{u},\boldsymbol{v},\boldsymbol{w},\boldsymbol{z},\varphi,\lambda)$. The following Hilbert space is introduced:

$$
\mathbb{H} = \boldsymbol{H}^1_D(\Omega_p) \times \boldsymbol{L}^2(\Omega_p) \times \boldsymbol{H}^1_D(\Omega_p) \times \boldsymbol{L}^2(\Omega_p) \times H^1_D(\Omega_a) \times L^2(\Omega_a),
$$

equipped with the following scalar product

$$
\begin{aligned}
(\mathcal{U}_1,\mathcal{U}_2)_{\mathbb{H}} = &(\rho\boldsymbol{v}_1,\boldsymbol{v}_2)_{\Omega_p} + (\rho_f\boldsymbol{z}_1,\boldsymbol{v}_2)_{\Omega_p} + (\rho_f\boldsymbol{v}_1,\boldsymbol{z}_2)_{\Omega_p} + (\rho_w\boldsymbol{z}_1,\boldsymbol{z}_2)_{\Omega_p}\\
&+ (\mathbb{C} : \boldsymbol{\epsilon}(\boldsymbol{u}_1),\boldsymbol{\epsilon}(\boldsymbol{u}_2))_{\Omega_p} + (m\nabla\cdot(\beta\boldsymbol{u}_1 + \boldsymbol{w}_1), \nabla\cdot(\beta\boldsymbol{u}_2 + \boldsymbol{w}_2))_{\Omega_p}\\
&+ (\rho_a c^{-2}\lambda_1,\lambda_2)_{\Omega_a} + (\rho_a\nabla\varphi_1,\nabla\varphi_2)_{\Omega_a}.
\end{aligned}
$$

Notice that

$$
\begin{aligned}
&(\rho\boldsymbol{v}_1,\boldsymbol{v}_2)_{\Omega_p} + (\rho_f\boldsymbol{z}_1,\boldsymbol{v}_2)_{\Omega_p} + (\rho_f\boldsymbol{v}_1,\boldsymbol{z}_2)_{\Omega_p} + (\rho_w\boldsymbol{z}_1,\boldsymbol{z}_2)_{\Omega_p} =\\
&(\tilde{\rho}_s\boldsymbol{v}_1,\boldsymbol{v}_2)_{\Omega_p} + (\tilde{\rho}_w\boldsymbol{z}_1,\boldsymbol{z}_2)_{\Omega_p} + \left(\rho_f[\phi^{1/2}\boldsymbol{v}_1 + \phi^{-1/2}\boldsymbol{z}_1], \phi^{1/2}\boldsymbol{v}_2 + \phi^{-1/2}\boldsymbol{z}_2\right),
\end{aligned}
$$

where $\tilde{\rho}_s = (1-\phi)\rho_f$, $\tilde{\rho}_w = \frac{a_0}{\phi}\rho_f$ and $a = 1 + a_0$.

The operator $A : \mathcal{D}(A) \subset \mathbb{H} \to \mathbb{H}$ has been defined as

$$A\mathcal{U} = \begin{Bmatrix} -\boldsymbol{v} \\ -\frac{\rho_w}{\rho_T}\nabla\cdot\boldsymbol{\sigma} - \frac{\rho_f}{\rho_T}\frac{\eta}{k}\boldsymbol{z} - \frac{\rho_f}{\rho_T}\nabla p \\ -\boldsymbol{z} \\ \frac{\rho_f}{\rho_T}\nabla\cdot\boldsymbol{\sigma} + \frac{\rho}{\rho_T}\frac{\eta}{k}\boldsymbol{z} + \frac{\rho}{\rho_T}\nabla p \\ -\lambda \\ -c^2\Delta\varphi \end{Bmatrix},$$

with $\rho_T = \rho\rho_w - \rho_f^2 > 0$, where the domain $\mathcal{D}(A)$ of the operator is the linear subspace of $\mathbb{H}$ defined as follows:

$$\begin{aligned} \mathcal{D}(A) = \{\mathcal{U} \in \mathbb{H} : \boldsymbol{u} \in \boldsymbol{H}^{\Delta}_{\mathbb{C}}(\Omega_p) \cap \boldsymbol{H}^2_*(\Omega_p), \boldsymbol{v} \in \boldsymbol{H}^1_D(\Omega_p), \boldsymbol{w} \in \boldsymbol{H}^2_*(\Omega_p), \\ \boldsymbol{z} \in \boldsymbol{H}^1_D(\Omega_p), \varphi \in H^{\Delta}(\Omega_a), \lambda \in H^1_D(\Omega_a); \\ (\boldsymbol{\sigma} + \rho_a\lambda\boldsymbol{I})\cdot\boldsymbol{n}_p = \boldsymbol{0}, \ \text{ on } \Gamma_I, \\ (p - \rho_a\lambda)\boldsymbol{n}_p = \boldsymbol{0}, \ \text{ on } \Gamma_I, \\ (\nabla\varphi + \boldsymbol{v} + \boldsymbol{z})\cdot\boldsymbol{n}_a = 0, \ \text{ on } \Gamma_I\}. \end{aligned}$$

Finally, let

$$\mathcal{F}(t) = \begin{Bmatrix} \boldsymbol{0} \\ (\rho_w\boldsymbol{f}_p - \rho_f\boldsymbol{g}_p)/\rho_T \\ \boldsymbol{0} \\ (\rho\boldsymbol{g}_p - \rho_f\boldsymbol{f}_p)/\rho_T \\ 0 \\ c^2 f_a \end{Bmatrix}.$$

With the above notation, problem (1.11) can be reformulated as follows:
given $\mathcal{F} \in C^1([0,T],\mathbb{H})$ and $\mathcal{U}_0 \in \mathcal{D}(A)$, find $\mathcal{U} \in C^1([0,T];\mathbb{H}) \cap C^0([0,T];\mathcal{D}(A))$ s.t.

$$\begin{cases} \dfrac{\mathrm{d}\mathcal{U}}{\mathrm{dt}} + A\mathcal{U}(t) = \mathcal{F}(t), & t \in (0,T], \\ \mathcal{U}(\boldsymbol{0}) = \mathcal{U}_0. \end{cases}$$

Owing to the Hille-Yoside theorem, this problem is well-posed provided A is maximal monotone, i.e. $(A\mathcal{U},\mathcal{U})_{\mathbb{H}} \geq 0 \ \forall\, \mathcal{U} \in \mathcal{D}(A)$ and $I + A$ is surjective from $\mathcal{D}(A)$ to $\mathbb{H}$.
By definition of the scalar product in $\mathbb{H}$, it follows:

$$\begin{aligned} (A\mathcal{U},\mathcal{U})_{\mathbb{H}} = &-\left(\rho\frac{\rho_w}{\rho_T}\nabla\cdot\boldsymbol{\sigma} + \rho\frac{\rho_f}{\rho_T}\frac{\eta}{k}\boldsymbol{z} + \rho\frac{\rho_f}{\rho_T}\nabla p, \boldsymbol{v}\right)_{\Omega_p} \\ &+\left(\rho_f\frac{\rho_f}{\rho_T}\nabla\cdot\boldsymbol{\sigma} + \rho\frac{\rho_f}{\rho_T}\frac{\eta}{k}\boldsymbol{z} + \rho\frac{\rho_f}{\rho_T}\nabla p, \boldsymbol{v}\right)_{\Omega_p} \\ &-\left(\rho_f\frac{\rho_w}{\rho_T}\nabla\cdot\boldsymbol{\sigma} + \rho_f\frac{\rho_f}{\rho_T}\frac{\eta}{k}\boldsymbol{z} + \rho_f\frac{\rho_f}{\rho_T}\nabla p, \boldsymbol{z}\right)_{\Omega_p} \end{aligned}$$

$$
\begin{aligned}
&+\left(\rho_w\frac{\rho_f}{\rho_T}\nabla\cdot\boldsymbol{\sigma}+\rho_w\frac{\rho}{\rho_T}\frac{\eta}{k}\boldsymbol{z}+\rho\frac{\rho_w}{\rho_T}\nabla p,\boldsymbol{z}\right)_{\Omega_p}\\
&-(\mathbb{C}:\boldsymbol{\epsilon}(\boldsymbol{v}),\boldsymbol{\epsilon}(\boldsymbol{u}))_{\Omega_p}-(\rho_a\Delta\varphi,\lambda)_{\Omega_a}\\
&-(\rho_a\nabla\lambda,\nabla\varphi)_{\Omega_a}-(m\nabla\cdot(\beta\boldsymbol{v}+\boldsymbol{z}),\nabla\cdot(\beta\boldsymbol{u}+\boldsymbol{w}))_{\Omega_p}\\
=&-(\nabla\cdot\boldsymbol{\sigma},\boldsymbol{v})_{\Omega_p}+(\nabla p,\boldsymbol{z})_{\Omega_p}+(\frac{\eta}{k}\boldsymbol{z},\boldsymbol{z})_{\Omega_p}\\
&-(\mathbb{C}:\boldsymbol{\epsilon}(\boldsymbol{v}),\boldsymbol{\epsilon}(\boldsymbol{u}))_{\Omega_p}-(\rho_a\Delta\varphi,\lambda)_{\Omega_a}\\
&-(\rho_a\nabla\lambda,\nabla\varphi)_{\Omega_a}-(m\nabla\cdot(\beta\boldsymbol{v}+\boldsymbol{z}),\nabla\cdot(\beta\boldsymbol{u}+\boldsymbol{w}))_{\Omega_p}\\
=&(\mathbb{C}:\boldsymbol{\epsilon}(\boldsymbol{u}),\boldsymbol{\epsilon}(\boldsymbol{v}))_{\Omega_p}+(m\nabla\cdot(\beta\boldsymbol{u}+\boldsymbol{w}),\nabla\cdot(\beta\boldsymbol{v}))_{\Omega_p}-(\boldsymbol{\sigma}\boldsymbol{n}_p,\boldsymbol{v})_{\Gamma_I}\\
&+(m\nabla\cdot(\beta\boldsymbol{u}+\boldsymbol{w}),\nabla\cdot\boldsymbol{z})_{\Omega_p}-(p\boldsymbol{n}_p,\boldsymbol{z})_{\Gamma_I}+\left(\frac{\eta}{k}\boldsymbol{z},\boldsymbol{z}\right)_{\Omega_p}\\
&-(\mathbb{C}:\boldsymbol{\epsilon}(\boldsymbol{v}),\boldsymbol{\epsilon}(\boldsymbol{u}))_{\Omega_p}+(\rho_a\nabla\varphi,\nabla\lambda)_{\Omega_a}-(\rho_a\nabla\varphi\cdot\boldsymbol{n}_a,\lambda)_{\Gamma_I}\\
&-(\rho_a\nabla\lambda,\nabla\varphi)_{\Omega_a}-(m\nabla\cdot(\beta\boldsymbol{u}+\boldsymbol{w}),\nabla\cdot(\beta\boldsymbol{v}+\boldsymbol{z}))_{\Omega_p}\\
=&\left\|\left(\frac{\eta}{k}\right)^{1/2}\boldsymbol{z}\right\|^2_{\Omega_p}\geq 0.
\end{aligned}
$$

Notice that the terms that live on Γ_I vanish due to interface conditions imposed.
A is therefore monotone. It remains to verify that for any $\mathcal{F}\in\mathbb{H}$, there exists a unique $\mathcal{U}\in\mathcal{D}(A)$ s.t. $\mathcal{U}+A\mathcal{U}=\mathcal{F}$, that is:

$$
\begin{cases}
\boldsymbol{u}-\boldsymbol{v}=\boldsymbol{F}_1, & \text{(1.12a)}\\
\boldsymbol{v}-\frac{\rho_w}{\rho_T}\nabla\cdot\boldsymbol{\sigma}-\frac{\rho_f}{\rho_T}\frac{\eta}{k}\boldsymbol{z}-\frac{\rho_f}{\rho_T}\nabla p=\boldsymbol{F}_2, & \text{(1.12b)}\\
\boldsymbol{w}-\boldsymbol{z}=\boldsymbol{F}_3, & \text{(1.12c)}\\
\boldsymbol{z}+\frac{\rho_f}{\rho_T}\nabla\cdot\boldsymbol{\sigma}+\frac{\rho}{\rho_T}\frac{\eta}{k}\boldsymbol{z}+\frac{\rho}{\rho_T}\nabla p=\boldsymbol{F}_4, & \text{(1.12d)}\\
\varphi-\lambda=F_5, & \text{(1.12e)}\\
\lambda-c^2\Delta\varphi=F_6. & \text{(1.12f)}
\end{cases}
$$

Observe that (1.12a), (1.12c) and (1.12e) can be further rewritten as $\boldsymbol{v}=\boldsymbol{u}-\boldsymbol{F}_1$, $\boldsymbol{z}=\boldsymbol{w}-\boldsymbol{F}_3$ and $\lambda=\varphi-F_5$, respectively. By using equations (1.12a), (1.12c) and (1.12e) , the system can be reformulated as follows:

$$
\begin{cases}
\rho\left(\boldsymbol{v}-\frac{\rho_w}{\rho_T}\nabla\cdot\boldsymbol{\sigma}-\frac{\rho_f}{\rho_T}\frac{\eta}{k}\boldsymbol{z}-\frac{\rho_f}{\rho_T}\nabla p\right)+\rho_f\left(\boldsymbol{z}+\frac{\rho_f}{\rho_T}\nabla\cdot\boldsymbol{\sigma}+\frac{\rho}{\rho_T}\frac{\eta}{k}\boldsymbol{z}+\frac{\rho}{\rho_T}\nabla p\right)=\\
\rho\boldsymbol{F}_2+\rho_f\boldsymbol{F}_4,\\
\rho_f\left(\boldsymbol{v}-\frac{\rho_w}{\rho_T}\nabla\cdot\boldsymbol{\sigma}-\frac{\rho_f}{\rho_T}\frac{\eta}{k}\boldsymbol{z}-\frac{\rho_f}{\rho_T}\nabla p\right)+\rho_w\left(\boldsymbol{z}+\frac{\rho_f}{\rho_T}\nabla\cdot\boldsymbol{\sigma}+\frac{\rho}{\rho_T}\frac{\eta}{k}\boldsymbol{z}+\frac{\rho}{\rho_T}\nabla p\right)=\\
\rho_f\boldsymbol{F}_2+\rho_w\boldsymbol{F}_4,\\
\rho_a c^{-2}\left(\lambda-c^2\Delta\varphi\right)=\rho_a c^{-2}F_6,
\end{cases}
$$

which implies

$$\begin{cases} \rho \boldsymbol{u} + \rho_f \boldsymbol{w} - \nabla \cdot \boldsymbol{\sigma} = \rho(\boldsymbol{F}_1 + \boldsymbol{F}_2) + \rho_f(\boldsymbol{F}_3 + \boldsymbol{F}_4) = \boldsymbol{G}_1, \\ \rho_f \boldsymbol{u} + \rho_w \boldsymbol{w} + \dfrac{\eta}{k}\boldsymbol{w} + \nabla p = \rho_f(\boldsymbol{F}_1 + \boldsymbol{F}_2) + \rho_w(\boldsymbol{F}_3 + \boldsymbol{F}_4) + \dfrac{\eta}{k}\boldsymbol{F}_3 = \boldsymbol{G}_2, \\ \rho_a c^{-2}\varphi - \rho_a \Delta\varphi = \rho_a c^{-2}(F_5 + F_6) = G_3. \end{cases} \tag{1.13}$$

Since $\boldsymbol{n}_p = -\boldsymbol{n}_a$ on Γ_I and owing to (1.12a), (1.12c) and (1.12e) and to the transmission conditions on Γ_I embedded in the definition of $\mathcal{D}(A)$, the variational formulation of the above problem reads:
Find $(\boldsymbol{u}, \boldsymbol{w}, \varphi) \in \boldsymbol{H}^1_D(\Omega_p) \times \boldsymbol{H}^1_D(\Omega_p) \times H^1_D(\Omega_a)$ s.t. for any $(\boldsymbol{v}, \boldsymbol{z}, \lambda) \in \boldsymbol{H}^1_D(\Omega_p) \times \boldsymbol{H}^1_D(\Omega_p) \times H^1_D(\Omega_a)$, it holds:

$$\mathcal{A}((\boldsymbol{u}, \boldsymbol{w}, \varphi), (\boldsymbol{v}, \boldsymbol{z}, \lambda)) = \mathcal{L}(\boldsymbol{v}, \boldsymbol{z}, \lambda),$$

where:

$$\begin{aligned} \mathcal{A}((\boldsymbol{u}, \boldsymbol{w}, \varphi), (\boldsymbol{v}, \boldsymbol{z}, \lambda)) =& (\rho \boldsymbol{u}, \boldsymbol{v})_{\Omega_p} + (\rho_f \boldsymbol{w}, \boldsymbol{v})_{\Omega_p} \\ &+ (\mathbb{C}\boldsymbol{\epsilon}(\boldsymbol{u}), \boldsymbol{\epsilon}(\boldsymbol{v}))_{\Omega_p} + (m\nabla \cdot (\beta \boldsymbol{u} + \boldsymbol{w}), \nabla \cdot (\beta \boldsymbol{v} + \boldsymbol{z}))_{\Omega_p} \\ &+ \left(\frac{\eta}{k}\boldsymbol{w}, \boldsymbol{z}\right)_{\Omega_p} + (\rho_a c^{-2}\varphi, \lambda)_{\Omega_a} + (\rho_a \nabla\varphi, \nabla\lambda)_{\Omega_a} \\ &+ (\rho_f \boldsymbol{u}, \boldsymbol{z})_{\Omega_p} + (\rho_w \boldsymbol{w}, \boldsymbol{z})_{\Omega_p} \\ &+ (\rho_a \varphi \boldsymbol{n}_p, \boldsymbol{v} + \boldsymbol{z})_{\Gamma_I} - (\rho_a(\boldsymbol{u} + \boldsymbol{w}) \cdot \boldsymbol{n}_p, \lambda)_{\Gamma_I} \end{aligned}$$

and

$$\mathcal{L}(\boldsymbol{v}, \boldsymbol{z}, \lambda) = (\boldsymbol{G}_1, \boldsymbol{v})_{\Omega_p} + (\boldsymbol{G}_2, \boldsymbol{z})_{\Omega_p} + (G_3, \lambda)_{\Omega_a}.$$

This problem is well posed thanks to the Lax-Milgram Lemma (see [66]). Notice that the bilinear form $\mathcal{A}$ is coercive since the interface contribution vanish when $\boldsymbol{v} = \boldsymbol{u}$, $\boldsymbol{z} = \boldsymbol{w}$ and $\lambda = \varphi$. In addition, thanks to (1.12b), it can be inferred that $\boldsymbol{u} \in \boldsymbol{H}^{\Delta}_{\mathbb{C}}(\Omega_p) \cap \boldsymbol{H}^2_*(\Omega_p) \cap \boldsymbol{H}^1_D(\Omega_p)$, $\boldsymbol{w} \in \boldsymbol{H}^2_*(\Omega_p) \cap \boldsymbol{H}^1_D(\Omega_p)$ and $\varphi \in H^{\Delta}(\Omega_a) \cap H^1_D(\Omega_a)$. Moreover, this gives $(\boldsymbol{v}, \boldsymbol{z}, \lambda) \in \boldsymbol{H}^1_D(\Omega_p) \times \boldsymbol{H}^1_D(\Omega_p) \times H^1_D(\Omega_a)$, thanks to (1.12a), (1.12c) and (1.12e). Then $\mathcal{U} \in \mathcal{D}(A)$ and the proof is complete. □

1.6 Weak Formulation

We multiply equations (1.2) and (1.3) by test functions $\boldsymbol{v}, \boldsymbol{\xi} \in \boldsymbol{H}^1_D(\Omega_p)$ and $\psi \in H^1_D(\Omega_a)$ and integrate by parts. We obtain:

$$\begin{cases} (\rho\ddot{\boldsymbol{u}}, \boldsymbol{v}) + (\rho_f\ddot{\boldsymbol{w}}, \boldsymbol{v}) + (\mathbb{C} : \boldsymbol{\epsilon}(\boldsymbol{u}), \boldsymbol{\epsilon}(\boldsymbol{v})) \\ +(\beta m(\beta\nabla\cdot\boldsymbol{u} + \nabla\cdot\boldsymbol{w})\boldsymbol{I}, \boldsymbol{\epsilon}(\boldsymbol{v})) - \langle\mathbb{C} : \boldsymbol{\epsilon}(\boldsymbol{u})\cdot\boldsymbol{n}_p, \boldsymbol{v}\rangle \\ -\langle\beta m(\beta\nabla\cdot\boldsymbol{u} + \nabla\cdot\boldsymbol{w})\boldsymbol{n}_p, \boldsymbol{v}\rangle = (\boldsymbol{f}_p, \boldsymbol{v}), \end{cases} \tag{1.14a}$$

$$\begin{cases} (\rho_f\ddot{\boldsymbol{u}}, \boldsymbol{\xi}) + (\rho_w\ddot{\boldsymbol{w}}, \boldsymbol{\xi}) + (\eta k^{-1}\dot{\boldsymbol{w}}, \boldsymbol{\xi}) + (m(\beta\nabla\cdot\boldsymbol{u} + \nabla\cdot\boldsymbol{w}), \nabla\cdot\boldsymbol{\xi}) \\ -\langle m(\beta\nabla\cdot\boldsymbol{u} + \nabla\cdot\boldsymbol{w})\boldsymbol{n}_p, \boldsymbol{\xi}\rangle = (\boldsymbol{g}_p, \boldsymbol{\xi}), \end{cases} \tag{1.14b}$$

$$(\rho_a c^{-2}\ddot{\varphi}, \psi) + (\rho_a\nabla\varphi, \nabla\psi) - \langle\rho_a\nabla\varphi\cdot\boldsymbol{n}_a, \psi\rangle = (\rho_a f_a, \psi). \tag{1.14c}$$

To derive equations (1.14a)-(1.14c), it has been used a well-known corollary of the Divergence Theorem (see [66] for more details). In particular, given $V \subset \mathbb{R}^n$ compact set (with a regular enough boundary ∂V), a sufficiently regular vectorial field $\boldsymbol{F}$ and a scalar function g, the following identity holds:

$$\int_V [\boldsymbol{F}\cdot\nabla g + (\nabla\cdot\boldsymbol{F})g]\, dV = \oint_{\partial V} g\boldsymbol{F}\cdot\boldsymbol{n}\, d\gamma. \tag{1.15}$$

More precisely, equation (1.14a) has been derived through a proper generalization to tensorial analysis of this last identity. Equation (1.14b) is ensured instead by simply setting in (1.15) $g = p$. The last integration has been computed by considering $\boldsymbol{F} = \nabla\varphi$ and the same definition of the Laplacian operator: $\Delta\varphi = \nabla\cdot\nabla\varphi$.
We remark that, at this point the constitutive laws have not yet been used, in order to correctly impose the coupling conditions. It should also be noted that the boundary terms perfectly match (on Γ_I) with the following interface conditions in weak form, imposed on the interface Γ_I:

$$-\langle\boldsymbol{\sigma}\cdot\boldsymbol{n}_p, \boldsymbol{v}\rangle = \langle\rho_a\dot{\varphi}\boldsymbol{n}_p, \boldsymbol{v}\rangle = \mathcal{C}_p(\varphi, \boldsymbol{v}), \tag{1.16}$$

$$k_{int}\langle p\boldsymbol{n}_p, \boldsymbol{\xi}\rangle = k_{int}\langle\rho_a\dot{\varphi}\boldsymbol{n}_p, \boldsymbol{\xi}\rangle = k_{int}\mathcal{C}_p(\varphi, \boldsymbol{\xi}), \tag{1.17}$$

$$-\langle\rho_a\nabla\varphi\cdot\boldsymbol{n}_a, \psi\rangle = \rho_a\langle(\dot{\boldsymbol{u}} + k_{int}\dot{\boldsymbol{w}})\cdot\boldsymbol{n}_a, \psi\rangle = \mathcal{C}_a(\boldsymbol{u}, \psi) + k_{int}\mathcal{C}_a(\boldsymbol{w}, \psi). \tag{1.18}$$

It is important to stress the fact that equation (1.17) cancels out when $k_{int} = 0$, as expected by equation (1.9) and the resulting condition $\dot{\boldsymbol{w}}\cdot\boldsymbol{n} = \boldsymbol{0}$ is inherited by condition (1.8).

Moreover, by plugging into equations (1.14a-1.14c) the constitutive laws defined in equations (1.4) and (1.5) and the newly introduced coupling bilinear forms, a the solu-

tion of (1.11) satisfies the following system:

for any $t \in (0,T]$, find $(\boldsymbol{u},\boldsymbol{v},\varphi) \in \boldsymbol{H}^1_D(\Omega_p)\times\boldsymbol{H}^1_D(\Omega_p)\times H^1_D(\Omega_a)$ s.t. for all $(\boldsymbol{v},\boldsymbol{\xi},\psi) \in \boldsymbol{H}^1_D(\Omega_p)\times\boldsymbol{H}^1_D(\Omega_p)\times H^1_D(\Omega_a)$, it holds:

$$\begin{aligned}
&(\rho\ddot{\boldsymbol{u}},\boldsymbol{v})_{\Omega_p} + (\rho_f\ddot{\boldsymbol{w}},\boldsymbol{v})_{\Omega_p} + \mathcal{A}^p(\boldsymbol{u},\boldsymbol{v}) + \mathcal{B}^p(\beta\boldsymbol{u}+\boldsymbol{w},\beta\boldsymbol{v}) + \mathcal{C}_p(\varphi,\boldsymbol{v})\\
&+ (\rho_f\ddot{\boldsymbol{u}},\boldsymbol{\xi})_{\Omega_p} + (\rho_w\ddot{\boldsymbol{w}},\boldsymbol{\xi})_{\Omega_p} + \eta k^{-1}(\dot{\boldsymbol{w}},\boldsymbol{\xi})_{\Omega_p} + \mathcal{B}^p(\beta\boldsymbol{u}+\boldsymbol{w},\boldsymbol{\xi}) + k_{int}\mathcal{C}_p(\varphi,\boldsymbol{\xi})\\
&+ (\rho_a c^{-2}\ddot{\varphi},\psi)_{\Omega_a} + \mathcal{A}^a(\varphi,\psi) + \mathcal{C}_a(\boldsymbol{u},\psi) + k_{int}\mathcal{C}_a(\boldsymbol{w},\psi)\\
&= (\boldsymbol{f}_p,\boldsymbol{v})_{\Omega_p} + (\boldsymbol{g}_p,\boldsymbol{\xi})_{\Omega_p} + (\rho_a f_a,\psi)_{\Omega_a}.
\end{aligned} \tag{1.19}$$

The bilinear forms $\mathcal{A}^p : \boldsymbol{H}^1_D(\Omega_p)\times\boldsymbol{H}^1_D(\Omega_p)\to\mathbb{R}$, $\mathcal{B}^p : \boldsymbol{H}^1_D(\Omega_p)\times\boldsymbol{H}^1_D(\Omega_p)\to\mathbb{R}$, $\mathcal{A}^a : H^1_D(\Omega_a)\times H^1_D(\Omega_a)\to\mathbb{R}$, $\mathcal{C}_p : H^1_D(\Omega_a)\times\boldsymbol{H}^1_D(\Omega_p)\to\mathbb{R}$ and $\mathcal{C}_a : \boldsymbol{H}^1_D(\Omega_p)\times H^1_D(\Omega_a)\to\mathbb{R}$ are defined as follows:

$$\begin{aligned}
\mathcal{A}^p(\boldsymbol{u},\boldsymbol{v}) &= (\mathbb{C}:\boldsymbol{\epsilon}(\boldsymbol{u}),\boldsymbol{\epsilon}(\boldsymbol{v}))_{\Omega_p} && \forall\ (\boldsymbol{u},\boldsymbol{v}) \in \boldsymbol{H}^1_D(\Omega_p)\times\boldsymbol{H}^1_D(\Omega_p),\\
\mathcal{B}^p(\boldsymbol{u},\boldsymbol{v}) &= (m\nabla\cdot\boldsymbol{u},\nabla\cdot\boldsymbol{v})_{\Omega_p} && \forall\ (\boldsymbol{u},\boldsymbol{v}) \in \boldsymbol{H}^1_D(\Omega_p)\times\boldsymbol{H}^1_D(\Omega_p),\\
\mathcal{A}^a(\varphi,\psi) &= (\rho_a\nabla\varphi,\nabla\psi)_{\Omega_a} && \forall\ (\varphi,\psi) \in H^1_D(\Omega_a)\times H^1_D(\Omega_a),\\
\\
\mathcal{C}_p(\varphi,\boldsymbol{v}) &= \langle\rho_a\dot{\varphi}\boldsymbol{n}_p,\boldsymbol{v}\rangle_{\Gamma_I} && \forall\ (\varphi,\boldsymbol{v}) \in H^1_D(\Omega_a)\times\boldsymbol{H}^1_D(\Omega_p),\\
\mathcal{C}_a(\boldsymbol{u},\psi) &= \langle\rho_a\dot{\boldsymbol{u}}\cdot\boldsymbol{n}_a,\psi\rangle_{\Gamma_I} && \forall\ (\boldsymbol{u},\psi) \in \boldsymbol{H}^1_D(\Omega_p)\times H^1_D(\Omega_a).
\end{aligned}$$

As already mentioned in Section 1.4, the coupling bilinear forms $\mathcal{C}_p(\cdot,\cdot)$ and $\mathcal{C}_a(\cdot,\cdot)$ are (skew) symmetric, property ensured by the fact that $\boldsymbol{n}_p = -\boldsymbol{n}_a$.

1.7 Stability of the continuous problem

In this section we will address the stability of the weak solution $(\boldsymbol{u},\boldsymbol{w},\varphi)$ of problem (1.19). In particular, the goal is to derive a priori estimates to bound the energy norm of the solution in terms of problem's data.
To start with, we consider (1.19) and we choose as test functions $(\dot{\boldsymbol{u}},\dot{\boldsymbol{w}},\dot{\varphi})$, to obtain:

$$\begin{aligned}
&(\rho\ddot{\boldsymbol{u}},\dot{\boldsymbol{u}})_{\Omega_p} + (\rho_f\ddot{\boldsymbol{w}},\dot{\boldsymbol{u}})_{\Omega_p} + \mathcal{A}^p(\boldsymbol{u},\dot{\boldsymbol{u}}) + \mathcal{B}^p(\beta\boldsymbol{u}+\boldsymbol{w},\beta\dot{\boldsymbol{u}})\\
&+ (\rho_f\ddot{\boldsymbol{u}},\dot{\boldsymbol{w}})_{\Omega_p} + (\rho_w\ddot{\boldsymbol{w}},\dot{\boldsymbol{w}})_{\Omega_p} + \eta k^{-1}(\dot{\boldsymbol{w}},\dot{\boldsymbol{w}})_{\Omega_p} + \mathcal{B}^p(\beta\boldsymbol{u}+\boldsymbol{w},\dot{\boldsymbol{w}})\\
&+ (\rho_a c^{-2}\ddot{\varphi},\dot{\varphi})_{\Omega_a} + \mathcal{A}^a(\varphi,\dot{\varphi}) = (\boldsymbol{f}_p,\dot{\boldsymbol{u}})_{\Omega_p} + (\boldsymbol{g}_p,\dot{\boldsymbol{w}})_{\Omega_p} + (\rho_a f_a,\dot{\varphi})_{\Omega_a}.
\end{aligned} \tag{1.20}$$

We remark that $\mathcal{C}_a(\boldsymbol{u},\dot{\varphi})+\mathcal{C}_p(\varphi,\dot{\boldsymbol{u}})=0$ due to skew-symmetry. Moreover, for the forthcoming analysis, we introduce the following energy norms:

$$\|\boldsymbol{u}\|^2_{\mathcal{E},e}=\|\tilde{\rho}_s\dot{\boldsymbol{u}}\|^2_{\Omega_p}+\left\|\mathbb{C}^{1/2}\boldsymbol{\epsilon}(\boldsymbol{u})\right\|^2_{\Omega_p},$$
$$\|\varphi\|^2_{\mathcal{E},a}=\left\|c^{-1}\rho_a^{1/2}\dot{\varphi}\right\|^2_{\Omega_a}+\|\nabla\varphi\|^2_{\Omega_a},$$

where $\tilde{\rho}_s=(1-\phi)\rho_s$. Moreover the tortuosity $a>1$ is rewritten as $a=1+a_0$, with $a_0>0$. Equation (1.20) is therefore accordingly rewritten, by expliciting densities:

$$\begin{aligned}\frac{1}{2}\frac{d}{dt}\Big[\|\boldsymbol{u}\|^2_{\mathcal{E},e}+\|\varphi\|^2_{\mathcal{E},a}+\left\|m^{1/2}\nabla\cdot(\beta\boldsymbol{u}+\boldsymbol{w})\right\|^2_{\Omega_p}+\\ \left\|\phi^{1/2}\rho_f^{1/2}\dot{\boldsymbol{u}}\right\|^2_{\Omega_p}+\left\|\left(\frac{a}{\phi}\right)^{1/2}\rho_f^{1/2}\dot{\boldsymbol{w}}\right\|^2_{\Omega_p}+2(\rho_f\dot{\boldsymbol{w}},\dot{\boldsymbol{u}})\Big]+\\ \eta k^{-1}\|\dot{\boldsymbol{w}}\|^2_{\Omega_p}=(\boldsymbol{f}_p,\dot{\boldsymbol{u}})_{\Omega_p}+(\boldsymbol{g}_p,\dot{\boldsymbol{w}})_{\Omega_p}+(\rho_a f_a,\dot{\varphi})_{\Omega_a}.\end{aligned}\tag{1.21}$$

By observing that:

$$\left\|\phi^{1/2}\rho_f^{1/2}\dot{\boldsymbol{u}}\right\|^2_{\Omega_p}+\left\|\left(\frac{a}{\phi}\right)^{1/2}\rho_f^{1/2}\dot{\boldsymbol{w}}\right\|^2_{\Omega_p}+2(\rho_f\dot{\boldsymbol{w}},\dot{\boldsymbol{u}})=$$
$$\left\|\phi^{1/2}\rho_f^{1/2}\dot{\boldsymbol{u}}\right\|^2_{\Omega_p}+\left\|\left(\frac{\rho_f}{\phi}\right)^{1/2}\dot{\boldsymbol{w}}\right\|^2_{\Omega_p}+\left\|\left(\frac{\rho_f a_0}{\phi}\right)^{1/2}\dot{\boldsymbol{w}}\right\|^2_{\Omega_p}+$$
$$2(\rho_f\dot{\boldsymbol{w}},\dot{\boldsymbol{u}})=\left\|\rho_f^{1/2}\left(\phi^{1/2}\dot{\boldsymbol{u}}+\phi^{-1/2}\dot{\boldsymbol{w}}\right)\right\|^2_{\Omega_p}+\left\|\tilde{\rho}_w^{1/2}\dot{\boldsymbol{w}}\right\|^2_{\Omega_p},$$

where $\tilde{\rho}_w=\left(\frac{\rho_f a_0}{\phi}\right)^{1/2}$, the following energy norm can therefore be defined:

$$\|\boldsymbol{U}(t)\|^2_{\mathcal{E}}=\|\boldsymbol{u}(t)\|^2_{\mathcal{E},e}+\|\varphi(t)\|^2_{\mathcal{E},a}+\left\|m^{1/2}\nabla\cdot(\beta\boldsymbol{u}+\boldsymbol{w})\right\|^2_{\Omega_p}+$$
$$\left\|\rho_f^{1/2}\left(\phi^{1/2}\dot{\boldsymbol{u}}+\phi^{-1/2}\dot{\boldsymbol{w}}\right)\right\|^2_{\Omega_p}+\left\|\tilde{\rho}_w^{1/2}\dot{\boldsymbol{w}}\right\|^2_{\Omega_p},$$

where $\boldsymbol{U}=(\boldsymbol{u},\boldsymbol{w},\varphi)$.

Theorem 2 (Stability of the continuous formulation)**.** *For any $t\in(0,T]$, let $(\boldsymbol{u},\boldsymbol{w},\varphi)$ be the solution of (1.19). Then, the following bound holds*

$$\|\boldsymbol{U}(t)\|_{\mathcal{E}}\leq\|\boldsymbol{U}(0)\|_{\mathcal{E}}+\int_0^t\left(\left\|\tilde{\rho}_s^{-1/2}\boldsymbol{f}_p\right\|_{\Omega_p}+\left\|\tilde{\rho}_w^{-1/2}\boldsymbol{g}_p\right\|_{\Omega_p}+\left\|c\rho_a^{1/2}f_a\right\|_{\Omega_a}\right)d\tau,$$

Proof. Equation (1.21) is rewritten as:

$$\frac{1}{2}\frac{d}{dt}\left\|\boldsymbol{U}(t)\right\|_{\mathcal{E}}^2+\eta k^{-1}\left\|\dot{\boldsymbol{w}}\right\|_{\Omega_p}^2=(\boldsymbol{f}_p,\dot{\boldsymbol{u}})_{\Omega_p}+(\boldsymbol{g}_p,\dot{\boldsymbol{w}})_{\Omega_p}+(\rho_a f_a,\dot{\varphi})_{\Omega_a}.$$

By integrating with respect to time in $[0,t]$, it follows:

$$\left\|\boldsymbol{U}(t)\right\|_{\mathcal{E}}^2\leq\left\|\boldsymbol{U}(0)\right\|_{\mathcal{E}}^2-2\eta k^{-1}\left\|\dot{\boldsymbol{w}}\right\|_{\Omega_p}^2+2\int_0^t\left((\boldsymbol{f}_p,\dot{\boldsymbol{u}})_{\Omega_p}+(\boldsymbol{g}_p,\dot{\boldsymbol{w}})_{\Omega_p}+(\rho_a f_a,\dot{\varphi})_{\Omega_a}\right)d\tau.$$

Observe now that $\left\|\boldsymbol{U}(t)\right\|_{\mathcal{E}}^2\lesssim\left\|\boldsymbol{U}(t)\right\|_{\mathcal{E}}^2+2\eta k^{-1}\left\|\dot{\boldsymbol{w}}\right\|_{\Omega_p}^2$, so that:

$$\left\|\boldsymbol{U}(t)\right\|_{\mathcal{E}}^2\leq\left\|\boldsymbol{U}(0)\right\|_{\mathcal{E}}^2+2\int_0^t\left((\boldsymbol{f}_p,\dot{\boldsymbol{u}})_{\Omega_p}+(\boldsymbol{g}_p,\dot{\boldsymbol{w}})_{\Omega_p}+(\rho_a f_a,\dot{\varphi})_{\Omega_a}\right)d\tau. \tag{1.22}$$

By applying the Cauchy-Schwartz inequality, (1.22) is rewritten as:

$$\begin{aligned}\left\|\boldsymbol{U}(t)\right\|_{\mathcal{E}}^2\leq&\left\|\boldsymbol{U}(0)\right\|_{\mathcal{E}}^2\\&+2\int_0^t\left(\left\|\tilde{\rho}_s^{-1/2}\boldsymbol{f}_p\right\|_{\Omega_p}+\left\|\tilde{\rho}_w^{-1/2}\boldsymbol{g}_p\right\|_{\Omega_p}+\left\|c\rho_a^{1/2}\rho_a f_a\right\|_{\Omega_a}\right)\left\|\boldsymbol{U}(\tau)\right\|_{\mathcal{E}}d\tau,\end{aligned}$$

By employing Gronwall's lemma (see [66]), we obtain:

$$\left\|\boldsymbol{U}(t)\right\|_{\mathcal{E}}\leq\left\|\boldsymbol{U}(0)\right\|_{\mathcal{E}}+\int_0^t\left(\left\|\tilde{\rho}_s^{-1/2}\boldsymbol{f}_p\right\|_{\Omega_p}+\left\|\tilde{\rho}_w^{-1/2}\boldsymbol{g}_p\right\|_{\Omega_p}+\left\|c\rho_a^{1/2}f_a\right\|_{\Omega_a}\right)d\tau,$$

and the thesis follows. □

Chapter 2

The numerical model

2.1 Discrete setting

As in [4, 6, 7, 24, 25], the domains Ω_p and Ω_a are assumed to be polygonal and we introduce a *polytopic* mesh $\mathcal{T}_h$ of meshsize h over Ω. Meshsize is defined as $h = \max_{k\in\mathcal{T}_h} h_k$, with h_k diameter of every element $k \in \mathcal{T}_h$, whose measure is instead denoted with $|k|$. $\mathcal{T}_h$ is decomposed as follows:

$$\mathcal{T}_h = \mathcal{T}_h^p \cup \mathcal{T}_h^a,$$

where $\mathcal{T}_h^p = \{k \in \mathcal{T}_h : \overline{k} \subseteq \overline{\Omega}_p\}$ and $\mathcal{T}_h^a = \{k \in \mathcal{T}_h : \overline{k} \subseteq \overline{\Omega}_a\}$ denote poroelastic and acoustic polytopic meshes, respectively. The elements $k \in \mathcal{T}_h$ can be general polygons (in 2d) or polyhedra (in 3d).
Implicit in this decomposition there is the assumption that the meshes $\mathcal{T}_h^a$ and $\mathcal{T}_h^p$ are aligned with Ω_a and Ω_p, respectively. A polynomial degree is associated with each element of $\mathcal{T}_h^p$ and $\mathcal{T}_h^a$: $p_{p,k} \geq 1$ for the poroelastic domain and $p_{a,k} \geq 1$ for the acoustic one.
It has been moreover assumed that $\mathbb{C}$, ρ_a and βm are element-wise constant, respectively:

$$\begin{aligned}
&\overline{\mathbb{C}}_k = (|\mathbb{C}^{1/2}|_2^2)_{|k} && \forall k \in \mathcal{T}_h^p,\\
&\overline{\rho}_{a,k} = \rho_{a|k} && \forall k \in \mathcal{T}_h^a,\\
&(\overline{m})_{p,k} = (m)_{p|k} && \forall k \in \mathcal{T}_h^p.
\end{aligned}$$

The symbol $|\cdot|_2$ stands for the norm induced by the ℓ^2-norm on $\mathbb{R}^n$, where n is the dimension of the space of second-order symmetric tensors, so that $n = 3$ if $d = 2$ and $n = 6$ if $d = 3$.
Finite-dimensional subspaces are introduced as follows:

$$\boldsymbol{V}_h^p = [\mathcal{P}_{p_p}(\mathcal{T}_h^p)]^d = \{\boldsymbol{v}_h \in \boldsymbol{L}^2(\Omega_p) : \boldsymbol{v}_{h|k} \in [\mathcal{P}_{p_{p,k}}(k)]^d \ \ \forall k \in \mathcal{T}_h^p\}$$

$$V_h^a = \mathcal{P}_{p_a}(\mathcal{T}_h^a) = \{\psi_h \in L^2(\Omega_a) : \psi_{h|k} \in \mathcal{P}_{p_{a,k}}(k) \ \ \forall k \in \mathcal{T}_h^a\}$$

For an integer $l \geq 1$, we also define the broken Sobolev spaces as:

$$\boldsymbol{H}^l(\mathcal{T}_h^p) = \{\boldsymbol{v} \in \boldsymbol{L}^2(\Omega_p) : \boldsymbol{v}_{|k} \in \boldsymbol{H}^l(k) \ \ \forall k \in \mathcal{T}_h^p\}$$
$$H^l(\mathcal{T}_h^a) = \{\psi \in L^2(\Omega_a) : \psi_{|k} \in H^l(k) \ \ \forall k \in \mathcal{T}_h^a\}.$$

2.2 Grid assumptions

In order to deal with polygonal and polyhedral elements, mesh *interfaces* are introduced, intuitively defined as the intersection of the $(d-1)$-dimensional faces of two any neighbouring elements. It is important to stress the fact that the term *interface* here used, refers to interface of single elements and not to interface between poroelastic and acoustic domains, fact that will be discussed later on. A distinction between cases $d = 3$ and $d = 2$ is however needed:

- when $d = 3$, interface includes general polygons that could be moreover decomposed into a set of triangles, denoted by $\mathcal{F}_h$. This latter notation will be used for generally dealing with faces.
- when $d = 2$, concepts of interface and face are equivalent, since a line segment will be taken into account. Notation used will be again $\mathcal{F}_h$ to consider faces.

From now on, symbol $\mathcal{F}_h$ will then denote a set of $(d-1)$-dimensional simplices (lines or polygons).
We next introduce some notation to take into account interface between Ω_p and Ω_a. Let

$$\mathcal{T}_{h,I} = \{k \in \mathcal{T}_h : \partial k \cap \Gamma_I \neq \emptyset\}$$

denote the set of elements that share a part of their boundary with the interface Γ_I. Intuitively other two sets can be defined as follows:

$$\mathcal{T}_{h,I}^p = \mathcal{T}_{h,I} \cap \mathcal{T}_h^p,$$

$$\mathcal{T}_{h,I}^a = \mathcal{T}_{h,I} \cap \mathcal{T}_h^a.$$

These last two notation allow to split the polytopic mesh into poroelastic and acoustic parts. By defining by $\mathcal{F}_h$ the set of the faces of $\mathcal{T}_h$, we set:

$$\mathcal{F}_{h,I} = \{F \in \mathcal{F}_h : F \subset \partial k^p \cap \partial k^a, k^p \in \mathcal{T}_{h,I}^p, k^a \in \mathcal{T}_{h,I}^a\}.$$

By introducing $\mathcal{F}_h^p$ and $\mathcal{F}_h^a$, indicating all faces of $\mathcal{T}_h^p$ and $\mathcal{T}_h^a$ respectively not laying on Γ_I, $\mathcal{F}_h$ can be decomposed as:

$$\mathcal{F}_h = \mathcal{F}_h^p \cup \mathcal{F}_{h,I} \cup \mathcal{F}_h^a.$$

Finally, faces of $\mathcal{T}_h^p$ and $\mathcal{T}_h^a$ are written as the union of *internal* (i) and *boundary* (b) faces:

$$\mathcal{F}_h^p = \mathcal{F}_h^{p,i} \cup \mathcal{F}_h^{p,b},$$
$$\mathcal{F}_h^a = \mathcal{F}_h^{a,i} \cup \mathcal{F}_h^{a,b}.$$

We next introduce the main assumption on $\mathcal{T}_h$, as done in [5, 7, 25].

Definition 2.2.1. A mesh $\mathcal{T}_h$ is said to be *polytopic-regular* if $\forall\ k \in \mathcal{T}_h$, $\exists\ \{S_k^F\}_{F \subset \partial k}$ a set of non-overlapping d-dimensional simplices contained in k, *s.t.* $\forall\ F \subset \partial k$, the following condition holds:

$$h_k \lesssim \frac{d|S_k^F|}{|F|}. \tag{2.1}$$

Note that $\bigcup_{F \subset \partial k} \overline{S}_k^F \subseteq \overline{k}$, that reveals the fact that in general the union of simplices does not have to cover the whole element k. Moreover this definition does impose any restriction on either the number of faces per element or on their measure relative to the diameter of the element they belong to. This concept is confirmed by the fact that the hidden constant in equation (2.1) does not depend on discretization parameters, as introduced in Section 2.1. Moreover, it imposes a further condition on the choice of the size of a face $F \subseteq \partial k$: in fact $|F|$ could be arbitrarily small compared to h_k, if the same h_k and the height of the considered simplex are comparable. In Figure 2.1 two examples of elements of a *polytopic regular mesh* are shown: notice how triangles S_k^F have height comparable to the meshsize h_k. In particular, in Figure 2.1b it is shown an example of union of simplices non covering the whole element. This definition allows

(a) (b)

Figure 2.1: Examples of elements that satisfy the *polytopic regularity* assumption. In blue non-overlapping simplices (triangles)

thus to introduce the following assumption:

Assumption 2.2.1. The sequence of meshes $\{\mathcal{T}_h\}_m$ is assumed to be *uniformly polytopic regular*.

Under this assumption, the following *trace-inverse inequality* holds:

$$\forall\ k \in \mathcal{T}_h,\ \forall v \in \mathcal{P}_p(k), \qquad ||v||_{L^2(\partial k)} \lesssim p h_k^{-1/2} ||v||_{L^2(k)}, \tag{2.2}$$

where the hidden constant is independent of the discretization parameters. For more details on equation (2.2), see reference [66].

Definition 2.2.2. A *covering* $\mathcal{T}_{\#} = \{\mathcal{K}\}$ associated with the polytopic mesh $\mathcal{T}_h$ is a set of regular shaped d-dimensional simplices $\mathcal{K}$, s.t. $\forall\ k \in \mathcal{T}_h$, $\exists\ \mathcal{K} \in \mathcal{T}_{\#}$ s.t. $k \subsetneq \mathcal{K}$.

Assumption 2.2.2. There exists a covering $\mathcal{T}_{\#}$ of $\mathcal{T}_h$ and a positive constant C_Ω s.t.

$$\max_{k\in\mathcal{T}_k} \text{card}\{k' \in \mathcal{T}_h : k' \cap \mathcal{K} \neq \emptyset,\ \mathcal{K} \in \mathcal{T}_h^{\#} \text{s.t. } k \subset \mathcal{K}\} \leq C_\Omega$$

and $diam(\mathcal{K}) \lesssim h_k$ for each pair $k \in \mathcal{T}_h,\ \mathcal{K} \in \mathcal{T}_h^{\#}$, with $k \subset \mathcal{K}$.

Assumption 2.2.3. Let k^+ and k^- be two any neighbouring elements of $\mathcal{T}_h$. The following *hp-local bounded variation property* is assumed to hold for both meshsize and the polynomial degree:

$$h_{k^+} \lesssim h_{k^-} \lesssim h_{k^+}, \quad p_{k^+} \lesssim p_{k^-} \lesssim p_{k^+},$$

where hidden constants do not depend on the discretization parameters, the number of faces per element and the physical parameters.

2.3 Trace operators

In order to consider a dG-formulation of the semi-discrete problem, as in [9, 10, 62], the average and jump operators have to be introduced. These operators, at the center of the analysis and design of dG methods, are defined on faces, in particular both on *internal* and *boundary* faces. Averages and jumps for scalar, vector or tensor fields ψ, $\boldsymbol{v}$ and $\boldsymbol{\tau}$, respectively are defined on an *internal* face $F \in \mathcal{F}_h^{p,i} \cup \mathcal{F}_h^{a,i}$, $F \subset \partial k^+ \cup \partial k^-$, with k^+ and k^- neighbouring elements in $\mathcal{T}_h^p$ and $\mathcal{T}_h^a$, as follows:

$$\begin{aligned}
[\![\psi]\!] &= \psi^+ \boldsymbol{n}^+ + \psi^- \boldsymbol{n}^-, & \{\!\{\psi\}\!\} &= \frac{\psi^+ + \psi^-}{2}, \\
[\![\boldsymbol{v}]\!] &= \boldsymbol{v}^+ \otimes \boldsymbol{n}^+ + \boldsymbol{v}^- \otimes \boldsymbol{n}^-, & \{\!\{\boldsymbol{v}\}\!\} &= \frac{\boldsymbol{v}^+ + \boldsymbol{v}^-}{2}, \\
[\![\boldsymbol{\tau}]\!] &= \boldsymbol{\tau}^+ \boldsymbol{n}^+ + \boldsymbol{\tau}^- \boldsymbol{n}^-, & \{\!\{\boldsymbol{\tau}\}\!\} &= \frac{\boldsymbol{\tau}^+ + \boldsymbol{\tau}^-}{2},
\end{aligned}$$

where $\boldsymbol{a} \otimes \boldsymbol{b}$ denotes the tensor product of $\boldsymbol{a}, \boldsymbol{b} \in \mathbb{R}^3$, $\cdot^\pm$ is the trace of the scalar, vector or tensor element on F, taken from the interior of $k^\pm$ and $\boldsymbol{n}^\pm$ is the outer unit normal to $\partial k^\pm$, respectively.
Accordingly, on *boundary* faces $F \in \mathcal{F}_h^{p,b} \cup \mathcal{F}_h^{a,b}$, averages and jumps are defined:

$$\begin{aligned}
[\![\psi]\!] &= \psi \boldsymbol{n}, & \{\!\{\psi\}\!\} &= \psi, \\
[\![\boldsymbol{v}]\!] &= \boldsymbol{v} \otimes \boldsymbol{n}, & \{\!\{\boldsymbol{v}\}\!\} &= \boldsymbol{v}, \\
[\![\boldsymbol{\tau}]\!] &= \boldsymbol{\tau} \boldsymbol{n}, & \{\!\{\boldsymbol{\tau}\}\!\} &= \boldsymbol{\tau}.
\end{aligned}$$

2.4 Semi-discrete problem

The semi-discrete dG formulation reads:
For any time $t \in [0,T]$, find $(\boldsymbol{u}_h, \boldsymbol{w}_h, \varphi_h) \in C^2([0,T]; \boldsymbol{V}_h^p) \times C^2([0,T]; \boldsymbol{V}_h^p) \times C^2([0,T]; V_h^a)$, s.t. for all $(\boldsymbol{v}_h, \boldsymbol{\xi}_h, \psi_h) \in \boldsymbol{V}_h^p \times \boldsymbol{V}_h^p \times V_h^a$,

$$\begin{aligned}
&(\rho \ddot{\boldsymbol{u}}_h, \boldsymbol{v}_h)_{\Omega_p} + (\rho_f \ddot{\boldsymbol{w}}_h, \boldsymbol{v}_h)_{\Omega_p} + \mathcal{A}_h^p(\boldsymbol{u}_h, \boldsymbol{v}_h) \\
&\quad + \mathcal{B}_h^p(\beta \boldsymbol{u}_h + \boldsymbol{w}_h, \beta \boldsymbol{v}_h) + \mathcal{C}_{h,p}(\varphi_h, \boldsymbol{v}_h) \\
&+ (\rho_f \ddot{\boldsymbol{u}}_h, \boldsymbol{\xi}_h)_{\Omega_p} + (\rho_w \ddot{\boldsymbol{w}}_h, \boldsymbol{\xi}_h)_{\Omega_p} + \eta k^{-1} (\dot{\boldsymbol{w}}_h, \boldsymbol{\xi}_h)_{\Omega_p} \\
&\quad + \mathcal{B}_h^p(\beta \boldsymbol{u}_h + \boldsymbol{w}_h, \boldsymbol{\xi}_h) + k_{int} \mathcal{C}_{h,p}(\varphi_h, \boldsymbol{\xi}_h) \\
&+ (\rho_a c^{-2} \ddot{\varphi}_h, \psi_h)_{\Omega_a} + \mathcal{A}_h^a(\varphi_h, \psi_h) + \mathcal{C}_{h,a}(\boldsymbol{u}_h, \psi_h) + k_{int} \mathcal{C}_{h,a}(\boldsymbol{w}_h, \psi_h) \\
&\quad = (\boldsymbol{f}_p, \boldsymbol{v}_h)_{\Omega_p} + (\boldsymbol{g}_p, \boldsymbol{\xi}_h)_{\Omega_p} + (\rho_a f_a, \psi_h)_{\Omega_a}.
\end{aligned} \tag{2.3}$$

The bilinear forms appearing in (2.3) are defined as:

$$\begin{aligned}
\mathcal{A}_h^p(\boldsymbol{u}, \boldsymbol{v}) =& (\boldsymbol{\sigma}_h(\boldsymbol{u}), \boldsymbol{\epsilon}_h(\boldsymbol{v}))_{\Omega_p} - \langle \{\!\{ \boldsymbol{\sigma}_h(\boldsymbol{u}) \}\!\}, [\![\boldsymbol{v}]\!] \rangle_{\mathcal{F}_h^p} \\
&+ \theta \langle [\![\boldsymbol{u}]\!], \{\!\{ \boldsymbol{\sigma}_h(\boldsymbol{v}) \}\!\} \rangle_{\mathcal{F}_h^p} + \langle \eta [\![\boldsymbol{u}]\!], [\![\boldsymbol{v}]\!] \rangle_{\mathcal{F}_h^p}, \qquad \forall\, (\boldsymbol{u}, \boldsymbol{v}) \in \boldsymbol{V}_h^p,
\end{aligned}$$

$$\begin{aligned}
\mathcal{B}_h^p(\boldsymbol{u}, \boldsymbol{v}) =& (m \nabla_h \cdot \boldsymbol{u}, \nabla_h \cdot \boldsymbol{v})_{\Omega_p} - \langle \{\!\{ m(\nabla_h \cdot \boldsymbol{u}) \boldsymbol{I} \}\!\}, [\![\boldsymbol{v}]\!] \rangle_{\mathcal{F}_h^p} \\
&+ \theta \langle [\![\boldsymbol{u}]\!], \{\!\{ m(\nabla_h \cdot \boldsymbol{v}) \boldsymbol{I} \}\!\} \rangle_{\mathcal{F}_h^p} + \langle \gamma [\![\boldsymbol{u}]\!], [\![\boldsymbol{v}]\!] \rangle_{\mathcal{F}_h^p}, \qquad \forall\, (\boldsymbol{u}, \boldsymbol{v}) \in \boldsymbol{V}_h^p,
\end{aligned}$$

$$\begin{aligned}
\mathcal{A}_h^a(\varphi, \psi) =& (\rho_a \nabla_h \varphi, \nabla_h \psi)_{\Omega_a} - \langle \{\!\{ \rho_a \nabla_h \varphi \}\!\}, [\![\psi]\!] \rangle_{\mathcal{F}_h^a} \\
&+ \theta \langle [\![\varphi]\!], \{\!\{ \rho_a \nabla_h \psi \}\!\} \rangle_{\mathcal{F}_h^a} + \langle \chi [\![\varphi]\!], [\![\psi]\!] \rangle_{\mathcal{F}_h^a}, \qquad \forall\, (\varphi, \psi) \in V_h^a,
\end{aligned}$$

$$\begin{aligned}
\mathcal{C}_{h,p}^1(\varphi, \boldsymbol{v}) &= \langle \rho_a \dot{\varphi} \boldsymbol{n}_p, \boldsymbol{v} \rangle_{\mathcal{F}_{h,I}}, \qquad && \forall\, (\varphi, \boldsymbol{v}) \in V_h^a \times \boldsymbol{V}_h^p, \\
\mathcal{C}_{h,a}^1(\boldsymbol{u}, \psi) &= \langle -\rho_a \dot{\boldsymbol{u}} \cdot \boldsymbol{n}_p, \psi \rangle_{\mathcal{F}_{h,I}}, && \forall\, (\boldsymbol{u}, \psi) \in \boldsymbol{V}_h^p \times V_h^a,
\end{aligned} \tag{2.4}$$

where ∇_h is the broken gradient on $\mathcal{T}_h$ and operators $\boldsymbol{\epsilon}_h$ and $\boldsymbol{\sigma}_h$ are defined as follows:

$$\boldsymbol{\epsilon}_h(\boldsymbol{v}) = \frac{\nabla_h \boldsymbol{v} + \nabla_h \boldsymbol{v}^T}{2},$$

$$\boldsymbol{\sigma}_h(\boldsymbol{v}) = \mathbb{C} : \boldsymbol{\epsilon}_h(\boldsymbol{v}).$$

We remark that the bilinear forms appearing in (2.4) take into account interface terms, differently from previous ones introduced in Section 1.6. DG operators have been here used as in [62], by extending integration by parts to dG framework. In particular, it

has been chosen to consider a *Symmetric Interior Penalty Galerkin* (SIPG) method [8, 76], by considering $\theta = -1$. Other methods are suitable, such as the *Non-symmetric Interior Penalty Galerkin* (NIPG) [63], with $\theta = 1$ and the *Incomplete Interior Penalty Galerkin* (IIPG) methods, $\theta = 0$ [29].

We also point out that in (2.4) we have used the short-hand notation $(\cdot,\cdot)_\Omega$ and $\langle\cdot,\cdot\rangle_{\mathcal{F}_h}$ in place of the sum all over the triangulation and faces, respectively, i.e.: $(\cdot,\cdot)_\Omega = \sum_{K\in\mathcal{T}_h}\int_K \cdot$ and $\langle\cdot,\cdot\rangle_{\mathcal{F}_h} = \sum_{F\in\mathcal{F}_h}\int_F \cdot$.

The stabilization functions $\eta \in L^\infty(\mathcal{F}_h^p)$ and $\gamma \in L^\infty(\mathcal{F}_h^p)$ appearing in (2.4) for the poroelastic part and $\chi \in L^\infty(\mathcal{F}_h^a)$ for the acoustic one, are defined as follows:

$$\eta|_F = \begin{cases} c_1 \max\limits_{k\in\{k^+,k^-\}} \left(\dfrac{\overline{\mathbb{C}}_k\ p_{p,k}^2}{h_k}\right) & \forall F \in \mathcal{F}_h^{p,i}, \quad F \subseteq \partial k^+ \cap \partial k^- \\ \dfrac{\overline{\mathbb{C}}_k\ p_{p,k}^2}{h_k} & \forall F \in \mathcal{F}_h^{p,b}, \quad F \subseteq \partial k \end{cases} \tag{2.5}$$

$$\gamma|_F = \begin{cases} c_2 \max\limits_{k\in\{k^+,k^-\}} \left(\dfrac{\overline{m}_k\ p_{p,k}^2}{h_k}\right) & \forall F \in \mathcal{F}_h^{p,i}, \quad F \subseteq \partial k^+ \cap \partial k^- \\ \dfrac{\overline{m}_k\ p_{p,k}^2}{h_k} & \forall F \in \mathcal{F}_h^{p,b}, \quad F \subseteq \partial k \end{cases} \tag{2.6}$$

$$\chi|_F = \begin{cases} c_3 \max\limits_{k\in\{k^+,k^-\}} \left(\dfrac{\overline{\rho}_{a,k}\ p_{a,k}^2}{h_k}\right) & \forall F \in \mathcal{F}_h^{a,i}, \quad F \subseteq \partial k^+ \cap \partial k^- \\ \dfrac{\overline{\rho}_{a,k}\ p_{a,k}^2}{h_k} & \forall F \in \mathcal{F}_h^{a,b}, \quad F \subseteq \partial k, \end{cases} \tag{2.7}$$

with $c_1,\ c_2,\ c_3 > 0$ positive constants, to be properly chosen.
We next introduce the following norms:

$$\begin{aligned}
\|\boldsymbol{v}\|_{\mathrm{dG,e}}^2 &= \left\|\mathbb{C}^{1/2}\boldsymbol{\epsilon}_h(\boldsymbol{v})\right\|_{\Omega_p}^2 + \left\|\eta^{1/2}[\![\boldsymbol{v}]\!]\right\|_{\mathcal{F}_h^p}^2, && \forall\ \boldsymbol{v} \in \boldsymbol{H}^1(\mathcal{T}_h^p) \supset \boldsymbol{V}_h^p, \\
|||\boldsymbol{v}|||_{\mathrm{dG,e}}^2 &= \|\boldsymbol{v}\|_{\mathrm{dG,e}}^2 + \left\|\eta^{-1/2}\{\!\{\mathbb{C} : \boldsymbol{\epsilon}_h(\boldsymbol{v})\}\!\}\right\|_{\mathcal{F}_h^p}^2, && \forall\ \boldsymbol{v} \in \boldsymbol{H}^2(\mathcal{T}_h^p), \\
\|\psi\|_{\mathrm{dG,a}}^2 &= \left\|\rho_a^{1/2}\nabla_h\psi\right\|_{\Omega_a}^2 + \left\|\chi^{1/2}[\![\psi]\!]\right\|_{\mathcal{F}_h^a}^2, && \forall\ \psi \in H^1(\mathcal{T}_h^a) \supset V_h^a, \\
|||\psi|||_{\mathrm{dG,a}}^2 &= \|\psi\|_{\mathrm{dG,a}}^2 + \left\|\chi^{-1/2}\{\!\{\rho_a\nabla_h\psi\}\!\}\right\|_{\mathcal{F}_h^a}^2, && \forall\ \psi \in H^2(\mathcal{T}_h^a), \\
\|\boldsymbol{z}\|_{\mathrm{dG,p}}^2 &= \left\|m^{1/2}\nabla_h\cdot\boldsymbol{z}\right\|_{\Omega_p}^2 + \left\|\gamma^{1/2}[\![\boldsymbol{z}]\!]\right\|_{\mathcal{F}_h^p}^2, && \forall\ \boldsymbol{z} \in \boldsymbol{H}^1(\mathcal{T}_h^p) \supset \boldsymbol{V}_h^p,
\end{aligned}$$

$$|||\boldsymbol{z}|||^2_{\mathrm{dG,p}} = \|\boldsymbol{z}\|^2_{\mathrm{dG,p}} + \left\|\gamma^{-1/2}\{\!\{(\nabla_h \cdot \boldsymbol{z})\boldsymbol{I}\}\!\}\right\|^2_{\mathcal{F}_h^p}, \qquad \forall\ \boldsymbol{z} \in \boldsymbol{H}^2(\mathcal{T}_h^p).$$

The following results follow based on employing standard arguments [6, 7, 62].

Lemma 1 (Coercivity and boundedness of $\mathcal{A}_h^p$, $\mathcal{A}_h^a$ and $\mathcal{B}_h^p$)**.** *Provided that $\mathcal{T}_h$ satisfies Assumptions 2.2.1, 2.2.2 and 2.2.3 and that c_1, c_2 and c_3 in (2.5), (2.6) and (2.7), respectively, are chosen sufficiently large, the following continuity and coercivity bounds hold:*

$$\begin{aligned}
&\mathcal{A}_h^p(\boldsymbol{u},\boldsymbol{v}) \lesssim \|\boldsymbol{u}\|_{\mathrm{dG,e}}\,\|\boldsymbol{v}\|_{\mathrm{dG,e}}\,, && \forall\ \boldsymbol{u},\boldsymbol{v} \in \boldsymbol{V}_h^p,\\
&\mathcal{A}_h^p(\boldsymbol{u},\boldsymbol{u}) \gtrsim \|\boldsymbol{u}\|^2_{\mathrm{dG,e}}\,, && \forall\ \boldsymbol{u} \in \boldsymbol{V}_h^p,\\
&\mathcal{A}_h^a(\varphi,\psi) \lesssim \|\varphi\|_{\mathrm{dG,a}}\,\|\psi\|_{\mathrm{dG,a}}\,, && \forall\ \varphi,\psi \in V_h^a,\\
&\mathcal{A}_h^a(\varphi,\varphi) \gtrsim \|\varphi\|^2_{\mathrm{dG,a}}\,, && \forall\ \varphi \in V_h^a,\\
&\mathcal{B}_h^p(\boldsymbol{w},\boldsymbol{z}) \lesssim \|\boldsymbol{w}\|_{\mathrm{dG,p}}\,\|\boldsymbol{z}\|_{\mathrm{dG,p}}\,, && \forall\ \boldsymbol{w},\boldsymbol{z} \in \boldsymbol{V}_h^p,\\
&\mathcal{B}_h^p(\boldsymbol{w},\boldsymbol{w}) \gtrsim \|\boldsymbol{w}\|^2_{\mathrm{dG,p}}\,, && \forall\ \boldsymbol{w} \in \boldsymbol{V}_h^p.
\end{aligned}$$

Moreover

$$\begin{aligned}
&\mathcal{A}_h^p(\boldsymbol{u},\boldsymbol{v}) \lesssim |||\boldsymbol{u}|||_{\mathrm{dG,e}}\,\|\boldsymbol{v}\|_{\mathrm{dG,e}}\,, && \forall\ \boldsymbol{u},\boldsymbol{v} \in \boldsymbol{H}^2(\mathcal{T}_h^p) \times \boldsymbol{V}_h^p,\\
&\mathcal{A}_h^a(\varphi,\psi) \lesssim |||\varphi|||_{\mathrm{dG,a}}\,\|\psi\|_{\mathrm{dG,a}}\,, && \forall\ \varphi,\psi \in H^2(\mathcal{T}_h^a) \times \boldsymbol{V}_h^a,\\
&\mathcal{B}_h^p(\boldsymbol{w},\boldsymbol{z}) \lesssim |||\boldsymbol{w}|||_{\mathrm{dG,p}}\,\|\boldsymbol{z}\|_{\mathrm{dG,p}}\,, && \forall\ \boldsymbol{w},\boldsymbol{z} \in \boldsymbol{H}^2(\mathcal{T}_h^p) \times \boldsymbol{V}_h^p.
\end{aligned}$$

The proof of the above results are based on arguments along the same lines as in the proof of Lemma 3 of Section 2.5.

2.5 Stability of the semi-discrete formulation

In order to prove the stability of the semi-discrete problem, we introduce the following norms that will be used in the following analysis. Let $(\boldsymbol{v},\boldsymbol{z},\psi) \in C^1([0,T];\boldsymbol{V}_h^p) \times C^1([0,T];\boldsymbol{V}_h^p)) \times C^1([0,T];V_h^a)$, we define the following mesh dependent energy norm:

$$\|(\boldsymbol{v},\boldsymbol{z},\psi)\|^2_{\mathcal{E}} = \|\boldsymbol{v}\|^2_{\mathcal{E},e} + \|\beta\boldsymbol{v}+\boldsymbol{z}\|^2_{\mathcal{E},p} + \|\psi\|^2_{\mathcal{E},a}\,, \tag{2.8}$$

where:

$$\|\boldsymbol{v}\|^2_{\mathcal{E},e} = \left\|\tilde{\rho}_s^{1/2}\dot{\boldsymbol{v}}\right\|^2_{\Omega_p} + \|\boldsymbol{v}\|^2_{\mathrm{dG,e}}\,, \tag{2.9}$$

$$\|\beta\boldsymbol{v}+\boldsymbol{z}\|^2_{\mathcal{E},p} = \|\beta\boldsymbol{v}+\boldsymbol{z}\|^2_{\mathrm{dG,p}} + \left\|\rho_f^{1/2}\left(\phi^{1/2}\dot{\boldsymbol{v}} + \phi^{-1/2}\dot{\boldsymbol{z}}\right)\right\|^2_{\Omega_p} + \|\tilde{\rho}_w\dot{\boldsymbol{z}}\|^2_{\Omega_p}\,, \tag{2.10}$$

$$\|\psi\|^2_{\mathcal{E},a} = \left\|c^{-1}\rho_a^{1/2}\dot{\psi}\right\|^2_{\Omega_a} + \|\psi\|^2_{\mathrm{dG,a}}\,. \tag{2.11}$$

Before stating the main result of this section (i.e. the stability of the numerical solution), the following lemmas, that will be used in the sequel, have been introduced.

Lemma 2. *The following bounds hold:*

$$\left\|\eta^{-1/2}\{\!\{\boldsymbol{\sigma}_h(\boldsymbol{v})\}\!\}\right\|_{\mathcal{F}_h^p} \lesssim \frac{1}{\sqrt{c_1}}\left\|\mathbb{C}^{1/2}\boldsymbol{\epsilon}_h(\boldsymbol{v})\right\|_{\Omega_p}, \qquad \forall \boldsymbol{v}\in \boldsymbol{V}_h^p, \tag{2.12}$$

$$\left\|\chi^{-1/2}\{\!\{\rho_a\nabla_h\psi\}\!\}\right\|_{\mathcal{F}_h^a} \lesssim \frac{1}{\sqrt{c_2}}\left\|\rho_a^{1/2}\nabla_h\psi\right\|_{\Omega_a}, \qquad \forall \psi\in V_h^a, \tag{2.13}$$

$$\left\|\gamma^{-1/2}m\{\!\{(\nabla_h\cdot\boldsymbol{z})I\}\!\}\right\|_{\mathcal{F}_h^p} \lesssim \frac{1}{\sqrt{c_3}}\left\|m^{1/2}\nabla_h\cdot\boldsymbol{z}\right\|_{\Omega_p}, \qquad \forall \boldsymbol{z}\in \boldsymbol{V}_h^p, \tag{2.14}$$

where c_1, c_2 and c_3 are the stability parameters appearing in (2.5),(2.6) and (2.7), respectively.

Proof. By taking into account that for simplices it holds the trace-inverse inequality, a simplex $T\subset\mathbb{R}^d$ and a polynomial degree $p\geq 1$ are considered. Indeed, it holds that, for all $v\in\mathcal{P}_p(T)$:

$$\|v\|_F^2 \lesssim p^2\frac{|F|}{|T|}\|v\|_T^2\,.$$

Moreover by the definition of $\overline{\mathbb{C}}_k$ and η and Assumption 2.2.1, it follows:

$$\begin{aligned}\left\|\eta^{-1/2}\{\!\{\boldsymbol{\sigma}_h(\boldsymbol{v})\}\!\}\right\|^2_{\mathcal{F}_h^p} &\leq \sum_{k\in\mathcal{T}_h^p}\sum_{F\subset\partial k}\overline{\mathbb{C}}_k\left\|\eta^{-1/2}\mathbb{C}^{1/2}\boldsymbol{\epsilon}_h(\boldsymbol{v})\right\|^2_F\\ &\leq \sum_{k\in\mathcal{T}_h^p}\sum_{F\subset\partial k}\eta^{-1}\overline{\mathbb{C}}_k p_{p,k}^2\frac{|F|}{|k_\flat^F|}\left\|\mathbb{C}^{1/2}\boldsymbol{\epsilon}_h(\boldsymbol{v})\right\|^2_{k_\flat^F}\\ &\lesssim \frac{1}{c_1}\left\|\mathbb{C}^{1/2}\boldsymbol{\epsilon}_h(\boldsymbol{v})\right\|^2_{\Omega_p}.\end{aligned}$$

Proofs of (2.13) and (2.14) are analogous to the proof of (2.12). □

Lemma 3. *For any $\boldsymbol{u}_h\in C^1([0,T];\boldsymbol{V}_h^p)$, $\boldsymbol{z}_h\in C^1([0,T];\boldsymbol{V}_h^p)$ and $\varphi_h\in C^1([0,T];V_h^a)$, it holds:*

$$\|\boldsymbol{u}_h\|^2_{\mathcal{E},e} \lesssim \|\boldsymbol{u}_h\|^2_{\mathcal{E},e} - 2\langle\{\!\{\boldsymbol{\sigma}_h(\boldsymbol{u}_h)\}\!\},[\![\boldsymbol{u}_h]\!]\rangle_{\mathcal{F}_h^p} \lesssim \|\boldsymbol{u}_h\|^2_{\mathcal{E},e}\,, \tag{2.15}$$

$$\|\varphi_h\|^2_{\mathcal{E},a} \lesssim \|\varphi_h\|^2_{\mathcal{E},a} - 2\langle\{\!\{\nabla_h\varphi_h\}\!\},[\![\varphi_h]\!]\rangle_{\mathcal{F}_h^a} \lesssim \|\varphi_h\|^2_{\mathcal{E},a}\,, \tag{2.16}$$

$$\|\boldsymbol{z}_h\|^2_{\mathrm{dG,p}} \lesssim \|\boldsymbol{z}_h\|^2_{\mathrm{dG,p}} - 2m\langle\{\!\{(\nabla_h\cdot\boldsymbol{z}_h\boldsymbol{I})\}\!\},[\![\boldsymbol{z}_h]\!]\rangle_{\mathcal{F}_h^p} \lesssim \|\boldsymbol{z}_h\|^2_{\mathrm{dG,p}}\,, \tag{2.17}$$

provided that the penalization constants c_1, c_2 and c_3 appearing in equations (2.5), (2.6) and (2.7) are chosen sufficiently large.

Proof. For the proof of (2.15) and (2.16) see [6], Lemma A.2.
Concerning (2.17), it holds

$$\|\boldsymbol{z}_h\|^2_{\mathrm{dG,p}} - 2m\langle \{\!\{(\nabla_h \cdot \boldsymbol{z}_h)\boldsymbol{I}\}\!\}, [\![\boldsymbol{z}_h]\!]\rangle_{\mathcal{F}_h^p} \lesssim \|\boldsymbol{z}_h\|^2_{\mathrm{dG,p}}$$

by the Cauchy-Schwarz inequality, the definition of $\|\cdot\|^2_{\mathrm{dG,p}}$ and Lemma 2. Indeed,

$$\begin{aligned}
&\|\boldsymbol{z}_h\|^2_{\mathrm{dG,p}} - 2m\langle \{\!\{(\nabla_h \cdot \boldsymbol{z}_h)\boldsymbol{I}\}\!\}, [\![\boldsymbol{z}_h]\!]\rangle_{\mathcal{F}_h^p} \\
\lesssim &\|\boldsymbol{z}_h\|^2_{\mathrm{dG,p}} + \left\| m\gamma^{-1/2} \{\!\{(\nabla_h \cdot \boldsymbol{z}_h)\boldsymbol{I}\}\!\} \right\|_{\mathcal{F}_h^p} \left\| \gamma^{1/2} [\![\boldsymbol{z}_h]\!] \right\|_{\mathcal{F}_h^p} \\
\lesssim &\|\boldsymbol{z}_h\|^2_{\mathrm{dG,p}} + \frac{1}{\sqrt{c_2}} \left\| m^{1/2} \nabla_h \cdot \boldsymbol{z}_h \right\|_{\Omega_p} \|\boldsymbol{z}_h\|_{\mathrm{dG,p}} \lesssim \|\boldsymbol{z}_h\|^2_{\mathrm{dG,p}}\,.
\end{aligned}$$

To prove the second bound, we observe that, for any $\delta > 0$

$$\begin{aligned}
\langle m\{\!\{(\nabla_h \cdot \boldsymbol{z}_h)\boldsymbol{I}\}\!\}, [\![\boldsymbol{z}_h]\!]\rangle_{\mathcal{F}_h^p} \leq &\sum_{F \in \mathcal{F}_h^p} \left\| \gamma^{-1/2} m \{\!\{(\nabla_h \cdot \boldsymbol{z}_h)\boldsymbol{I}\}\!\} \right\|_F \left\| \gamma^{1/2} [\![\boldsymbol{z}_h]\!] \right\|_F \\
\leq &\frac{1}{2\delta} \left\| \gamma^{-1/2} m \{\!\{(\nabla_h \cdot \boldsymbol{z}_h)\boldsymbol{I}\}\!\} \right\|^2_{\mathcal{F}_h^p} + \frac{\delta}{2} \left\| \gamma^{1/2} [\![\boldsymbol{z}_h]\!] \right\|^2_{\mathcal{F}_h^p}.
\end{aligned}$$

Hence, from the definition of the norm $\|\cdot\|_{\mathrm{dG,p}}$ on $\boldsymbol{V}_h^p$, it follows that:

$$\begin{aligned}
&\|\boldsymbol{z}_h\|^2_{\mathrm{dG,p}} - 2m\langle \{\!\{(\nabla_h \cdot \boldsymbol{z}_h \boldsymbol{I})\}\!\}, [\![\boldsymbol{z}_h]\!]\rangle_{\mathcal{F}_h^p} \\
\gtrsim &\left\| m^{1/2} \nabla_h \cdot \boldsymbol{z}_h \right\|^2_{\Omega_p} + (1-\delta) \left\| \gamma^{1/2} [\![\boldsymbol{z}_h]\!] \right\|^2_{\mathcal{F}_h^p} - \frac{1}{\delta} \left\| \gamma^{-1/2} m \{\!\{(\nabla_h \cdot \boldsymbol{z}_h)\boldsymbol{I}\}\!\} \right\|^2_{\mathcal{F}_h^p} \\
\gtrsim &\left(1 - \frac{C}{c_3 \delta}\right) \left\| m^{1/2} \nabla_h \cdot \boldsymbol{z}_h \right\|^2_{\Omega_p} + (1-\delta) \left\| \gamma^{1/2} [\![\boldsymbol{z}_h]\!] \right\|^2_{\mathcal{F}_h^p}.
\end{aligned}$$

Then, choosing $\delta = \frac{1}{2}$ and $c_3 = 4C$, the thesis follows. □

The main result can be therefore stated through the following theorem.

Theorem 3 (Stability of the semi-discrete formulation)**.** *For any $t \in (0, T]$, let $(\boldsymbol{u}_h, \boldsymbol{w}_h, \varphi_h)$ be the solution of (2.3). Let Assumptions 2.2.1, 2.2.2 and 2.2.3 on $\mathcal{T}_h$ be satisfied. For sufficiently large penalty parameter c_1, c_2 and c_3 in (2.5), (2.6) and (2.7), respectively, the following bound holds*

$$\|\boldsymbol{U}_h(t)\|_{\mathcal{E}} \lesssim \|\boldsymbol{U}_h(0)\|_{\mathcal{E}} + \int_0^t \left(\left\| \tilde{\rho}_s^{-1/2} \boldsymbol{f}_p \right\|_{\Omega_p} + \left\| \tilde{\rho}_w^{-1/2} \boldsymbol{g}_p \right\|_{\Omega_p} + \left\| c \rho_a^{1/2} f_a \right\|_{\Omega_a} \right) d\tau,$$

where $U_h(t) = (\boldsymbol{u}_h, \boldsymbol{w}_h, \varphi_h)$.

Proof. By taking in (2.3) test functions $(\boldsymbol{v}_h, \boldsymbol{\xi}_h, \psi_h)$ equal to $(\dot{\boldsymbol{u}}_h, \dot{\boldsymbol{w}}_h, \dot{\varphi}_h)$, it follows:

$$(\rho \ddot{\boldsymbol{u}}_h, \dot{\boldsymbol{u}}_h)_{\Omega_p} + (\rho_f \ddot{\boldsymbol{w}}_h, \dot{\boldsymbol{u}}_h)_{\Omega_p} + \mathcal{A}_h^p(\boldsymbol{u}_h, \dot{\boldsymbol{u}}_h)$$

$$
\begin{aligned}
&+ \mathcal{B}_h^p(\beta \boldsymbol{u}_h + \boldsymbol{w}_h, \beta \dot{\boldsymbol{u}}_h) + \mathcal{C}_{h,p}(\varphi_h, \dot{\boldsymbol{u}}_h) \\
&+ (\rho_f \ddot{\boldsymbol{u}}_h, \dot{\boldsymbol{w}}_h)_{\Omega_p} + (\rho_w \ddot{\boldsymbol{w}}_h, \dot{\boldsymbol{w}}_h)_{\Omega_p} + \eta k^{-1} (\dot{\boldsymbol{w}}_h, \dot{\boldsymbol{w}}_h)_{\Omega_p} \\
&+ \mathcal{B}_h^p(\beta \boldsymbol{u}_h + \boldsymbol{w}_h, \dot{\boldsymbol{w}}_h) + k_{int} \mathcal{C}_{h,p}(\varphi_h, \dot{\boldsymbol{w}}_h) \\
&+ (\rho_a c^{-2} \ddot{\varphi}_h, \dot{\varphi}_h)_{\Omega_a} + \mathcal{A}_h^a(\varphi_h, \dot{\varphi}_h) + \mathcal{C}_{h,a}(\boldsymbol{u}_h, \dot{\varphi}_h) + k_{int} \mathcal{C}_{h,a}(\boldsymbol{w}_h, \dot{\varphi}_h) \\
&= (\boldsymbol{f}_p, \dot{\boldsymbol{u}}_h)_{\Omega_p} + (\boldsymbol{g}_p, \dot{\boldsymbol{w}}_h)_{\Omega_p} + (\rho_a f_a, \dot{\varphi}_h)_{\Omega_a}.
\end{aligned}
$$

Using the definition of the bilinear forms A_h^p, A_h^a and B_h^p the skew-symmetry of the coupling bilinear forms, we obtain:

$$
\begin{aligned}
&(\rho \ddot{\boldsymbol{u}}_h, \dot{\boldsymbol{u}}_h)_{\Omega_p} + (\rho_f \ddot{\boldsymbol{w}}_h, \dot{\boldsymbol{u}}_h)_{\Omega_p} \\
&+ (\boldsymbol{\sigma}_h(\boldsymbol{u}_h), \boldsymbol{\epsilon}_h(\dot{\boldsymbol{u}}_h))_{\Omega_p} - \langle \{\!\{ \boldsymbol{\sigma}_h(\boldsymbol{u}_h) \}\!\}, [\![\dot{\boldsymbol{u}}_h]\!] \rangle_{\mathcal{F}_h^p} - \langle [\![\boldsymbol{u}_h]\!], \{\!\{ \boldsymbol{\sigma}_h(\dot{\boldsymbol{u}}_h) \}\!\} \rangle_{\mathcal{F}_h^p} + \langle \eta [\![\boldsymbol{u}_h]\!], [\![\dot{\boldsymbol{u}}_h]\!] \rangle_{\mathcal{F}_h^p} \\
&+ (m \nabla_h \cdot (\beta \boldsymbol{u}_h + \boldsymbol{w}_h), \beta \nabla_h \cdot \dot{\boldsymbol{u}}_h)_{\Omega_p} - \langle m \{\!\{ (\nabla_h \cdot (\beta \boldsymbol{u}_h + \boldsymbol{w}_h)) \boldsymbol{I} \}\!\}, [\![\beta \dot{\boldsymbol{u}}_h]\!] \rangle_{\mathcal{F}_h^p} \\
&- \langle m [\![\beta \boldsymbol{u}_h + \boldsymbol{w}_h]\!], \{\!\{ (\beta \nabla_h \cdot \dot{\boldsymbol{u}}_h) \boldsymbol{I} \}\!\} \rangle_{\mathcal{F}_h^p} + \langle \gamma [\![\beta \boldsymbol{u}_h + \boldsymbol{w}_h]\!], [\![\beta \dot{\boldsymbol{u}}_h]\!] \rangle_{\mathcal{F}_h^p} \\
&+ (\rho_f \ddot{\boldsymbol{u}}_h, \dot{\boldsymbol{w}}_h)_{\Omega_p} + (\rho_w \ddot{\boldsymbol{w}}_h, \dot{\boldsymbol{w}}_h)_{\Omega_p} + \eta k^{-1} (\dot{\boldsymbol{w}}_h, \dot{\boldsymbol{w}}_h)_{\Omega_p} \\
&+ (m \nabla_h \cdot (\beta \boldsymbol{u}_h + \boldsymbol{w}_h), \nabla_h \cdot \dot{\boldsymbol{w}}_h)_{\Omega_p} - \langle m \{\!\{ (\nabla_h \cdot (\beta \boldsymbol{u}_h + \boldsymbol{w}_h)) \boldsymbol{I} \}\!\}, [\![\dot{\boldsymbol{w}}_h]\!] \rangle_{\mathcal{F}_h^p} \\
&- \langle m [\![\beta \boldsymbol{u}_h + \boldsymbol{w}_h]\!], \{\!\{ (\nabla_h \cdot \dot{\boldsymbol{w}}_h) \boldsymbol{I} \}\!\} \rangle_{\mathcal{F}_h^p} + \langle \gamma [\![\beta \boldsymbol{u}_h + \boldsymbol{w}_h]\!], [\![\dot{\boldsymbol{w}}_h]\!] \rangle_{\mathcal{F}_h^p} \\
&+ (\rho_a c^{-2} \ddot{\varphi}_h, \dot{\varphi}_h)_{\Omega_a} + (\rho_a \nabla_h \varphi_h, \nabla_h \dot{\varphi}_h)_{\Omega_a} - \langle \{\!\{ \rho_a \nabla_h \varphi_h \}\!\}, [\![\dot{\varphi}_h]\!] \rangle_{\mathcal{F}_h^a} \\
&- \langle [\![\varphi_h]\!], \{\!\{ \rho_a \nabla_h \dot{\varphi}_h \}\!\} \rangle_{\mathcal{F}_h^a} + \langle \chi [\![\varphi]\!], [\![\dot{\varphi}_h]\!] \rangle_{\mathcal{F}_h^a} \\
&= (\boldsymbol{f}_p, \dot{\boldsymbol{u}}_h)_{\Omega_p} + (\boldsymbol{g}_p, \dot{\boldsymbol{w}}_h)_{\Omega_p} + (\rho_a f_a, \dot{\varphi}_h)_{\Omega_a}.
\end{aligned} \tag{2.18}
$$

The left-hand side of (2.18) can be rewritten firstly as:

$$
\begin{aligned}
&\frac{d}{dt} \Bigg[\frac{1}{2} \left\| \rho^{1/2} \dot{\boldsymbol{u}}_h \right\|_{\Omega_p}^2 + \frac{1}{2} \left\| \boldsymbol{u}_h \right\|_{\mathrm{dG,e}}^2 - \langle \{\!\{ \boldsymbol{\sigma}_h(\boldsymbol{u}_h) \}\!\}, [\![\boldsymbol{u}_h]\!] \rangle_{\mathcal{F}_h^p} + \\
&\quad \frac{1}{2} \left\| c^{-1} \rho_a^{1/2} \dot{\varphi}_h \right\|_{\Omega_a}^2 + \frac{1}{2} \left\| \varphi_h \right\|_{\mathrm{dG,a}}^2 - \langle \{\!\{ \nabla_h \varphi_h \}\!\}, [\![\varphi_h]\!] \rangle_{\mathcal{F}_h^a} + \\
&\quad \frac{1}{2} \left\| \rho_w^{1/2} \dot{\boldsymbol{w}}_h \right\|_{\Omega_a}^2 + (\rho_f \dot{\boldsymbol{w}}_h, \dot{\boldsymbol{u}}_h)_{\Omega_p} + \\
&\quad \left\| \beta \boldsymbol{u}_h + \boldsymbol{w}_h \right\|_{\mathrm{dG,p}}^2 - \langle m \{\!\{ \nabla_h \cdot (\beta \boldsymbol{u}_h + \boldsymbol{w}_h) \boldsymbol{I} \}\!\}, [\![\beta \boldsymbol{u}_h + \boldsymbol{w}_h]\!] \rangle_{\mathcal{F}_h^p} + \\
&\quad \eta k^{-1} \left\| \dot{\boldsymbol{w}}_h \right\|_{\Omega_p}^2 .
\end{aligned} \tag{2.19}
$$

We next observe that

$$
\begin{aligned}
\left\| \rho^{1/2} \dot{\boldsymbol{u}}_h \right\|_{\Omega_p}^2 &= \rho \left\| \dot{\boldsymbol{u}}_h \right\|_{\Omega_p}^2 = [(1-\phi)\rho_s + \phi \rho_f] \left\| \dot{\boldsymbol{u}}_h \right\|_{\Omega_p}^2 = (1-\phi)\rho_s \left\| \dot{\boldsymbol{u}}_h \right\|_{\Omega_p}^2 + \phi \rho_f \left\| \dot{\boldsymbol{u}}_h \right\|_{\Omega_p}^2 \\
&= \left\| (1-\phi)^{1/2} \rho_s^{1/2} \dot{\boldsymbol{u}}_h \right\|_{\Omega_p}^2 + \left\| \phi^{1/2} \rho_f^{1/2} \dot{\boldsymbol{u}}_h \right\|_{\Omega_p}^2 = \left\| \tilde{\rho}_s^{1/2} \dot{\boldsymbol{u}}_h \right\|_{\Omega_p}^2 + \left\| \phi^{1/2} \rho_f^{1/2} \dot{\boldsymbol{u}}_h \right\|_{\Omega_p}^2 ,
\end{aligned}
$$

$$\left\|\rho_w^{1/2}\dot{\boldsymbol{w}}_h\right\|_{\Omega_p}^2 = \left\|\left(\frac{a}{\phi}\right)^{1/2}\rho_f^{1/2}\dot{\boldsymbol{w}}_h\right\|_{\Omega_p}^2 = \left\|\left(\frac{1+a_0}{\phi}\right)^{1/2}\rho_f^{1/2}\dot{\boldsymbol{w}}_h\right\|_{\Omega_p}^2$$
$$= \left\|\left(\frac{\rho_f}{\phi}\right)^{1/2}\dot{\boldsymbol{w}}_h\right\|_{\Omega_p}^2 + \left\|\left(\frac{a_0\rho_f}{\phi}\right)^{1/2}\dot{\boldsymbol{w}}_h\right\|_{\Omega_p}^2,$$

where the tortuosity $a > 1$ has been written as $a = 1 + a_0$, with $a_0 > 0$. It has been moreover introduced $\tilde{\rho}_s = (1-\phi)\rho_s$ and $\tilde{\rho}_w = \frac{a_0\rho_f}{\phi}$.
According to the above notation, it follows that:

$$\left\|\rho^{1/2}\dot{\boldsymbol{u}}_h\right\|_{\Omega_p}^2 + \left\|\rho_w^{1/2}\dot{\boldsymbol{w}}_h\right\|_{\Omega_p}^2 + 2(\rho_f\dot{\boldsymbol{w}}_h, \dot{\boldsymbol{u}}_h)_{\Omega_p} =$$
$$\left\|\tilde{\rho}_s^{1/2}\dot{\boldsymbol{u}}_h\right\|_{\Omega_p}^2 + \left\|\phi^{1/2}\rho_f^{1/2}\dot{\boldsymbol{u}}_h + \phi^{-1/2}\rho_f^{1/2}\dot{\boldsymbol{w}}_h\right\|_{\Omega_p}^2 + \left\|\tilde{\rho}_w^{1/2}\dot{\boldsymbol{w}}_h\right\|_{\Omega_p}^2.$$

By using definitions (2.8), (2.9), (2.10) and (2.11) and plugging them into (2.19), it follows that the right hand side of (2.18) can be written as:

$$\frac{1}{2}\frac{d}{dt}\Big[\, \|\boldsymbol{u}_h\|_{\mathcal{E},e}^2 + \|\varphi_h\|_{\mathcal{E},a}^2 + \|\beta\boldsymbol{u}_h + \boldsymbol{w}_h\|_{\mathcal{E},p}^2 -$$
$$2\langle\{\!\{\boldsymbol{\sigma}_h(\boldsymbol{u}_h)\}\!\}, [\![\boldsymbol{u}_h]\!]\rangle_{\mathcal{F}_h^p} - 2\langle\{\!\{\nabla_h\varphi_h\}\!\}, [\![\varphi_h]\!]\rangle_{\mathcal{F}_h^a} -$$
$$2\langle m\{\!\{\nabla_h\cdot(\beta\boldsymbol{u}_h + \boldsymbol{w}_h)\boldsymbol{I}\}\!\}, [\![\beta\boldsymbol{u}_h + \boldsymbol{w}_h]\!]\rangle_{\mathcal{F}_h^p} +$$
$$\eta k^{-1}\|\dot{\boldsymbol{w}}_h\|_{\Omega_p}^2 \equiv \frac{1}{2}\frac{d}{dt}\Big[\, \mathrm{I}\,\Big].$$

Equation (2.18) is therefore rewritten as:

$$\frac{1}{2}\frac{d}{dt}\Big[\, \mathrm{I}\,\Big] + \eta k^{-1}\|\dot{\boldsymbol{w}}_h\|_{\Omega_p}^2 = (\boldsymbol{f}_p, \dot{\boldsymbol{u}}_h)_{\Omega_p} + (\boldsymbol{g}_p, \dot{\boldsymbol{w}}_h)_{\Omega_p} + (\rho_a f_a, \dot{\varphi}_h)_{\Omega_a}. \tag{2.20}$$

By integrating in the time interval $[0, t]$, equation (2.20) reduces to:

$$\Big[\, \mathrm{I}\,\Big]_0^t = 2\int_0^t (\boldsymbol{f}_p, \dot{\boldsymbol{u}}_h)_{\Omega_p} + (\boldsymbol{g}_p, \dot{\boldsymbol{w}}_h)_{\Omega_p} + (\rho_a f_a, \dot{\varphi}_h)_{\Omega_a} d\tau - 2\eta k^{-1}\int_0^t \|\dot{\boldsymbol{w}}_h\|_{\Omega_p}^2(\tau) d\tau. \tag{2.21}$$

By using the results in Lemma 3 and proceeding as in Section 1.7, it follows:

$$\|\boldsymbol{U}_h(t)\|_{\mathcal{E}}^2 \lesssim \|\boldsymbol{U}_h(0)\|_{\mathcal{E}}^2 + 2\int_0^t \big((\boldsymbol{f}_p, \dot{\boldsymbol{u}}_h)_{\Omega_p} + (\boldsymbol{g}_p, \dot{\boldsymbol{w}}_h)_{\Omega_p} + (\rho_a f_a, \dot{\varphi}_h)_{\Omega_a}\big) d\tau$$
$$-2\eta k^{-1}\int_0^t \|\dot{\boldsymbol{w}}_h\|_{\Omega_p}^2(\tau) d\tau, \qquad t \in (0, T].$$

Since $\|\boldsymbol{U}_h(t)\|_{\mathcal{E}}^2 \lesssim \|\boldsymbol{U}_h(t)\|_{\mathcal{E}}^2 + 2\eta k^{-1}\int_0^t \|\dot{\boldsymbol{w}}_h\|_{\Omega_p}^2(\tau)d\tau$, it holds:

$$\|\boldsymbol{U}_h(t)\|_{\mathcal{E}}^2 \lesssim \|\boldsymbol{U}_h(0)\|_{\mathcal{E}}^2 + 2\int_0^t \left((\boldsymbol{f}_p, \dot{\boldsymbol{u}}_h)_{\Omega_p} + (\boldsymbol{g}_p, \dot{\boldsymbol{w}}_h)_{\Omega_p} + (\rho_a f_a, \dot{\varphi}_h)_{\Omega_a}\right)d\tau, \qquad t \in (0,T],$$

that implies:

$$\begin{aligned}\|\boldsymbol{U}_h(t)\|_{\mathcal{E}}^2 \lesssim\ & \|\boldsymbol{U}_h(0)\|_{\mathcal{E}}^2 \\ & + \int_0^t \left(\left\|\tilde{\rho}_s^{-1/2}\boldsymbol{f}_p\right\|_{\Omega_p} + \left\|\tilde{\rho}_w^{-1/2}\boldsymbol{g}_p\right\|_{\Omega_p} + \left\|c\rho_a^{1/2}f_a\right\|_{\Omega_a}\right)\|\boldsymbol{U}_h(\tau)\|_{\mathcal{E}}d\tau, \qquad t \in (0,T],\end{aligned}$$

from the Cauchy-Schwarz inequality. We obtain, by applying Gronwall's lemma (see [66]):

$$\begin{aligned}\|\boldsymbol{U}_h(t)\|_{\mathcal{E}} \lesssim\ & \|\boldsymbol{U}_h(0)\|_{\mathcal{E}} \\ & + \int_0^t \left(\left\|\tilde{\rho}_s^{-1/2}\boldsymbol{f}_p\right\|_{\Omega_p} + \left\|\tilde{\rho}_w^{-1/2}\boldsymbol{g}_p\right\|_{\Omega_p} + \left\|c\rho_a^{1/2}f_a\right\|_{\Omega_a}\right)d\tau, \qquad t \in (0,T],\end{aligned}$$

so that stability is stated. □

2.6 Error estimates

In this section we prove an a-priori error estimate for the semi-discrete problem (2.3). For an open bounded polytopic domain $D \subset \mathbb{R}^d$ and a generic polytopic mesh $\mathcal{T}_h$ over D satisfying Assumptions 2.2.1, 2.2.2 and 2.2.3, for any $k \in \mathcal{T}_h$ and $m \in \mathbb{N}_0$, the extension operator $\tilde{\mathcal{E}} : H^m(k) \to H^m(\mathbb{R}^d)$ can be introduced, s.t. $\tilde{\mathcal{E}}v|_k = v$ and $\left\|\tilde{\mathcal{E}}v\right\|_{m,\mathbb{R}^d} \lesssim \|v\|_{m,k}$, as in [6].
The corresponding vector-valued version mapping $\boldsymbol{H}^m(k)$ onto $\boldsymbol{H}^m(\mathbb{R}^d)$ acts component-wise and is denoted in the same way. The result below is a consequence of the *hp*-approximation properties stated in [24] and of Assumptions 2.2.1, 2.2.2 and 2.2.3.

Lemma 4 (Interpolation estimates)**.** *For any functions $\boldsymbol{v} \in \boldsymbol{H}^m(\mathcal{T}_h^p)$, $m \geq 2$ and $\varphi \in H^n(\mathcal{T}_h^a)$, $n \geq 2$, there exists $\boldsymbol{v}_I \in \boldsymbol{V}_h^p$ and $\varphi_I \in V_h^a$ s.t.*

$$\begin{aligned}|||\boldsymbol{v} - \boldsymbol{v}_I|||_{\mathrm{dG,e}}^2 &\lesssim \sum_{k\in\mathcal{T}_h^p} \frac{h^{2s_k^v-2}}{p_{v,k}^{2m-3}}\left\|\tilde{\mathcal{E}}\boldsymbol{v}\right\|_{m,\mathcal{K}}^2,\\ |||\boldsymbol{v} - \boldsymbol{v}_I|||_{\mathrm{dG,p}}^2 &\lesssim \sum_{k\in\mathcal{T}_h^p} \frac{h^{2s_k^v-2}}{p_{v,k}^{2m-3}}\left\|\tilde{\mathcal{E}}\boldsymbol{v}\right\|_{m,\mathcal{K}}^2,\\ |||\varphi - \varphi_I|||_{\mathrm{dG,a}}^2 &\lesssim \sum_{k\in\mathcal{T}_h^a} \frac{h^{2s_k^\varphi-2}}{p_{\varphi,k}^{2n-3}}\left\|\tilde{\mathcal{E}}\varphi\right\|_{n,\mathcal{K}}^2,\end{aligned}$$

with $s_k^v = \min\{p_k^v + 1, m\}$ *and* $s_k^\varphi = \min\{p_k^\varphi + 1, n\}$.
Additionally, if $\boldsymbol{v} \in C^1((0,T];\boldsymbol{H}^m(\mathcal{T}_h^p))$, $m \geq 2$ *and* $\varphi \in C^1((0,T];H^m(\mathcal{T}_h^a))$, $n \geq 2$*:*

$$\|\boldsymbol{v} - \boldsymbol{v}_I\|_{\mathcal{E},e}^2 \lesssim \sum_{k\in\mathcal{T}_h^p} \frac{h^{2s_k^v-2}}{p_{v,k}^{2m-3}} \left(\left\|\tilde{\mathcal{E}}\dot{\boldsymbol{v}}\right\|_{m,\mathcal{K}}^2 + \left\|\tilde{\mathcal{E}}\boldsymbol{v}\right\|_{m,\mathcal{K}}^2 \right),$$

$$\|\varphi - \varphi_I\|_{\mathcal{E},a}^2 \lesssim \sum_{k\in\mathcal{T}_h^a} \frac{h^{2s_k^\varphi-2}}{p_{\varphi,k}^{2n-3}} \left(\left\|\tilde{\mathcal{E}}\dot{\varphi}\right\|_{n,\mathcal{K}}^2 + \left\|\tilde{\mathcal{E}}\varphi\right\|_{n,\mathcal{K}}^2 \right).$$

Proof. See [6]. □

From Lemma 4 we can prove the following result.

Lemma 5. *For any* $(\boldsymbol{u},\boldsymbol{w},\varphi)$ *such that* $\boldsymbol{u} \in C^1([0,T];\boldsymbol{H}^m(\mathcal{T}_h^p))$, $\boldsymbol{w} \in C^1([0,T];\boldsymbol{H}^l(\mathcal{T}_h^p))$ *and* $\varphi \in C^1([0,T];H^n(\mathcal{T}_h^a))$*, with* $m,l,n \geq 2$*, there exists* $(\boldsymbol{u}_I,\boldsymbol{w}_I,\varphi_I) \in \boldsymbol{V}_h^p \times \boldsymbol{V}_h^p \times V_h^a$ *s.t.:*

$$\begin{aligned}\|(\boldsymbol{u}-\boldsymbol{u}_I,\boldsymbol{w}-\boldsymbol{w}_I,\varphi-\varphi_I)\|_{\mathcal{E}}^2 \lesssim & \sum_{k\in\mathcal{T}_h^p} \frac{h_k^{2(s_k^u-1)}}{p_{u,k}^{2m-3}} \left(\left\|\tilde{\mathcal{E}}\dot{\boldsymbol{u}}\right\|_{m,\mathcal{K}}^2 + \left\|\tilde{\mathcal{E}}\boldsymbol{u}\right\|_{m,\mathcal{K}}^2 \right) \\ & + \sum_{k\in\mathcal{T}_h^p} \frac{h_k^{2(s_k^w-1)}}{p_{w,k}^{2l-3}} \left(\left\|\tilde{\mathcal{E}}\dot{\boldsymbol{w}}\right\|_{l,\mathcal{K}}^2 + \left\|\tilde{\mathcal{E}}\boldsymbol{w}\right\|_{l,\mathcal{K}}^2 \right) \\ & + \sum_{k\in\mathcal{T}_h^a} \frac{h_k^{2(s_k^\varphi-1)}}{p_{\varphi,k}^{2n-3}} \left(\left\|\tilde{\mathcal{E}}\dot{\varphi}\right\|_{n,\mathcal{K}}^2 + \left\|\tilde{\mathcal{E}}\varphi\right\|_{n,\mathcal{K}}^2 \right).\end{aligned}$$

Proof. The proof follows by applying estimates of Lemma 4 and reasoning as in [7, 62]. □

By defining $\|\cdot\|_E$ as:

$$\|\boldsymbol{U}_h\|_E^2 = \|\boldsymbol{u}_h\|_{\mathcal{E},e}^2 + \|\varphi_h\|_{\mathcal{E},a}^2 + \|\beta\boldsymbol{u}_h + \boldsymbol{w}_h\|_{\mathcal{E},p}^2,$$

with $\boldsymbol{U}_h(t) := (\boldsymbol{u}_h(t),\boldsymbol{w}_h(t),\varphi_h(t))$ and $\boldsymbol{E}(t) = (\boldsymbol{u}-\boldsymbol{u}_h,\boldsymbol{w}-\boldsymbol{w}_h,\varphi-\varphi_h)(t) = (\boldsymbol{e}^u,\boldsymbol{e}^w,e^\varphi)(t)$, the following theorem is stated.

Theorem 4 (A-priori error estimate in the energy norm)**.** *Let Assumptions 2.2.1, 2.2.2 and 2.2.3 hold. Assume that the exact solution of problem (1.11) is such that* $\boldsymbol{u} \in C^2([0,T];\boldsymbol{H}^2(\Omega_p)\cap\boldsymbol{H}^m(\mathcal{T}_h^p))$, $\boldsymbol{w} \in C^2([0,T];\boldsymbol{H}^2(\Omega_p)\cap\boldsymbol{H}^l(\mathcal{T}_h^p))$ *and* $\varphi \in C^2([0,T];H^2(\Omega_a)\cap H^n(\mathcal{T}_h^a))$*, with* $m,n,l \geq 2$*. Let* $(\boldsymbol{u}_h,\boldsymbol{w}_h,\varphi_h) \in C^2([0,T];\boldsymbol{V}_h^p)\times C^2([0,T];\boldsymbol{V}_h^p)\times C^2([0,T];V_h^a)$ *be the corresponding solution of the semi-discrete problem (2.3), with sufficiently large*

penalty parameters c_1, c_2 and c_3. Then, the following bound holds for the discretization error $\boldsymbol{E}(t)$:

$$\begin{aligned}\|\boldsymbol{E}\|_E \lesssim & \sum_{k\in\mathcal{T}_h^p} \frac{h_k^{2(s_k^u-1)}}{p_{u,k}^{m-3/2}} \left(\left\|\tilde{\mathcal{E}}\dot{\boldsymbol{u}}\right\|_{m,\mathcal{K}} + \left\|\tilde{\mathcal{E}}\boldsymbol{u}\right\|_{m,\mathcal{K}} + \int_0^t \left[\left\|\tilde{\mathcal{E}}\ddot{\boldsymbol{u}}\right\|_{m,\mathcal{K}} + \left\|\tilde{\mathcal{E}}\dot{\boldsymbol{u}}\right\|_{m,\mathcal{K}} \right] d\tau \right) \\ & + \sum_{k\in\mathcal{T}_h^p} \frac{h_k^{2(s_k^w-1)}}{p_{w,k}^{l-3/2}} \left(\left\|\tilde{\mathcal{E}}\dot{\boldsymbol{w}}\right\|_{l,\mathcal{K}} + \left\|\tilde{\mathcal{E}}\boldsymbol{w}\right\|_{l,\mathcal{K}} + \int_0^t \left[\left\|\tilde{\mathcal{E}}\ddot{\boldsymbol{w}}\right\|_{l,\mathcal{K}} + \left\|\tilde{\mathcal{E}}\dot{\boldsymbol{w}}\right\|_{l,\mathcal{K}} \right] d\tau \right) \\ & + \sum_{k\in\mathcal{T}_h^a} \frac{h_k^{2(s_k^\varphi-1)}}{p_{\varphi,k}^{n-3/2}} \left(\left\|\tilde{\mathcal{E}}\dot{\varphi}\right\|_{n,\mathcal{K}} + \left\|\tilde{\mathcal{E}}\varphi\right\|_{n,\mathcal{K}} + \int_0^t \left[\left\|\tilde{\mathcal{E}}\ddot{\varphi}\right\|_{n,\mathcal{K}} + \left\|\tilde{\mathcal{E}}\dot{\varphi}\right\|_{n,\mathcal{K}} \right] d\tau \right),\end{aligned}$$

Proof. From the *strong consistency* of the semi-discrete formulation, for any $t \in (0, T]$, the exact solution $(\boldsymbol{u}(t), \boldsymbol{w}(t), \varphi(t))$ satisfies the semi-discrete formulation (2.3), that is:

$$\begin{aligned}(\rho\ddot{\boldsymbol{u}}, \boldsymbol{v})_{\Omega_p} + (\rho_f\ddot{\boldsymbol{w}}, \boldsymbol{v})_{\Omega_p} + \mathcal{A}_h^p(\boldsymbol{u}, \boldsymbol{v}) + \mathcal{B}_h^p(\beta\boldsymbol{u} + \boldsymbol{w}, \beta\boldsymbol{v}) + \mathcal{C}_{h,p}(\varphi, \boldsymbol{v}) \\ + (\rho_f\ddot{\boldsymbol{u}}, \boldsymbol{\xi})_{\Omega_p} + (\rho_w\ddot{\boldsymbol{w}}, \boldsymbol{\xi})_{\Omega_p} + \eta k^{-1}(\dot{\boldsymbol{w}}, \boldsymbol{\xi})_{\Omega_p} \\ + \mathcal{B}_h^p(\beta\boldsymbol{u} + \boldsymbol{w}, \boldsymbol{\xi}) + k_{int}\mathcal{C}_{h,p}(\varphi, \boldsymbol{\xi}) \\ + (\rho_a c^{-2}\ddot{\varphi}, \psi)_{\Omega_a} + \mathcal{A}_h^a(\varphi, \psi) + \mathcal{C}_{h,a}(\boldsymbol{u}, \psi) + k_{int}\mathcal{C}_{h,a}(\boldsymbol{w}, \psi) \\ = (\boldsymbol{f}_p, \boldsymbol{v})_{\Omega_p} + (\boldsymbol{g}_p, \boldsymbol{\xi})_{\Omega_p} + (\rho_a f_a, \psi)_{\Omega_a}, \\ \forall\ (\boldsymbol{v}, \boldsymbol{\xi}, \psi) \in \boldsymbol{V}_h^p \times \boldsymbol{V}_h^p \times V_h^a.\end{aligned}$$

By subtracting the semi-discrete formulation from the above equation, the *error equation* reads as follows:

$$\begin{aligned}(\rho\ddot{\boldsymbol{e}}_u, \boldsymbol{v})_{\Omega_p} + (\rho_f\ddot{\boldsymbol{e}}_w, \boldsymbol{v})_{\Omega_p} + \mathcal{A}_h^p(\boldsymbol{e}_u, \boldsymbol{v}) + \mathcal{B}_h^p(\beta\boldsymbol{e}_u + \boldsymbol{e}_w, \beta\boldsymbol{v}) + \mathcal{C}_{h,p}(e_\varphi, \boldsymbol{v}) \\ + (\rho_f\ddot{\boldsymbol{e}}_u, \boldsymbol{\xi})_{\Omega_p} + (\rho_w\ddot{\boldsymbol{e}}_w, \boldsymbol{\xi})_{\Omega_p} + \eta k^{-1}(\dot{\boldsymbol{e}}_w, \boldsymbol{\xi})_{\Omega_p} \\ + \mathcal{B}_h^p(\beta\boldsymbol{e}_u + \boldsymbol{e}_w, \boldsymbol{\xi}) + k_{int}\mathcal{C}_{h,p}(e_\varphi, \boldsymbol{\xi}) \\ + (\rho_a c^{-2}\ddot{e}_\varphi, \psi)_{\Omega_a} + \mathcal{A}_h^a(e_\varphi, \psi) + \mathcal{C}_{h,a}(\boldsymbol{e}_u, \psi) + k_{int}\mathcal{C}_{h,a}(\boldsymbol{e}_w, \psi) = 0, \\ \forall\ (\boldsymbol{v}, \boldsymbol{\xi}, \psi) \in \boldsymbol{V}_h^p \times \boldsymbol{V}_h^p \times V_h^a. \qquad (2.22)\end{aligned}$$

The error $\boldsymbol{E} = (\boldsymbol{e}_u, \boldsymbol{e}_w, e_\varphi) = (\boldsymbol{u} - \boldsymbol{u}_h, \boldsymbol{w} - \boldsymbol{w}_h, \varphi - \varphi_h)$ can be split as:

$$\boldsymbol{E} = \boldsymbol{E}_I - \boldsymbol{E}_h,$$

where $\boldsymbol{E}_I = (\boldsymbol{e}_I^u, \boldsymbol{e}_I^w, e_I^\varphi) = (\boldsymbol{u} - \boldsymbol{u}_I, \boldsymbol{w} - \boldsymbol{w}_I, \varphi - \varphi_I)$, $\boldsymbol{E}_h = (\boldsymbol{e}_h^u, \boldsymbol{e}_h^w, e_h^\varphi) = (\boldsymbol{u}_h - \boldsymbol{u}_I, \boldsymbol{w}_h - \boldsymbol{w}_I, \varphi_h - \varphi_I)$ and $(\boldsymbol{u}_I, \boldsymbol{w}_I, \varphi_I) \in \boldsymbol{V}_h^p \times \boldsymbol{V}_h^p \times V_h^a$ are the interpolants defined in Lemma

4.

The error $\boldsymbol{E}$ is now estimated by means of the triangle inequality:

$$\|\boldsymbol{E}\|_E^2 \leq \|\boldsymbol{E}_h\|_E^2 + \|\boldsymbol{E}_I\|_E^2$$

and the result in Lemma 5 is used to bound the term $\boldsymbol{E}_I$. Then, by taking as test function $(\boldsymbol{v}, \boldsymbol{\xi}, \psi) = (\dot{\boldsymbol{e}}_h^u, \dot{\boldsymbol{e}}_h^w, \dot{e}_h^\varphi)$, identity (2.22) is rewritten as:

$$\begin{aligned}
(\rho\ddot{\boldsymbol{e}}_u, \dot{\boldsymbol{e}}_h^u)_{\Omega_p} + (\rho_f\ddot{\boldsymbol{e}}_w, \dot{\boldsymbol{e}}_h^u)_{\Omega_p} + \mathcal{A}_h^p(\boldsymbol{e}_u, \dot{\boldsymbol{e}}_h^u) + \mathcal{B}_h^p(\beta\boldsymbol{e}_u + \boldsymbol{e}_w, \beta\dot{\boldsymbol{e}}_h^u) + \mathcal{C}_{h,p}(e_\varphi, \dot{\boldsymbol{e}}_h^u) \\
+ (\rho_f\ddot{\boldsymbol{e}}_u, \dot{\boldsymbol{e}}_h^w)_{\Omega_p} + (\rho_w\ddot{\boldsymbol{e}}_w, \dot{\boldsymbol{e}}_h^w)_{\Omega_p} + \eta k^{-1}(\dot{\boldsymbol{e}}_w, \dot{\boldsymbol{e}}_h^w)_{\Omega_p} \\
+ \mathcal{B}_h^p(\beta\boldsymbol{e}_u + \boldsymbol{e}_w, \dot{\boldsymbol{e}}_h^w) + k_{int}\mathcal{C}_{h,p}(e_\varphi, \dot{\boldsymbol{e}}_h^w) \\
+ (\rho_a c^{-2}\ddot{e}_\varphi, \dot{e}_h^\varphi)_{\Omega_a} + \mathcal{A}_h^a(e_\varphi, \dot{e}_h^\varphi) + \mathcal{C}_{h,a}(\boldsymbol{e}_u, \dot{e}_h^\varphi) + k_{int}\mathcal{C}_{h,a}(\boldsymbol{e}_w, \dot{e}_h^\varphi) = 0,
\end{aligned}$$

that can be easily rewritten as:

$$\begin{aligned}
(\rho\ddot{\boldsymbol{e}}_h^u, \dot{\boldsymbol{e}}_h^u)_{\Omega_p} + (\rho_f\ddot{\boldsymbol{e}}_h^w, \dot{\boldsymbol{e}}_h^u)_{\Omega_p} + \mathcal{A}_h^p(\boldsymbol{e}_h^u, \dot{\boldsymbol{e}}_h^u) + \mathcal{B}_h^p(\beta\boldsymbol{e}_h^u + \boldsymbol{e}_h^w, \beta\dot{\boldsymbol{e}}_h^u) \\
+ (\rho_f\ddot{\boldsymbol{e}}_h^u, \dot{\boldsymbol{e}}_h^w)_{\Omega_p} + (\rho_w\ddot{\boldsymbol{e}}_h^w, \dot{\boldsymbol{e}}_h^w)_{\Omega_p} + \eta k^{-1}(\dot{\boldsymbol{e}}_h^w, \dot{\boldsymbol{e}}_h^w)_{\Omega_p} + \mathcal{B}_h^p(\beta\boldsymbol{e}_h^u + \boldsymbol{e}_h^w, \dot{\boldsymbol{e}}_h^w) \\
+ (\rho_a c^{-2}\ddot{e}_h^\varphi, \dot{e}_h^\varphi)_{\Omega_a} + \mathcal{A}_h^a(e_h^\varphi, \dot{e}_h^\varphi) \\
= \\
(\rho\ddot{\boldsymbol{e}}_I^u, \dot{\boldsymbol{e}}_h^u)_{\Omega_p} + (\rho_f\ddot{\boldsymbol{e}}_I^w, \dot{\boldsymbol{e}}_h^u)_{\Omega_p} + \mathcal{A}_h^p(\boldsymbol{e}_I^u, \dot{\boldsymbol{e}}_h^u) + \mathcal{B}_h^p(\beta\boldsymbol{e}_I^u + \boldsymbol{e}_I^w, \beta\dot{\boldsymbol{e}}_h^u) + \mathcal{C}_{h,p}(e_I^\varphi, \dot{\boldsymbol{e}}_h^u) \\
+ (\rho_f\ddot{\boldsymbol{e}}_I^u, \dot{\boldsymbol{e}}_h^w)_{\Omega_p} + (\rho_w\ddot{\boldsymbol{e}}_I^w, \dot{\boldsymbol{e}}_h^w)_{\Omega_p} + \eta k^{-1}(\dot{\boldsymbol{e}}_I^w, \dot{\boldsymbol{e}}_h^w)_{\Omega_p} \\
+ \mathcal{B}_h^p(\beta\boldsymbol{e}_I^u + \boldsymbol{e}_I^w, \dot{\boldsymbol{e}}_h^w) + k_{int}\mathcal{C}_{h,p}(e_I^\varphi, \dot{\boldsymbol{e}}_h^w) \\
+ (\rho_a c^{-2}\ddot{e}_I^\varphi, \dot{e}_h^\varphi)_{\Omega_a} + \mathcal{A}_h^a(e_I^\varphi, \dot{e}_h^\varphi) + \mathcal{C}_{h,a}(\boldsymbol{e}_I^u, \dot{e}_h^\varphi) + k_{int}\mathcal{C}_{h,a}(\boldsymbol{e}_I^w, \dot{e}_h^\varphi). \qquad (2.23)
\end{aligned}$$

Notice now that the coupling terms of left-hand side of the above equation have been neglected due to skew-symmetry. Moreover, as in Section 2.5, left-hand side could be rewritten, by collecting a first time derivative and introducing the energy norm. Indeed, by defining $\mathcal{N}(t)$ as follows:

$$\begin{aligned}
\mathcal{N}^2(t) = \|\boldsymbol{E}_h\|_E^2 - 2\langle\{\!\{\boldsymbol{\sigma}_h(\boldsymbol{e}_h^u)\}\!\}, [\![\boldsymbol{e}_h^u]\!]\rangle_{\mathcal{F}_h^p} - 2\langle\{\!\{\nabla_h e_h^\varphi\}\!\}, [\![e_h^\varphi]\!]\rangle_{\mathcal{F}_h^a} \\
-2m\langle\{\!\{\nabla_h \cdot (\beta\boldsymbol{e}_h^u + \boldsymbol{e}_h^w)\}\!\}, [\![\beta\boldsymbol{e}_h^u + \boldsymbol{e}_h^w]\!]\rangle_{\mathcal{F}_h^p},
\end{aligned}$$

the left-hand side of equation (2.23) is rewritten as:

$$\frac{1}{2}\frac{\mathrm{d}}{\mathrm{dt}}\mathcal{N}^2(t) + \eta k^{-1}\,\|\dot{\boldsymbol{e}}_h^w\|_{\Omega_p}^2$$

and in particular, from Lemma 3, it holds:

$$\int_0^t \frac{1}{2}\frac{\mathrm{d}}{\mathrm{dt}} \|\boldsymbol{E}_h\|_E^2 \, d\tau \lesssim \int_0^t \frac{1}{2}\frac{\mathrm{d}}{\mathrm{dt}} \mathcal{N}^2(t) d\tau + \int_0^t \eta k^{-1} \|\dot{\boldsymbol{e}}_h^w\|_{\Omega_p}^2 \, d\tau.$$

Next, we take into account the right-hand side of (2.23), that is

$$\begin{aligned}
&(\tilde{\rho}_s \ddot{\boldsymbol{e}}_I^u, \dot{\boldsymbol{e}}_h^u)_{\Omega_p} + \mathcal{A}_h^p(\boldsymbol{e}_I^u, \dot{\boldsymbol{e}}_h^u) + (\rho_a c^{-2} \ddot{e}_I^\varphi, \dot{e}_h^\varphi)_{\Omega_a} + \mathcal{A}_h^a(e_I^\varphi, \dot{e}_h^\varphi) \\
&\quad + (\phi \rho_f \ddot{\boldsymbol{e}}_I^u, \dot{\boldsymbol{e}}_h^u)_{\Omega_p} + (\rho_f \ddot{\boldsymbol{e}}_I^w, \dot{\boldsymbol{e}}_h^u)_{\Omega_p} + (\rho_f \ddot{\boldsymbol{e}}_I^u, \dot{\boldsymbol{e}}_h^w)_{\Omega_p} \\
&+ (\rho_f \phi^{-1} \ddot{\boldsymbol{e}}_I^w, \dot{\boldsymbol{e}}_h^w)_{\Omega_p} + (\tilde{\rho}_w \ddot{\boldsymbol{e}}_I^w, \dot{\boldsymbol{e}}_h^w)_{\Omega_p} + \mathcal{B}_h^p(\beta \boldsymbol{e}_I^u + \boldsymbol{e}_I^w, \beta \dot{\boldsymbol{e}}_h^u + \dot{\boldsymbol{e}}_h^w) \\
&+ \mathcal{C}_{h,p}(e_I^\varphi, \dot{\boldsymbol{e}}_h^u) + \mathcal{C}_{h,a}(\boldsymbol{e}_I^u, \dot{e}_h^\varphi) + k_{int}(\mathcal{C}_{h,p}(e_I^\varphi, \dot{\boldsymbol{e}}_h^w) + \mathcal{C}_{h,a}(\boldsymbol{e}_I^w, \dot{e}_h^\varphi)) \\
&\quad + \eta k^{-1} (\dot{\boldsymbol{e}}_I^w, \dot{\boldsymbol{e}}_h^w)_{\Omega_p}.
\end{aligned} \tag{2.24}$$

By employing the Cauchy-Schwarz inequality, it follows:

$$\begin{aligned}
&|(\tilde{\rho}_s \ddot{\boldsymbol{e}}_I^u, \dot{\boldsymbol{e}}_h^u)_{\Omega_p}| \lesssim \|\dot{\boldsymbol{e}}_I^u\|_{\mathcal{E},e} \|\boldsymbol{e}_I^u\|_{\mathcal{E},e}, \\
&|(\rho_a c^{-2} \ddot{e}_I^\varphi, \dot{e}_h^\varphi)_{\Omega_a}| \lesssim \left\|\dot{e}_I^\varphi\right\|_{\mathcal{E},a} \left\|e_I^\varphi\right\|_{\mathcal{E},a},
\end{aligned}$$

Moreover, it holds:

$$\begin{aligned}
&(\phi \rho_f \ddot{\boldsymbol{e}}_I^u, \dot{\boldsymbol{e}}_h^u)_{\Omega_p} + (\rho_f \ddot{\boldsymbol{e}}_I^w, \dot{\boldsymbol{e}}_h^u)_{\Omega_p} + (\rho_f \ddot{\boldsymbol{e}}_I^u, \dot{\boldsymbol{e}}_h^w)_{\Omega_p} + (\rho_f \phi^{-1} \ddot{\boldsymbol{e}}_I^w, \dot{\boldsymbol{e}}_h^w)_{\Omega_p} + (\tilde{\rho}_w \ddot{\boldsymbol{e}}_I^w, \dot{\boldsymbol{e}}_h^w)_{\Omega_p} \\
&= \left(\phi^{1/2} \rho_f^{1/2} \ddot{\boldsymbol{e}}_I^u + \rho_f^{1/2} \phi^{-1/2} \ddot{\boldsymbol{e}}_I^w, \phi^{1/2} \rho_f^{1/2} \dot{\boldsymbol{e}}_h^u + \rho_f^{1/2} \phi^{-1/2} \dot{\boldsymbol{e}}_h^w\right)_{\Omega_p} + (\tilde{\rho}_w^{1/2} \ddot{\boldsymbol{e}}_I^w, \tilde{\rho}_w^{1/2} \dot{\boldsymbol{e}}_h^w)_{\Omega_p} \\
&\leq \left\|\phi^{1/2} \rho_f^{1/2} \ddot{\boldsymbol{e}}_I^u + \rho_f^{1/2} \phi^{-1/2} \ddot{\boldsymbol{e}}_I^w\right\|_{\Omega_p} \left\|\phi^{1/2} \rho_f^{1/2} \dot{\boldsymbol{e}}_h^u + \rho_f^{1/2} \phi^{-1/2} \dot{\boldsymbol{e}}_h^w\right\|_{\Omega_p} \\
&\quad + \left\|\tilde{\rho}_w^{1/2} \ddot{\boldsymbol{e}}_I^w\right\|_{\Omega_p} \left\|\tilde{\rho}_w^{1/2} \dot{\boldsymbol{e}}_h^w\right\|_{\Omega_p},
\end{aligned}$$

where again it has been used the Cauchy-Schwarz inequality.
For $\mathcal{A}_h^p$- and $\mathcal{A}_h^a$- terms in (2.24), by employing continuity estimates in Lemma 1 and observing that $\|\cdot\|_{\mathrm{dG},\star} \leq \|\cdot\|_{\mathcal{E},\star}$, it follows:

$$\begin{aligned}
&\mathcal{A}_h^p(\boldsymbol{e}_I^u, \dot{\boldsymbol{e}}_h^u) + \mathcal{A}_h^a(e_I^\varphi, \dot{e}_h^\varphi) = \frac{\mathrm{d}}{\mathrm{dt}} \left(\mathcal{A}_h^p(\boldsymbol{e}_I^u, \boldsymbol{e}_h^u) + \mathcal{A}_h^a(e_I^\varphi, e_h^\varphi)\right) - \mathcal{A}_h^p(\dot{\boldsymbol{e}}_I^u, \boldsymbol{e}_h^u) + \mathcal{A}_h^a(\dot{e}_I^\varphi, e_h^\varphi) \lesssim \\
&\frac{\mathrm{d}}{\mathrm{dt}} \left(|||\boldsymbol{e}_I^u|||_{\mathrm{dG,e}} \|\boldsymbol{e}_h^u\|_{\mathcal{E},e} + |||e_I^\varphi|||_{\mathrm{dG,a}} \left\|e_h^\varphi\right\|_{\mathcal{E},a}\right) + \left(|||\dot{\boldsymbol{e}}_I^u|||_{\mathrm{dG,e}} \|\boldsymbol{e}_h^u\|_{\mathcal{E},e} + |||\dot{e}_I^\varphi|||_{\mathrm{dG,a}} \left\|e_h^\varphi\right\|_{\mathcal{E},a}\right).
\end{aligned}$$

$\mathcal{B}_h^p$-terms in (2.24) can be bounded, in the same way, as follows:

$$\begin{aligned}
&\mathcal{B}_h^p(\beta \boldsymbol{e}_I^u + \boldsymbol{e}_I^w, \beta \dot{\boldsymbol{e}}_h^u + \dot{\boldsymbol{e}}_h^w) = \\
&\frac{\mathrm{d}}{\mathrm{dt}} \left(\mathcal{B}_h(\beta \boldsymbol{e}_I^u + \boldsymbol{e}_I^w, \beta \boldsymbol{e}_h^u + \boldsymbol{e}_h^w)\right) - \mathcal{B}_h(\beta \dot{\boldsymbol{e}}_I^u + \dot{\boldsymbol{e}}_I^w, \beta \boldsymbol{e}_h^u + \boldsymbol{e}_h^w) \lesssim \\
&\frac{\mathrm{d}}{\mathrm{dt}} \left(|||\beta \boldsymbol{e}_I^u + \boldsymbol{e}_I^w|||_{\mathrm{dG,p}} \|\beta \boldsymbol{e}_I^u + \boldsymbol{e}_I^w\|_{\mathrm{dG,p}}\right) + |||\beta \dot{\boldsymbol{e}}_I^u + \dot{\boldsymbol{e}}_I^w|||_{\mathrm{dG,p}} \|\beta \boldsymbol{e}_h^u + \boldsymbol{e}_h^w\|_{\mathrm{dG,p}}.
\end{aligned}$$

For the coupling terms in (2.24), it follows that:

$$\mathcal{C}_{h,p}(e_I^{\varphi}, \dot{\boldsymbol{e}}_h^u) + \mathcal{C}_{h,a}(\boldsymbol{e}_I^u, \dot{e}_h^{\varphi}) + k_{int}(\mathcal{C}_{h,p}(e_I^{\varphi}, \dot{\boldsymbol{e}}_h^w) + \mathcal{C}_{h,a}(\boldsymbol{e}_I^w, \dot{e}_h^{\varphi})) = \mathcal{C}_{h,p}(e_I^{\varphi}, \dot{\boldsymbol{e}}_h^u + k_{int}\dot{\boldsymbol{e}}_h^w) + \mathcal{C}_{h,a}(\boldsymbol{e}_I^u + k_{int}\boldsymbol{e}_I^w, \dot{e}_h^{\varphi}),$$

for $k_{int} = \{0, 1\}$.
Now, recalling the definitions of the coupling bilinear forms, it follows:

$$\begin{aligned}
\mathcal{C}_{h,p}(e_I^{\varphi}, \dot{\boldsymbol{e}}_h^u + k_{int}\dot{\boldsymbol{e}}_h^w) &= \langle \rho_a \dot{e}_I^{\varphi} \boldsymbol{n}_p, \dot{\boldsymbol{e}}_h^u + k_{int}\dot{\boldsymbol{e}}_h^w \rangle_{\mathcal{F}_h^I} \\
&\lesssim \sum_{F \in \mathcal{F}_h^I} \left\| \rho_a \dot{e}_I^{\varphi} \right\|_F \left\| \dot{\boldsymbol{e}}_h^u + k_{int}\dot{\boldsymbol{e}}_h^w \right\|_F \\
&\lesssim \sum_{\substack{k_p \in \mathcal{T}_{h,p}^I \\ k_a \in \mathcal{T}_{h,a}^I}} \left\| \dot{e}_I^{\varphi} \right\|_{\partial k^a} \left\| \dot{\boldsymbol{e}}_h^u + k_{int}\dot{\boldsymbol{e}}_h^w \right\|_{\partial k^p} \\
&\lesssim \sum_{\substack{k_p \in \mathcal{T}_{h,p}^I \\ k_a \in \mathcal{T}_{h,a}^I}} p_{a,k^a} h_{k^a}^{-1/2} \left\| \dot{e}_I^{\varphi} \right\|_{\partial k^a} \left\| \dot{\boldsymbol{e}}_h^u + k_{int}\dot{\boldsymbol{e}}_h^w \right\|_{k^p} \\
&\lesssim \mathcal{I}_h^a(\dot{e}_I^{\varphi}) \left(\|\boldsymbol{e}_h^u\|_{\mathcal{E},e} + \left\| \tilde{\rho}_w^{1/2} \dot{\boldsymbol{e}}_h^w \right\|_{\Omega_p} \right),
\end{aligned}$$

where

$$\mathcal{I}_h^a(\varphi) = \sum_{\substack{k_p \in \mathcal{T}_{h,p}^I \\ k_a \in \mathcal{T}_{h,a}^I}} p_{a,k^a} h_{k^a}^{-1/2} \|\varphi\|_{\partial k^a}, \qquad \forall\ \varphi \in H^2(\Omega_a) \cap H^n(\mathcal{T}_h^a).$$

Analogously, by defining:

$$\mathcal{I}_h^p(\boldsymbol{v}) = \sum_{\substack{k_p \in \mathcal{T}_{h,p}^I \\ k_a \in \mathcal{T}_{h,a}^I}} p_{p,k^p} h_{k^p}^{-1/2} \|\boldsymbol{v}\|_{\partial k^p}, \qquad \forall\ \boldsymbol{v} \in \boldsymbol{H}^2(\Omega_p) \cap \boldsymbol{H}^m(\mathcal{T}_h^p)$$

it holds:

$$\mathcal{C}_{h,a}(\boldsymbol{e}_I^u + k_{int}\boldsymbol{e}_I^w, \dot{e}_h^{\varphi}) \lesssim \mathcal{I}_h^p(\dot{\boldsymbol{e}}_I^u + k_{int}\dot{\boldsymbol{e}}_I^w) \left\| e_h^{\varphi} \right\|_{\mathcal{E},a}.$$

Observe now, that since $\boldsymbol{e}_h^u(0) = \boldsymbol{e}_h^w(0) = e_h^{\varphi}(0) = 0$, by integrating in time in the interval $[0, t]$, it follows:

$$\begin{aligned}
\|\boldsymbol{E}_h\|_E^2 \lesssim & \int_0^t \left(\|\dot{\boldsymbol{e}}_I^u\|_{\mathcal{E},e} \|\boldsymbol{e}_I^u\|_{\mathcal{E},e} + \left\|\dot{e}_I^{\varphi}\right\|_{\mathcal{E},a} \left\|e_I^{\varphi}\right\|_{\mathcal{E},a} \right) d\tau \\
& + |||\boldsymbol{e}_I^u|||_{\mathrm{dG,e}} \|\boldsymbol{e}_h^u\|_{\mathcal{E},e} + |||e_I^{\varphi}|||_{\mathrm{dG,a}} \left\|e_h^{\varphi}\right\|_{\mathcal{E},a} \\
& + \int_0^t \left(|||\dot{\boldsymbol{e}}_I^u|||_{\mathrm{dG,e}} \|\boldsymbol{e}_h^u\|_{\mathcal{E},e} + |||\dot{e}_I^{\varphi}|||_{\mathrm{dG,a}} \left\|e_h^{\varphi}\right\|_{\mathcal{E},a} \right) d\tau \\
& + \int_0^t \left(\left\| \rho_f^{1/2} \left(\phi^{1/2} \ddot{\boldsymbol{e}}_I^u + \phi^{-1/2} \ddot{\boldsymbol{e}}_I^w \right) \right\|_{\Omega_p} \left\| \rho_f^{1/2} \left(\phi^{1/2} \dot{\boldsymbol{e}}_h^u + \phi^{-1/2} \dot{\boldsymbol{e}}_h^w \right) \right\|_{\Omega_p} \right) d\tau
\end{aligned}$$

$$
\begin{aligned}
&+ \int_0^t \left(\left\| \tilde{\rho}_w^{1/2} \ddot{\boldsymbol{e}}_I^w \right\|_{\Omega_p} \left\| \tilde{\rho}_w^{1/2} \dot{\boldsymbol{e}}_h^w \right\|_{\Omega_p} \right) \\
&+ |||\beta \boldsymbol{e}_I^u + \boldsymbol{e}_I^w)|||_{\mathrm{dG,p}} \, \|\beta \boldsymbol{e}_h^u + \boldsymbol{e}_h^w\|_{\mathrm{dG,p}} \\
&+ \int_0^t \left(|||\beta \dot{\boldsymbol{e}}_I^u + \dot{\boldsymbol{e}}_I^w|||_{\mathrm{dG,p}} \, \|\beta \boldsymbol{e}_h^u + \boldsymbol{e}_h^w\|_{\mathrm{dG,p}} \right) d\tau \\
&+ \int_0^t \mathcal{I}_h^a(\dot{e}_I^\varphi) \left(\|\boldsymbol{e}_h^u\|_{\mathcal{E},e} + \left\| \tilde{\rho}_w^{1/2} \dot{\boldsymbol{e}}_h^w \right\|_{\Omega_p} \right) d\tau \\
&+ \int_0^t \mathcal{I}_h^p(\dot{\boldsymbol{e}}_I^u + k_{int} \dot{\boldsymbol{e}}_I^w) \left\| e_h^\varphi \right\|_{\mathcal{E},a} d\tau \\
&+ \int_0^t \eta k^{-1} \left\| \dot{\boldsymbol{e}}_I^w \right\|_{\Omega_p}^2 d\tau. \qquad (2.25)
\end{aligned}
$$

By employing the Young's inequality, it holds:

$$
\begin{aligned}
\|\boldsymbol{E}_h\|_E^2 \lesssim & |||\boldsymbol{e}_I^u|||_{\mathrm{dG,e}}^2 + \left|||e_h^\varphi|||_{\mathrm{dG,a}}^2 + |||\beta \boldsymbol{e}_I^u + \boldsymbol{e}_I^w|||_{\mathrm{dG,p}}^2 \right. \\
& + \int_0^t \eta k^{-1} \left\| \dot{\boldsymbol{e}}_I^w \right\|_{\Omega_p}^2 d\tau \\
& + \int_0^t \left[\|\dot{\boldsymbol{e}}_I^u\|_{\mathcal{E},e} + \left\| \dot{e}_I^\varphi \right\|_{\mathcal{E},a} + \|\beta \dot{\boldsymbol{e}}_I^u + \dot{\boldsymbol{e}}_I^w\|_{\mathcal{E},p} \right. \\
& \quad + |||\dot{\boldsymbol{e}}_I^u|||_{\mathrm{dG,e}} + \left|||\dot{e}_I^\varphi|||_{\mathrm{dG,a}} + |||\beta \dot{\boldsymbol{e}}_I^u + \dot{\boldsymbol{e}}_I^w|||_{\mathrm{dG,p}} \right. \\
& \quad \left. \left. + \mathcal{I}_h^a(\dot{e}_I^\varphi) + \mathcal{I}_h^p(\dot{\boldsymbol{e}}_I^u + k_{int} \dot{\boldsymbol{e}}_I^w) \right] \|\boldsymbol{E}_h\|_{\mathcal{E}} \, d\tau. \right. \qquad (2.26)
\end{aligned}
$$

By defining:

$$
\begin{aligned}
\mathcal{C}^2(\boldsymbol{e}_I^u, \boldsymbol{e}_I^w, e_I^\varphi) &= |||\boldsymbol{e}_I^u|||_{\mathrm{dG,e}}^2 + \left|||e_h^\varphi|||_{\mathrm{dG,a}}^2 + |||\beta \boldsymbol{e}_I^u + \boldsymbol{e}_I^w|||_{\mathrm{dG,p}}^2 + \int_0^t \eta k^{-1} \left\| \dot{\boldsymbol{e}}_I^w \right\|_{\Omega_p}^2 d\tau \\
\mathcal{D}(\dot{\boldsymbol{e}}_I^u, \dot{\boldsymbol{e}}_I^w, \dot{e}_I^\varphi) &= \|\dot{\boldsymbol{e}}_I^u\|_{\mathcal{E},e} + \left\| \dot{e}_I^\varphi \right\|_{\mathcal{E},a} + \|\beta \dot{\boldsymbol{e}}_I^u + \dot{\boldsymbol{e}}_I^w\|_{\mathcal{E},p} \\
&\quad + |||\dot{\boldsymbol{e}}_I^u|||_{\mathrm{dG,e}} + \left|||\dot{e}_I^\varphi|||_{\mathrm{dG,a}} + |||\beta \dot{\boldsymbol{e}}_I^u + \dot{\boldsymbol{e}}_I^w|||_{\mathrm{dG,p}} + \mathcal{I}_h^a(\dot{e}_I^\varphi) + \mathcal{I}_h^p(\dot{\boldsymbol{e}}_I^u + k_{int} \dot{\boldsymbol{e}}_I^w),
\end{aligned}
$$

equation (2.26) reduces to:

$$
\|\boldsymbol{E}_h\|_E^2 \lesssim \mathcal{C}^2(\boldsymbol{e}_I^u, \boldsymbol{e}_I^w, e_I^\varphi) + \int_0^t \mathcal{D}(\dot{\boldsymbol{e}}_I^u, \dot{\boldsymbol{e}}_I^w, \dot{e}_I^\varphi) \, \|\boldsymbol{E}_h\|_E \, d\tau
$$

and, by employing Gronwall's lemma:

$$
\|\boldsymbol{E}_h\|_E \lesssim \mathcal{C}(\boldsymbol{e}_I^u, \boldsymbol{e}_I^w, e_I^\varphi) + \int_0^t \mathcal{D}(\dot{\boldsymbol{e}}_I^u, \dot{\boldsymbol{e}}_I^w, \dot{e}_I^\varphi) d\tau,
$$

We point out that in order to bound term $\mathcal{C}$ it has been used estimates in Lemma 4, together with standard estimates as in [62]. To estimate term $\mathcal{D}$, it has been used again

estimates in Lemma 5 and the following ones for $\mathcal{I}_h^a(e_I^\varphi)$ and $\mathcal{I}_h^p(\boldsymbol{e}_I^u + k_{int}\boldsymbol{e}_I^w)$:

$$\mathcal{I}_h^a(e_I^\varphi) \lesssim \sum_{k\in\mathcal{T}_{h,I}^a} \frac{h_k^{s_k^\varphi-1}}{p_{\varphi,k}^{n-3/2}} \left\|\tilde{\mathcal{E}}\varphi\right\|_{n,\mathcal{K}}$$

$$\mathcal{I}_h^p(\boldsymbol{e}_I^u + k_{int}\boldsymbol{e}_I^w) \lesssim \sum_{k\in\mathcal{T}_{h,I}^p} \frac{h_k^{s_k^u-1}}{p_{u,k}^{m-3/2}} \left\|\tilde{\mathcal{E}}\boldsymbol{u}\right\|_{m,\mathcal{K}} + \sum_{k\in\mathcal{T}_{h,I}^p} \frac{h_k^{s_k^w-1}}{p_{w,k}^{l-3/2}} \left\|\tilde{\mathcal{E}}\boldsymbol{w}\right\|_{l,\mathcal{K}}.$$

By collecting all bounds, the following error estimate is achieved:

$$\begin{aligned}
\|\boldsymbol{E}\|_E \lesssim & \sum_{k\in\mathcal{T}_h^p} \frac{h_k^{2(s_k^u-1)}}{p_{u,k}^{m-3/2}} \left(\left\|\tilde{\mathcal{E}}\dot{\boldsymbol{u}}\right\|_{m,\mathcal{K}} + \left\|\tilde{\mathcal{E}}\boldsymbol{u}\right\|_{m,\mathcal{K}} + \int_0^t \left[\left\|\tilde{\mathcal{E}}\ddot{\boldsymbol{u}}\right\|_{m,\mathcal{K}} + \left\|\tilde{\mathcal{E}}\dot{\boldsymbol{u}}\right\|_{m,\mathcal{K}} \right] d\tau \right) \\
& + \sum_{k\in\mathcal{T}_h^p} \frac{h_k^{2(s_k^w-1)}}{p_{w,k}^{l-3/2}} \left(\left\|\tilde{\mathcal{E}}\dot{\boldsymbol{w}}\right\|_{l,\mathcal{K}} + \left\|\tilde{\mathcal{E}}\boldsymbol{w}\right\|_{l,\mathcal{K}} + \int_0^t \left[\left\|\tilde{\mathcal{E}}\ddot{\boldsymbol{w}}\right\|_{l,\mathcal{K}} + \left\|\tilde{\mathcal{E}}\dot{\boldsymbol{w}}\right\|_{l,\mathcal{K}} \right] d\tau \right) \\
& + \sum_{k\in\mathcal{T}_h^a} \frac{h_k^{2(s_k^\varphi-1)}}{p_{\varphi,k}^{n-3/2}} \left(\left\|\tilde{\mathcal{E}}\dot{\varphi}\right\|_{n,\mathcal{K}} + \left\|\tilde{\mathcal{E}}\varphi\right\|_{n,\mathcal{K}} + \int_0^t \left[\left\|\tilde{\mathcal{E}}\ddot{\varphi}\right\|_{n,\mathcal{K}} + \left\|\tilde{\mathcal{E}}\dot{\varphi}\right\|_{n,\mathcal{K}} \right] d\tau \right), \quad (2.27)
\end{aligned}$$

that concludes the proof. □

2.7 Algebraic Formulation

In order to define the corresponding algebraic formulation, the dG bilinear forms listed in previous section are now associated to corresponding matrices. Observe that the dG structure of bilinear forms descending by the integration by parts, seen as the contribute of four terms, is now lost and simplified into the notation of a general matrix. Mass matrices have been simply associated to bilinear forms as shown here below:

$$\begin{aligned}
(\boldsymbol{M}_a)_{ij} &= \int_{\Omega_a} \rho_a c^{-2} \psi_j \psi_i, && \forall\ i,j \in \{1,\dots,N_{h,a}\}, \\
(\boldsymbol{M}_p)_{ij} &= \int_{\Omega_p} \boldsymbol{\phi}_j \boldsymbol{\phi}_i, && \forall\ i,j \in \{1,\dots,N_{h,p}\}, \\
(\boldsymbol{M}_p^\rho)_{ij} &= \int_{\Omega_p} \rho \boldsymbol{\phi}_j \boldsymbol{\phi}_i, && \forall\ i,j \in \{1,\dots,N_{h,p}\}, \\
(\boldsymbol{M}_p^{\rho_f})_{ij} &= \int_{\Omega_p} \rho_f \boldsymbol{\phi}_j \boldsymbol{\phi}_i, && \forall\ i,j \in \{1,\dots,N_{h,p}\}, \\
(\boldsymbol{M}_p^{\rho_w})_{ij} &= \int_{\Omega_p} \rho_w \boldsymbol{\phi}_j \boldsymbol{\phi}_i, && \forall\ i,j \in \{1,\dots,N_{h,p}\}.
\end{aligned}$$

Other matrices are defined as:

$$\begin{aligned}
(\boldsymbol{A}_a)_{ij} &= \mathcal{A}_h^a(\psi_j,\psi_i), && \forall\ i,j \in \{1,\dots,N_{h,a}\}, \\
(\boldsymbol{A}_p)_{ij} &= \mathcal{A}_h^p(\boldsymbol{\phi}_j,\boldsymbol{\phi}_i), && \forall\ i,j \in \{1,\dots,N_{h,p}\},
\end{aligned}$$

$$(\boldsymbol{B}_p)_{ij} = \mathcal{B}_h^p(\boldsymbol{\phi}_j, \boldsymbol{\phi}_i), \qquad \forall\, i,j \in \{1,\dots,N_{h,p}\}.$$

Here $N_{h,a}$ and $N_{h,p}$ denote the number of element-wise discontinuous basis functions defined over $\boldsymbol{V}_h^a$ and $\boldsymbol{V}_h^p$, respectively.
These last three elements could be moreover decomposed individually into the sum of the following four matrices:

- $\boldsymbol{V}$, volume term;
- $-\boldsymbol{I}$, consistency term;
- $-\boldsymbol{I}^T$, symmetry term;
- $\boldsymbol{S}$, stabilization term.

This structure will be considered in the numerical implementation of the proposed dG method.
More precisely for the three terms $\mathcal{A}^a$, $\mathcal{A}^p$ and $\mathcal{B}^p$ the decomposition reads as follows:

- $\boldsymbol{A}_a = \boldsymbol{V}_a - \boldsymbol{I}_a^T - \boldsymbol{I}_a + \boldsymbol{S}_a$, where:

$$\begin{aligned}
\boldsymbol{V}_a(i,j) &= \sum_{K\in\mathcal{T}_h^a} \int_K \rho_a \nabla_h\varphi_j \cdot \nabla_h\varphi_i,\\
\boldsymbol{I}_a(i,j) &= \sum_{F\in\mathcal{F}_h^a} \int_F [\![\varphi_j]\!] \cdot \{\!\{\rho_a \nabla_h\varphi_i\}\!\},\\
\boldsymbol{S}_a(i,j) &= \sum_{F\in\mathcal{F}_h^a} \int_F \chi [\![\varphi_j]\!] \cdot [\![\varphi_i]\!], \qquad \forall\, i,j \in \{1,\dots,N_{h,a}\}.
\end{aligned}$$

- $\boldsymbol{A}_p = \boldsymbol{V}_{p,1} - \boldsymbol{I}_{p,1}^T - \boldsymbol{I}_{p,1} + \boldsymbol{S}_{p,1}$, where:

$$\begin{aligned}
\boldsymbol{V}_{p,1}(i,j) &= \sum_{K\in\mathcal{T}_h^p} \int_K \boldsymbol{\sigma}_h(\boldsymbol{\phi}_j) : \boldsymbol{\epsilon}_h(\boldsymbol{\phi}_i),\\
\boldsymbol{I}_{p,1}(i,j) &= \sum_{F\in\mathcal{F}_h^p} \int_F [\![\boldsymbol{\phi}_j]\!] : \{\!\{\boldsymbol{\sigma}_h(\boldsymbol{\phi}_i)\}\!\},\\
\boldsymbol{S}_{p,1}(i,j) &= \sum_{F\in\mathcal{F}_h^p} \int_F \eta [\![\boldsymbol{\phi}_j]\!] : [\![\boldsymbol{\phi}_i]\!], \qquad \forall\, i,j \in \{1,\dots,N_{h,p}\}.
\end{aligned}$$

- $\boldsymbol{B}_p = \boldsymbol{V}_{p,2} - \boldsymbol{I}_{p,2}^T - \boldsymbol{I}_{p,2} + \boldsymbol{S}_{p,2}$, where:

$$\begin{aligned}
\boldsymbol{V}_{p,2}(i,j) &= \sum_{K\in\mathcal{T}_h^p} \int_K m(\nabla_h\cdot\boldsymbol{\phi}_j)(\nabla_h\cdot\boldsymbol{\phi}_i),\\
\boldsymbol{I}_{p,2}(i,j) &= \sum_{F\in\mathcal{F}_h^p} \int_F [\![\boldsymbol{\phi}_j]\!] \{\!\{m(\nabla_h\cdot\boldsymbol{\phi}_i)\boldsymbol{I}\}\!\},
\end{aligned}$$

$$\boldsymbol{S}_{p,2}(i,j) = \sum_{F\in\mathcal{F}_h^p} \int_F \gamma[\![\boldsymbol{\phi}_j]\!][\![\boldsymbol{\phi}_i]\!], \qquad \forall\ i,j \in \{1,\dots,N_{h,p}\}.$$

For the coupling bilinear forms, we define:

$$(\boldsymbol{C}_a)_{ij} = \mathcal{C}_h^a(\psi_j, \boldsymbol{\phi}_i), \qquad \forall i \in \{1,\dots,N_{h,p}\},\ \forall j \in \{1,\dots,N_{h,a}\},$$
$$(\boldsymbol{C}_p)_{ij} = \mathcal{C}_h^p(\boldsymbol{\phi}_j, \psi_i), \qquad \forall i \in \{1,\dots,N_{h,a}\},\ \forall j \in \{1,\dots,N_{h,p}\}.$$

Equation (2.3) can therefore be rewritten as:

$$\begin{aligned}
&\boldsymbol{M}_p^{\rho}\ddot{U}(t) + \boldsymbol{M}_p^{\rho_f}\ddot{W}(t) + \boldsymbol{A}_p U(t) + \beta^2 \boldsymbol{B}_p U(t) + \beta \boldsymbol{B}_p W(t) + \boldsymbol{C_p}\dot{\Phi}(t) \\
&+ \boldsymbol{M}_p^{\rho_f}\ddot{U}(t) + \boldsymbol{M}_p^{\rho_w}\ddot{W}(t) + \eta k^{-1}\boldsymbol{M}_p\dot{W}(t) + \beta \boldsymbol{B}_p U(t) + \boldsymbol{B}_p W(t) + k_{int}\boldsymbol{C_p}\dot{\Phi}(t) \\
&+ \boldsymbol{C}_a\dot{U}(t) + k_{int}\boldsymbol{C}_a\dot{W}(t) + \boldsymbol{M}_a\ddot{\Phi}(t) + \boldsymbol{A}_a\Phi(t) \\
&= \boldsymbol{F}_p(t) + \boldsymbol{G}_p(t) + \boldsymbol{F}_a(t),
\end{aligned} \tag{2.28}$$

with initial conditions:

$$\begin{cases} U(0) = U_0;\ W(0) = W_0;\ \Phi(0) = \Phi_0, \\ \dot{U}(0) = U_1;\ \dot{W}(0) = W_1;\ \dot{\Phi}(0) = \Phi_1. \end{cases}$$

In order to fully discretize equation (2.28), different time discretization schemes have been introduced, as it is described in the following.

2.7.1 Leapfrog scheme

A first approach considered is leapfrog method. The time interval $[0,T]$ has been discretized by introducing a timestep $\Delta t > 0$, such that $\forall\ k \in \mathbb{N}$, $t_{k+1} - t_k = \Delta t$, as shown in Figure 2.2. We define U^k as $U^k = U(t^k)$. Time derivatives are approximated

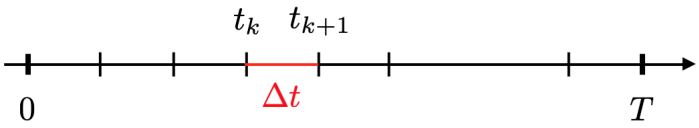

Figure 2.2: Discretization of time interval $[0,T]$

as follows:

$$\dot{U}^i \approx \frac{U^{i+1} - U^{i-1}}{2\Delta t} \tag{2.29}$$

$$\ddot{U}^i \approx \frac{U^{i-1} - 2U^i + U^{i+1}}{\Delta t^2}. \tag{2.30}$$

A notation $(\cdot^\star)$ has been introduced to take into account a general scenario (semi-implicit or fully-implicit). By plugging (2.29) and (2.30) into (2.28), we get:

$$\boldsymbol{M}_p^{\rho}\frac{U^{i-1}-2U^i+U^{i+1}}{\Delta t^2}+\boldsymbol{M}_p^{\rho_f}\frac{W^{i-1}-2W^i+W^{i+1}}{\Delta t^2}$$
$$+\boldsymbol{A}_pU^\star+\beta^2\boldsymbol{B}_pU^\star+\beta\boldsymbol{B}_pW^\star+\boldsymbol{C_p}\frac{\Phi^{i+1}-\Phi^{i-1}}{2\Delta t}=\boldsymbol{F}_p^\star,$$

$$\boldsymbol{M}_p^{\rho_f}\frac{U^{i-1}-2U^i+U^{i+1}}{\Delta t^2}+\boldsymbol{M}_p^{\rho_w}\frac{W^{i-1}-2W^i+W^{i+1}}{\Delta t^2}$$
$$+\eta k^{-1}\boldsymbol{M}_p\frac{W^{i+1}-W^{i-1}}{2\Delta t}+\beta\boldsymbol{B}_pU^\star+\boldsymbol{B}_pW^\star+k_{int}\boldsymbol{C_p}\frac{\Phi^{i+1}-\Phi^{i-1}}{2\Delta t}=\boldsymbol{G}_p^\star,$$

$$\boldsymbol{C}_a\frac{U^{i+1}-U^{i-1}}{2\Delta t}+k_{int}\boldsymbol{C}_a\frac{W^{i+1}-W^{i-1}}{2\Delta t}+\boldsymbol{M}_a\frac{\Phi^{i-1}-2\Phi^i+\Phi^{i+1}}{\Delta t^2}+\boldsymbol{A}_a\Phi^\star=\boldsymbol{F}_a^\star.$$

If $\star=i$, the semi-implicit case will be considered, whereas if $\star=i+1$, the fully-implicit one will be taken into account. The system has been therefore rewritten as:

$$\begin{cases}\boldsymbol{M}_p^{\rho}(U^{i-1}-2U^i+U^{i+1})+\boldsymbol{M}_p^{\rho_f}(W^{i-1}-2W^i+W^{i+1})\\ +\Delta t^2\boldsymbol{A}_pU^\star+\Delta t^2\beta^2\boldsymbol{B}_pU^\star+\Delta t^2\beta\boldsymbol{B}_pW^\star+\dfrac{\Delta t}{2}\boldsymbol{C_p}(\Phi^{i+1}-\Phi^{i-1})=\Delta t^2\boldsymbol{F}_p^\star,\\ \\ \boldsymbol{M}_p^{\rho_f}(U^{i-1}-2U^i+U^{i+1})+\boldsymbol{M}_p^{\rho_w}(W^{i-1}-2W^i+W^{i+1})\\ +\dfrac{\Delta t}{2}\eta k^{-1}\boldsymbol{M}_p(W^{i+1}-W^{i-1})+\Delta t^2\beta\boldsymbol{B}_pU^\star+\Delta t^2\boldsymbol{B}_pW^\star\\ +k_{int}\dfrac{\Delta t}{2}\boldsymbol{C_p}(\Phi^{i+1}-\Phi^{i-1})=\Delta t^2\boldsymbol{G}_p^\star,\\ \\ \dfrac{\Delta t}{2}\boldsymbol{C_a}(U^{i+1}-U^{i-1})+k_{int}\dfrac{\Delta t}{2}\boldsymbol{C_a}(W^{i+1}-W^{i-1})+\\ \boldsymbol{M}_a(\Phi^{i-1}-2\Phi^i+\Phi^{i+1})+\Delta t^2\boldsymbol{A}_a\Phi^\star=\Delta t^2\boldsymbol{F}_a^\star,\end{cases}$$

with initial conditions

$$\begin{cases}U^0=U_0;\ W^0=W_0;\ \Phi^0=\Phi_0,\\ U^1=U_1;\ W^1=W_1;\ \Phi^1=\Phi_1.\end{cases}$$

Collecting together matrices associated to the three time instants for the discretization, the semi-implicit and fully-implicit schemes are shown below.

Semi-implicit formulation:

$$\boldsymbol{K}^{i-1} = \begin{bmatrix} \boldsymbol{M}_p^{\rho} & \boldsymbol{M}_p^{\rho_f} & -\frac{\Delta t}{2}\boldsymbol{C}_p \\ \boldsymbol{M}_p^{\rho_f} & \boldsymbol{M}_p^{\rho_w} - \eta k^{-1}\frac{\Delta t}{2}\boldsymbol{M}_p & -k_{int}\frac{\Delta t}{2}\boldsymbol{C}_p \\ -\frac{\Delta t}{2}\boldsymbol{C}_a & -k_{int}\frac{\Delta t}{2}\boldsymbol{C}_a & \boldsymbol{M}_a \end{bmatrix},$$

$$\boldsymbol{K}^{i} = \begin{bmatrix} -2\boldsymbol{M}_p^{\rho} + \Delta t^2\boldsymbol{A}_p + \Delta t^2\beta^2\boldsymbol{B}_p & -2\boldsymbol{M}_p^{\rho_f} + \Delta t^2\beta\boldsymbol{B}_p & \boldsymbol{0} \\ -2\boldsymbol{M}_p^{\rho_f} + \Delta t^2\beta\boldsymbol{B}_p & -2\boldsymbol{M}_p^{\rho_w} + \Delta t^2\boldsymbol{B}_p & \boldsymbol{0} \\ \boldsymbol{0} & \boldsymbol{0} & -2\boldsymbol{M}_a + \Delta t^2\boldsymbol{A}_a \end{bmatrix},$$

$$\boldsymbol{K}^{i+1} = \begin{bmatrix} \boldsymbol{M}_p^{\rho} & \boldsymbol{M}_p^{\rho_f} & \frac{\Delta t}{2}\boldsymbol{C_p} \\ \boldsymbol{M}_p^{\rho_f} & \boldsymbol{M}_p^{\rho_w} + \eta k^{-1}\frac{\Delta t}{2}\boldsymbol{M}_p & k_{int}\frac{\Delta t}{2}\boldsymbol{C_p} \\ \frac{\Delta t}{2}\boldsymbol{C_a} & k_{int}\frac{\Delta t}{2}\boldsymbol{C_a} & \boldsymbol{M}_a \end{bmatrix}$$

and

$$\boldsymbol{F} = \Delta t^2 \begin{bmatrix} \boldsymbol{F}_p^i, & \boldsymbol{G}_p^i, & \boldsymbol{F}_a^i \end{bmatrix}^T.$$

Fully-implicit formulation:

$$\boldsymbol{K}^{i-1} = \begin{bmatrix} \boldsymbol{M}_p^{\rho} & \boldsymbol{M}_p^{\rho_f} & -\frac{\Delta t}{2}\boldsymbol{C_p} \\ \boldsymbol{M}_p^{\rho_f} & \boldsymbol{M}_p^{\rho_w} - \eta k^{-1}\frac{\Delta t}{2}\boldsymbol{M}_p & -k_{int}\frac{\Delta t}{2}\boldsymbol{C_p} \\ -\frac{\Delta t}{2}\boldsymbol{C_a} & -k_{int}\frac{\Delta t}{2}\boldsymbol{C_a} & \boldsymbol{M}_a \end{bmatrix},$$

$$\boldsymbol{K}^{i} = \begin{bmatrix} -2\boldsymbol{M}_p^{\rho} & -2\boldsymbol{M}_p^{\rho_f} & \boldsymbol{0} \\ -2\boldsymbol{M}_p^{\rho_f} & -2\boldsymbol{M}_p^{\rho_w} & \boldsymbol{0} \\ \boldsymbol{0} & \boldsymbol{0} & -2\boldsymbol{M}_a \end{bmatrix},$$

$$\boldsymbol{K}^{i+1} = \begin{bmatrix} \boldsymbol{M}_p^{\rho} + \Delta t^2\boldsymbol{A}_p + \Delta t^2\beta^2\boldsymbol{B}_p & \boldsymbol{M}_p^{\rho_f} + \Delta t^2\beta\boldsymbol{B}_p & \frac{\Delta t}{2}\boldsymbol{C_p} \\ \boldsymbol{M}_p^{\rho_f} + \Delta t^2\beta\boldsymbol{B}_p & \boldsymbol{M}_p^{\rho_w} + \eta k^{-1}\frac{\Delta t}{2}\boldsymbol{M}_p & k_{int}\frac{\Delta t}{2}\boldsymbol{C_p} \\ \frac{\Delta t}{2}\boldsymbol{C_a} & k_{int}\frac{\Delta t}{2}\boldsymbol{C_a} & \boldsymbol{M}_a + \Delta t^2\boldsymbol{A}_a \end{bmatrix}$$

and

$$\boldsymbol{F} = \Delta t^2 \begin{bmatrix} \boldsymbol{F}_p^{i+1}, & \boldsymbol{G}_p^{i+1}, & \boldsymbol{F}_a^{i+1} \end{bmatrix}^T.$$

A vector of unknowns has been introduced for each time instant and defined as:

$$\boldsymbol{X^*} = \begin{bmatrix} U^*, & W^*, & \Phi^* \end{bmatrix}^T,$$

where $\cdot^* := \cdot^{(i-1)}, \cdot^{(i)}, \cdot^{(i+1)}$.

Finally, the linear system reads as:

$$\boldsymbol{K}^{i-1}\boldsymbol{X}^{i-1} + \boldsymbol{K}^{i}\boldsymbol{X}^{i} + \boldsymbol{K}^{i+1}\boldsymbol{X}^{i+1} = \boldsymbol{F},$$

or equivalently:

$$\boldsymbol{K}^{i+1}\boldsymbol{X}^{i+1} = \tilde{\boldsymbol{F}}(\boldsymbol{X}^{i-1}, \boldsymbol{X}^{i}). \tag{2.31}$$

It's important to stress the fact that, differently from the fully-implicit scheme, the semi-implicit one needs a Courant-Friedrichs-Lewy (CFL, [30]) condition in order to avoid stability issues. In particular, the condition reads as $\Delta t \leq C_{CFL}\ h$, where the constant C_{CFL} is related to the polynomial degree and the characteristic velocities of the acoustic and poroelastic waves.

2.7.2 Newmark scheme

Another time discretization that can be used is the *Newmark-beta method* (see e.g. [34]). Equation (2.28) is rewritten in algebraic form as:

$$\begin{bmatrix} \boldsymbol{M}_p^{\rho} & \boldsymbol{M}_p^{\rho_f} & \boldsymbol{0} \\ \boldsymbol{M}_p^{\rho_f} & \boldsymbol{M}_p^{\rho_w} & \boldsymbol{0} \\ \boldsymbol{0} & \boldsymbol{0} & \boldsymbol{M}_a \end{bmatrix} \begin{bmatrix} \ddot{U} \\ \ddot{W} \\ \ddot{\Phi} \end{bmatrix} + \begin{bmatrix} \boldsymbol{0} & \boldsymbol{0} & \boldsymbol{C}_p \\ \boldsymbol{0} & \eta k^{-1}\boldsymbol{M}_p & k_{int}\boldsymbol{C}_p \\ \boldsymbol{C}_a & k_{int}\boldsymbol{C}_a & \boldsymbol{0} \end{bmatrix} \begin{bmatrix} \dot{U} \\ \dot{W} \\ \dot{\Phi} \end{bmatrix} +$$

$$\begin{bmatrix} \boldsymbol{A}_p + \beta^2\boldsymbol{B}_p & \beta\boldsymbol{B}_p & \boldsymbol{0} \\ \beta\boldsymbol{B}_p & \boldsymbol{B}_p & \boldsymbol{0} \\ \boldsymbol{0} & \boldsymbol{0} & \boldsymbol{A}_a \end{bmatrix} \begin{bmatrix} U^\star \\ W^\star \\ \Phi^\star \end{bmatrix} = \begin{bmatrix} \boldsymbol{F}_p^\star \\ \boldsymbol{G}_p^\star \\ \boldsymbol{F}_a^\star \end{bmatrix}. \tag{2.32}$$

Equation (2.32) can be rewritten in compact form:

$$\boldsymbol{A}\ddot{\boldsymbol{X}} + \boldsymbol{B}\dot{\boldsymbol{X}} + \boldsymbol{C}\boldsymbol{X} = \boldsymbol{F}. \tag{2.33}$$

By expliciting the second time derivative:

$$\ddot{\boldsymbol{X}} = \boldsymbol{A}^{-1}(\boldsymbol{F} - \boldsymbol{B}\dot{\boldsymbol{X}} - \boldsymbol{C}\boldsymbol{X}) = \boldsymbol{A}^{-1}\boldsymbol{F} - \boldsymbol{A}^{-1}\boldsymbol{B}\dot{\boldsymbol{X}} - \boldsymbol{A}^{-1}\boldsymbol{C}\boldsymbol{X} = \mathcal{L}(t, \boldsymbol{X}, \dot{\boldsymbol{X}}),$$

that yields to:

$$\begin{cases} \ddot{\boldsymbol{X}} = \mathcal{L}(t, \boldsymbol{X}, \dot{\boldsymbol{X}}) \\ \dot{\boldsymbol{X}}(0) = \boldsymbol{X}_0 \\ \boldsymbol{X}(0) = \boldsymbol{X}_1. \end{cases} \tag{2.34}$$

The Newmark scheme is defined by introducing a Taylor expansion for displacement and velocity, respectively:

$$\begin{cases} \boldsymbol{X}^{k+1} = \boldsymbol{X}^k + \Delta t \boldsymbol{Z}^k + \Delta t^2(\beta_N \mathcal{L}^{k+1} + (\frac{1}{2} - \beta_N)\mathcal{L}^k) \\ \boldsymbol{Z}^{k+1} = \boldsymbol{Z}^k + \Delta t(\gamma_N \mathcal{L}^{k+1} + (1 - \gamma_N)\mathcal{L}^k), \end{cases} \tag{2.35}$$

where $\boldsymbol{Z}^k = \dot{\boldsymbol{Z}}(t^k)$, $\mathcal{L}^k = \mathcal{L}(t^k, \boldsymbol{X}^k, \boldsymbol{Z}^k)$ and the Newmark parameters β_N and γ_N satisfy (see [57]) the following constraints:

$$0 \leq \gamma_N \leq 1,$$

$$0 \leq 2\beta_N \leq 1.$$

The typical choices of parameters are $\gamma_N = 1/2$ and $\beta_N = 1/4$.
By plugging the definition of $\mathcal{L}$ into (2.35), the time integration reduces to:

$$\begin{bmatrix} \boldsymbol{A} + \Delta t^2 \beta_N \boldsymbol{C} & \Delta t^2 \beta_N \boldsymbol{B} \\ \gamma_N \Delta t \boldsymbol{C} & \boldsymbol{A} + \gamma_N \Delta t \boldsymbol{B} \end{bmatrix} \begin{bmatrix} \boldsymbol{X}^{k+1} \\ \boldsymbol{Z}^{k+1} \end{bmatrix} =$$
$$\begin{bmatrix} \boldsymbol{A} - \Delta t^2(\frac{1}{2} - \beta_N)\boldsymbol{C} & \Delta t \boldsymbol{A} - \Delta t^2(\frac{1}{2} - \beta_N)\boldsymbol{B} \\ -(1 - \gamma_N)\Delta t \boldsymbol{C} & \boldsymbol{A} - (1 - \gamma_N)\Delta t \boldsymbol{B} \end{bmatrix} \begin{bmatrix} \boldsymbol{X}^k \\ \boldsymbol{Z}^k \end{bmatrix} +$$
$$\begin{bmatrix} \Delta t^2 \beta_N \boldsymbol{F}^{k+1} \\ \gamma_N \Delta t \boldsymbol{F}^{k+1} \end{bmatrix} + \begin{bmatrix} \Delta t^2(\frac{1}{2} - \beta_N)\boldsymbol{F}^k \\ (1 - \gamma_N)\Delta t \boldsymbol{F}^k \end{bmatrix}. \tag{2.36}$$

2.7.3 The generalized-α method

We consider also a generalization of the Newmark scheme, as in [35]. As done in the previous subsection, the system has been simplified into equation (2.33). Taylor expansions defined in equation (2.35) are again taken into account. By introducing parameters α_m and α_f, intermediate time discretization instants are considered as shown below:

$$\begin{aligned} \boldsymbol{X}^{k+1-\alpha_f} &= (1 - \alpha_f)\boldsymbol{X}^{k+1} + \alpha_f \boldsymbol{X}^k, \\ \boldsymbol{Z}^{k+1-\alpha_f} &= (1 - \alpha_f)\boldsymbol{Z}^{k+1} + \alpha_f \boldsymbol{Z}^k. \end{aligned} \tag{2.37}$$

In order to discretize the second time derivative, the notation $\boldsymbol{J}^k = \ddot{\boldsymbol{X}}(t^k)$ is introduced. Acceleration is discretized at intermediate nodes as:

$$\boldsymbol{J}^{k+1-\alpha_m} = (1-\alpha_m)\boldsymbol{J}^{k+1} + \alpha_m \boldsymbol{J}^k. \tag{2.38}$$

Equation (2.33) is rewritten in terms of intermediate nodes:

$$\boldsymbol{A}\boldsymbol{J}^{k+1-\alpha_m} + \boldsymbol{B}\boldsymbol{Z}^{k+1-\alpha_f} + \boldsymbol{C}\boldsymbol{X}^{k+1-\alpha_f} = \boldsymbol{F}^{k+1-\alpha_f}. \tag{2.39}$$

Equations (2.37) and (2.38) are plugged into equation (2.39), yielding:

$$\begin{aligned}
&\left[(1-\alpha_m)\boldsymbol{A} + \Delta t(1-\alpha_f)\gamma_N \boldsymbol{B} + \Delta t^2(1-\alpha_f)\beta_N \boldsymbol{C}\right]\boldsymbol{J}^{k+1} = \\
&-\boldsymbol{C}\boldsymbol{X}^k - \left[\boldsymbol{B} + \Delta t(1-\alpha_f)\boldsymbol{C}\right]\boldsymbol{Z}^k - \\
&\left[\alpha_m \boldsymbol{A} + \Delta t(1-\alpha_f)(1-\gamma_N)\boldsymbol{B} + \Delta t^2(1-\alpha_f)(\frac{1}{2}-\beta_N)\boldsymbol{C}\right]\boldsymbol{J}^k + \\
&(1-\alpha_f)\boldsymbol{F}^{k+1} + \alpha_f \boldsymbol{F}^k,
\end{aligned}$$

that leads to

$$\begin{cases}
\boldsymbol{J}^{k+1} = \boldsymbol{\phi}(t, \boldsymbol{X}^k, \boldsymbol{Z}^k, \boldsymbol{J}^k), \\
\boldsymbol{X}^0 = \boldsymbol{x}_0, \\
\boldsymbol{Z}^0 = \boldsymbol{z}_0, \\
\boldsymbol{J}^0 = \boldsymbol{A}^{-1}(\boldsymbol{F}^0 - \boldsymbol{B}\boldsymbol{Z}^0 - \boldsymbol{C}\boldsymbol{X}^0).
\end{cases} \tag{2.40}$$

In order to have an unconditionally stable method, the following constraints have to be satisfied:

$$\begin{aligned}
\gamma_N &= \frac{1}{2} - \alpha_m + \alpha_f, \\
\alpha_m &\leq \alpha_f \leq \frac{1}{2}, \\
\beta_N &\geq \frac{1}{4} + \frac{1}{2}(\alpha_f - \alpha_m).
\end{aligned}$$

Chapter 3

Numerical results

Numerical implementation has been carried out through the software MATLAB[1]. The code used in [6] has been modified by introducing matrices corresponding to the poroelastic part and ensuring appropriate boundary conditions. Different time discretizations presented in Section 2.7 have been implemented. Meshes have been generated through the `polymesher` software (see [60],[73]). The latter routine ensures a polygonal mesh generation, respecting grid Assumptions (2.2.1), (2.2.2) and (2.2.3) stated in Section 2.2. The `polymesher` function included in article [73] has been modified by overturning the generated square (rectangle), over the interface Γ_I. In Figure 3.1, some examples of meshes generated by varying the number of polygons are shown.

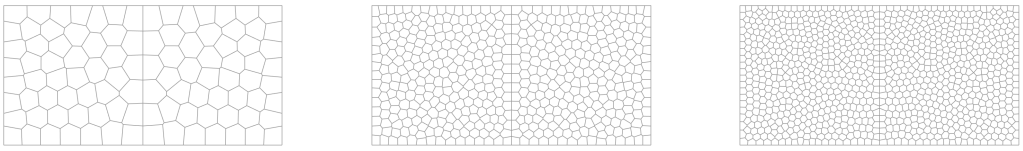

Figure 3.1: Examples of meshes generated with `polymesher`:
number of polygons $N = 100,\ 500,\ 1000$

3.1 Remarks on the Matlab code

From the MATLAB implementation point of view, the main coding work has been done by modifying the assembly phase defined in the `matrix2D.m` function. As presented in [7], a new theoretical dG analysis has extended previous theory on dG methods from triangles to polygons. From the practical point of view, since bilinear forms have been split by construction into volumetric and interface terms, two kinds of integration have been therefore considered. Sub-triangulation has been introduced as shown in Figure

[1]MATLAB 2019a, The MathWorks, Inc., Natick, Massachusetts, United States.

3.2a. It is shown the case for $p = 2$ polynomial degree and 2D quadrature nodes equal to $(2p + 1)^d$ for each triangle. 2D quadrature nodes have been used to compute integrals defined over the whole volumes, crucial aspect of this analysis when dealing with cost of computational time, drastically reduced through most recent quadrature free formula (see [7]). Instead interface integrals (and coupling integrals) have been calcu-

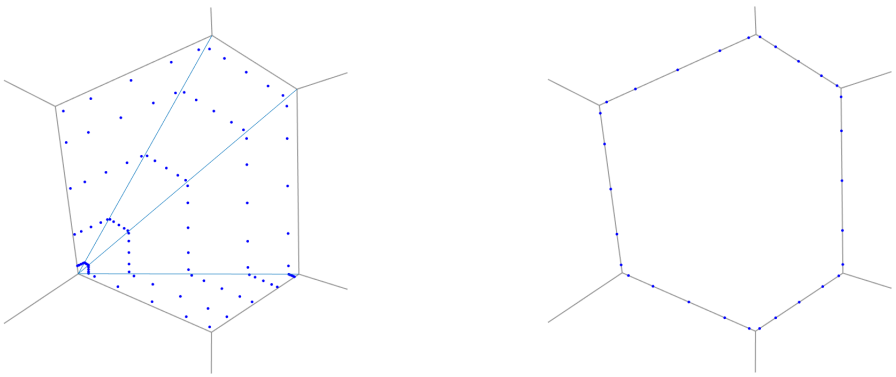

(a) Sub-triangulation and 2D quadrature nodes

(b) 1D quadrature nodes

Figure 3.2: Quadrature nodes over polygons for $p = 2$

lated by 1D quadrature formulas defined on edges of polygons, as shown in Figure 3.2b.

In the following pseudocode it has been resumed different `for` cycles that have been used inside the MATLAB function, in order to evaluate volume and interface integrals. For the sake of simplicity it has been chosen to keep only the skeleton of the function, avoiding to represent all variables involved.

Listing 3.1: Pseudocode of `matrix2D.m`

```
function [Matrices]= matrix2D(femregion,neighbour,Dati)

for ie=1:femregion.ne % loop over elements
        for iTria = 1:size(Tria,1) % loop over triangles
                for k=1:length(w_2D) % 2D quad nodes
                        for i=1:femregion.nln % shape functions
                                for i=1:femregion.nln
                                        % volume integrals
                                end
                        end
                end
        end

        for iedg=1:neighbour.nedges(ie) % loop over faces
                for k=1:nqn_1D % 1D quad nodes
                        for j=1:femregion.nln % shape functions
                                % interface integrals
                        end
                end
        end
end
```

3.2 Monodomain test

As a first test case, the following "simplified" poroelastic problem has been considered:

$$\begin{cases} \ddot{\boldsymbol{u}} - \nabla \cdot \tilde{\boldsymbol{\sigma}} - \nabla(\nabla \cdot \boldsymbol{u}) = \boldsymbol{f} & \text{in } \Omega \times (0,T], \\ \boldsymbol{u}(\cdot,0) = \boldsymbol{u}_0 & \text{in } \Omega, \\ \dot{\boldsymbol{u}}(\cdot,0) = \boldsymbol{u}_1 & \text{in } \Omega, \\ \boldsymbol{u} = \boldsymbol{0} & \text{on } \partial\Omega, \end{cases} \tag{3.1}$$

where symbol $\tilde{\boldsymbol{\sigma}}$ stands for the elastic stress tensor $\tilde{\boldsymbol{\sigma}} = \mathbb{C} : \boldsymbol{\epsilon}(\boldsymbol{u})$. Moreover, as it could be noticed from system (3.1), the whole boundary $\partial\Omega$ reduces to a Dirichlet boundary. At the semi-discrete level, system (3.1) reads as:

$$\boldsymbol{M}\ddot{U} + \boldsymbol{A}U + \boldsymbol{B}U = \boldsymbol{F}. \tag{3.2}$$

The domain is given by $\Omega = (0,1) \times (0,1)$ and the exact solution is chosen as:

$$\boldsymbol{u}(x,y;t) = \begin{pmatrix} x^2 \cos(\frac{\pi x}{2}) \sin(\pi x) \\ x^2 \cos(\frac{\pi x}{2}) \sin(\pi x) \end{pmatrix} \cos(\sqrt{2}\pi t).$$

The forcing term, boundary and initial conditions have been defined accordingly. The semi-implicit scheme has been used to integrate in time problem (3.2).

A convergence analysis measuring the errors in the L^2 and H^1 norms has been carried out by considering four meshes of $N = 80,\ 320,\ 1280,\ 5120$ polygons. Here we choose a polynomial approximation degree $p = 2$. The final time has been set to $T = 1$, while the timestep to $\Delta t = 10^{-5}$, in order to respect the CFL condition. As shown in Figure 3.3, H^1 error and L^2 error of gradient (H^1-seminorm) point out a convergence rate proportional to h^p, as prescribed by the theory. Figure 3.3 also show the error $||\boldsymbol{u} - \boldsymbol{u}_h||_\Omega$ as a function of h. It can be seen a convergence rate of h^{p+1}. The error

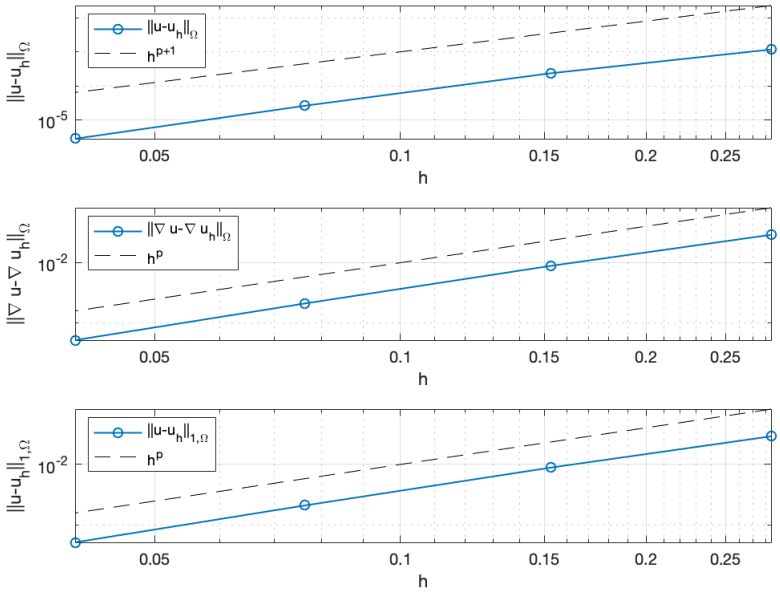

Figure 3.3: Monodomain test: computed errors as a function of meshsize h, $p = 2$

analysis has moreover focused on the trend of the $||\boldsymbol{u}-\boldsymbol{u}_h||_\Omega$, by varying the polynomial degree p from 1 to 5 and fixing the number of polygons to $N = 400$. The final time has been set to $T = 0.025$, in order to reduce time iterations to 2500. Figure 3.4 shows a semilogarithmic plot of L^2 norms, stating an exponential decay of the errors. The computed errors have been also reported in Table B.1 in the Appendix section.

3.3 Coupled domains test

An exact solution for the *sealed pores* case is constructed in order to respect constraints on the interface imposed by (1.7), (1.8) and (1.9). Moreover, $\boldsymbol{u}$ and $\boldsymbol{w}$ are chosen in such a way to have a null pressure in the whole poroelastic domain. Since solutions at the interface are identically zero, with their $x-$, $y-$ and $t-$ derivatives, interface coupling conditions are consequently null. This fact suggests to test both *sealed pores*

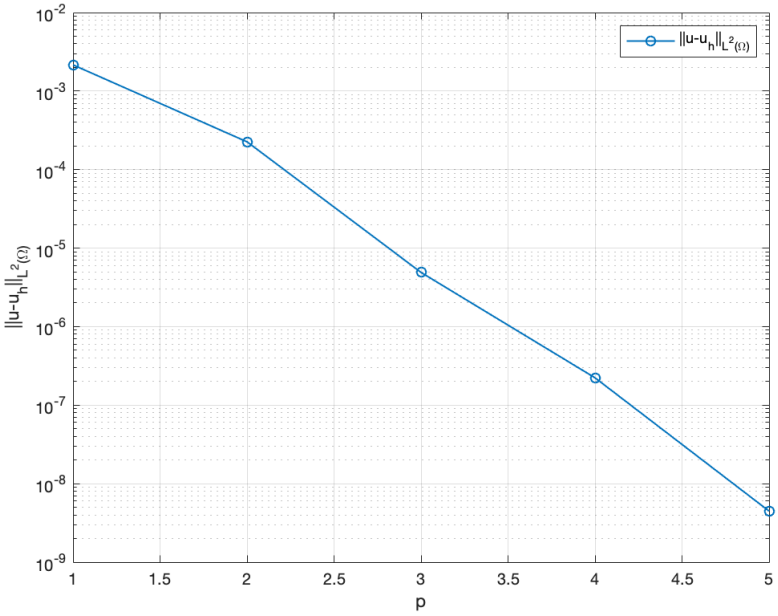

Figure 3.4: Monodomain test: L^2 errors as a function of polynomial degree p in semilogarithmic scale

and *open pores* with the same solutions. Physical parameters are set as shown in Table 3.1, the considered problem is solved in the domain $\Omega = (-1, 1) \times (0, 1)$, on *polygonal meshes* as in Figure 3.5. The poro-elasto-acoustic interface is given by $\Gamma_I = \{0\} \times [0, 1]$. As shown in Table 3.1, parameters has been set equal to 1, except for the dynamic

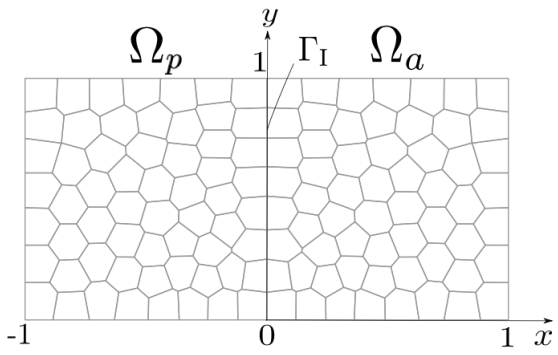

Figure 3.5: Polygonal mesh, with $N = 100$

viscosity, set to zero in order to simplify the study and $\rho_w = 2$ that have ensured a non vanishing second poroelastic equation.

Exact solutions are defined as follows:

$$\boldsymbol{u}(x, y; t) = \begin{pmatrix} x^2 \cos(\frac{\pi x}{2}) \sin(\pi x), \\ x^2 \cos(\frac{\pi x}{2}) \sin(\pi x), \end{pmatrix} \cos(\sqrt{2}\pi t)$$

Data	Adimensional Value
ρ_f, ρ_s	1
λ, μ	1
a	1
ϕ	0.5
η	0
ρ_w	2
β, m	1
c	1

Table 3.1: Coupled domains test: physical parameters

$$\boldsymbol{w}(x,y;t) = -\begin{pmatrix} x^2\cos(\frac{\pi x}{2})\sin(\pi x) \\ x^2\cos(\frac{\pi x}{2})\sin(\pi x) \end{pmatrix}\cos(\sqrt{2}\pi t)$$

$$\varphi(x,y;t) = (x^2\sin(\pi x)\sin(\pi y))\sin(\sqrt{2}\pi t).$$

Forcing terms have been calculated accordingly and read as follows:

$$\boldsymbol{f}_p(x,y;t) = \begin{pmatrix} \frac{\lambda+2\mu}{8} \\ \frac{\mu}{8} \end{pmatrix} h_1(x,y)\cos(\sqrt{2}\pi t),$$

$$\boldsymbol{g}_p(x,y;t) = \begin{pmatrix} 2\pi^2x^2\cos(\pi x/2)\sin(\pi x) \\ 2\pi^2x^2\cos(\pi x/2)\sin(\pi x) \end{pmatrix}\cos(\sqrt{2}\pi t),$$

$$f_a(x,y;t) = -2\left(2\pi x\cos(\pi x) + \sin(\pi x)\right)\sin(\pi y)\sin(\sqrt{2}\pi t),$$

where:

$$\begin{aligned} h_1(x,y) = {} & (-8\pi x\cos(\pi x/2) - 24\pi x\cos(3\pi x/2) \\ & + 2(-8 + 5\pi^2x^2 + (-8 + 9\pi^2x^2)\cos(\pi x))\sin(\pi x/2)). \end{aligned}$$

A first error analysis has been carried out on L^2-norms for *sealed* and *open* pores. Four sequentially refined polygonal meshes (the coarsest mesh containing 50 elements, the finest 400) have been considered, with uniform polynomial degree $p = 1, 2, 3$ set on any element. Final time T has been set equal to 0.25, in order to consider just 2500 time iterations, considering a timestep of $\Delta t = 10^{-4}$. L^2-errors are expected to converge proportional to h^{p+1}, while H^1-seminorm and H^1-norm proportional to h^p, as shown in Figure 3.6, for the case of $p = 3$ polynomials. Numerical results have been shown in Tables B.2 to B.10 in the Appendix section. Moreover, an L^2 error analysis on the pressure has been carried out, for $p = 3$ polynomials. Figure 3.7 shows the convergence proportional to h^p: as expected the trend is the same of the one of the gradient norm. Pressure has been computed through equation (1.5).

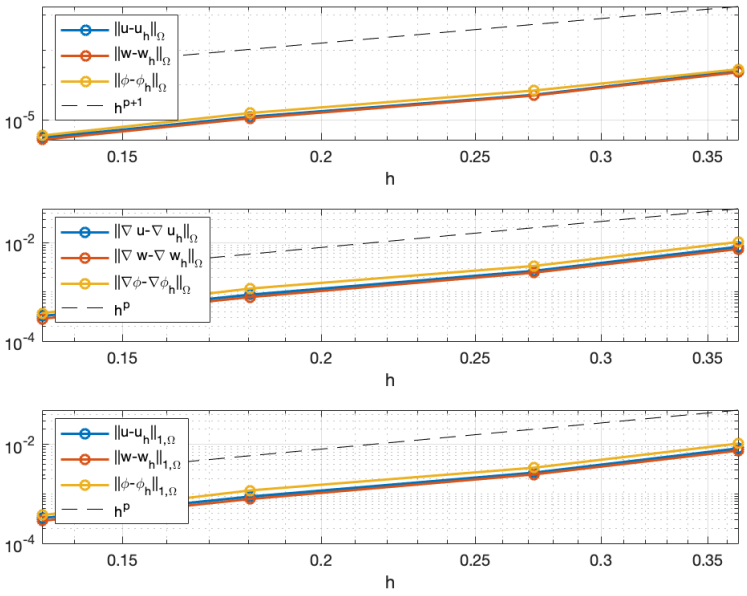

(a) Sealed pores

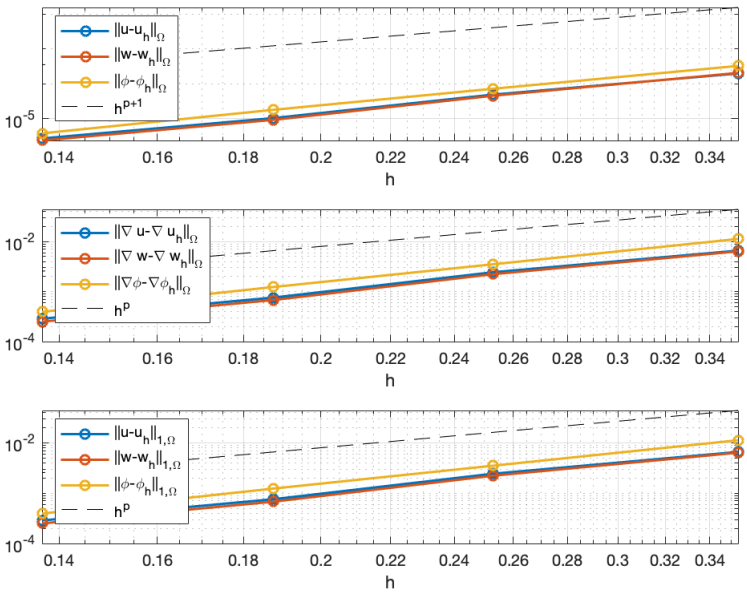

(b) Open pores

Figure 3.6: Coupled domains test: computed errors as a function of meshsize h with $p = 3$

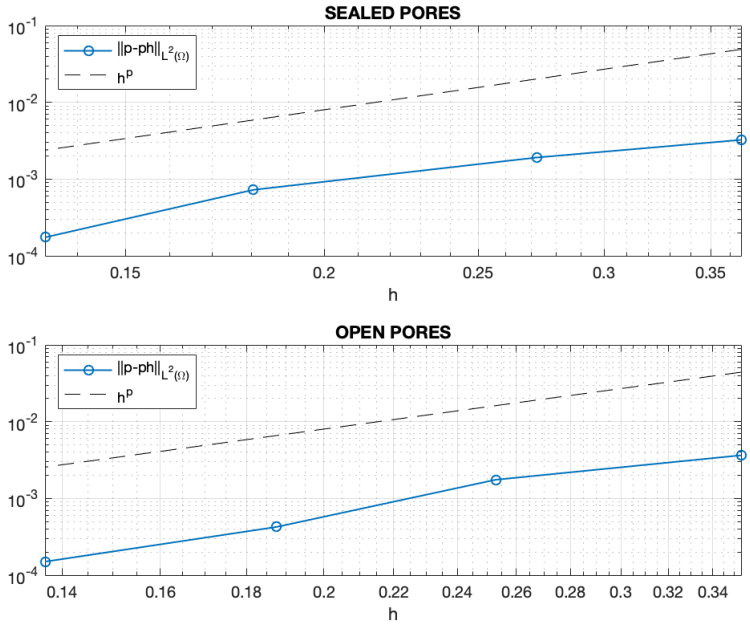

Figure 3.7: $||p - p_h||_{\Omega_p}$ as a function of meshsize h with $p = 3$

As done for the monodomain test, a convergence analysis of the computed errors measured in the L^2 and H^1-norms letting varying the polynomial degree p, has been taken into account. Figure 3.8 points out an exponential decay of the errors, through a semilogarithmic plot.

Since previous exact solutions introduced had vanishing interface conditions, other possible choices could be taken into account, in order to consider non-zero coupling conditions. Solutions will be now non identical for open and sealed pores scenarios, since they slightly differ in imposing pressure continuity (equation (1.9)).
Dealing with *sealed pores*, an exact solution, constructed as a combination of polynomials for space and an exponential for time variables, reads as follows:

$$\begin{cases} \boldsymbol{u}(x,y;t) = \left(1 + x^2 - 3xy, -9 + x^2\right) e^t \\ \boldsymbol{w}(x,y;t) = \left(-x + x^2 + xy, 1 + x + x^2 + y - 4xy + y^2\right) e^t \\ \varphi(x,y;t) = \left(-x + x^2 + 9y\right) e^t. \end{cases}$$

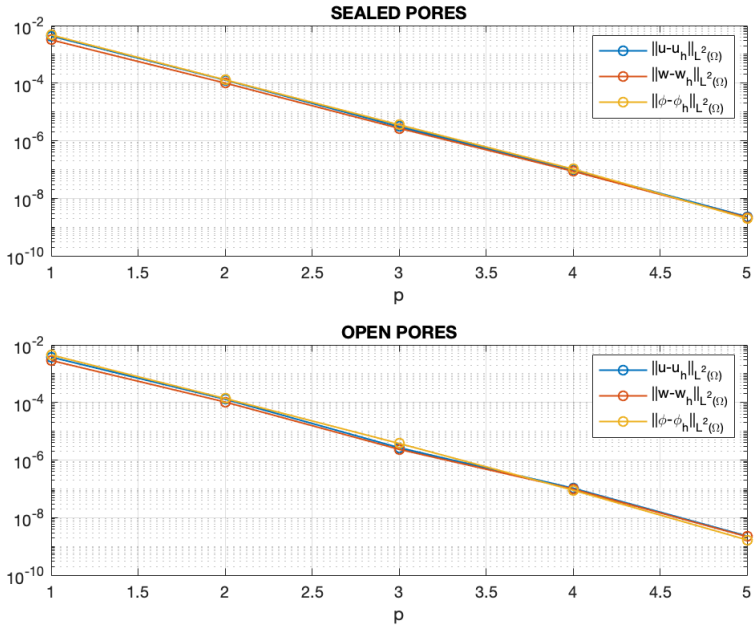

Figure 3.8: Coupled domains: computed errors as a function of polynomial degree p in semilogarithmic scale

Moreover, concerning with *open pores*, an analytical solution is proposed as follows:

$$\begin{cases} \boldsymbol{u}(x,y;t) = \left(9 + x + x^2 + y + 3y^2,\ -x - 3y - 6xy\right) e^t \\ \boldsymbol{w}(x,y;t) = \left(-1 - x - x^2 - y - 3y^2,\ x + 3y + 6xy\right) e^t \\ \varphi(x,y;t) = (-8x)\, e^t. \end{cases}$$

Even with these solutions, a convergence analysis has been carried out. By the way, by considering a $p = 2$ polynomial degree, the numerical solution incurs a saturation effect, due to the polynomial nature of the same analytical solution.

3.4 Physical examples

Test 1: Linear interface

A first test has been studied by considering the same rectangular polygonal mesh presented in the previous section. Once again, the domain Ω has been split into a poroelastic and an acoustic part, respectively $\Omega_p = (-200, 0) \times (0, 400)$ m^2 and $\Omega_a = (0, 200) \times (0, 400)$ m^2. A linear interface has been placed at $x = 0$ m, resulting in $\Gamma_I = 0 \times [0, 400]$ m.

Physical and dimensional parameters have been chosen as in [27] and listed in Table 3.2. Boundary and initial conditions have been set equal to zero both for the poroelastic and the acoustic domain. Forcing terms are null in Ω_p, while in Ω_a a forcing term

Fluid	Fluid density	ρ_f	1000	kg/m^3
	Wave velocity	c	1500	m/s
	Dynamic viscosity	η	0	Pa $\cdot$ s
Grain	Solid density	ρ_s	2690	kg/m^3
	Shear modulus	μ	$1.86{\cdot}10^9$	Pa
Matrix	Porosity	ϕ	0.38	
	Tortuosity	a	1.8	
	Permeability	k	$2.79 \cdot 10^{-11}$	m^2
	Lamé coefficient	λ_0	$1.2 \cdot 10^8$	Pa
	Biot's coefficient	m	$5.34 \cdot 10^9$	Pa
	Biot's coefficient	β	0.95	

Table 3.2: Test 1: straight interface. Physical parameters

is imposed until $t = 0.05$ s, by considering the following load:

$$\boldsymbol{f}_a = \boldsymbol{r}(x, y)h(t),$$

where

$$h(t) = \begin{cases} \sum_{k=1}^{4} \alpha_k \sin(\gamma_k \omega_0 t), & \text{if } 0 < t < \frac{1}{f_0} \\ 0, & \text{otherwise,} \end{cases} \tag{3.3}$$

with coefficients defined as: $\alpha_1 = 1$, $\alpha_2 = -21/32$, $\alpha_3 = 63/768$, $\alpha_4 = -1/512$, $\gamma_k = 2^{k-1}$, $\omega_0 = 2\pi f_0$ Hz, $f_0 = 20$ Hz . $h(t)$ function is shown in Figure 3.9. Function

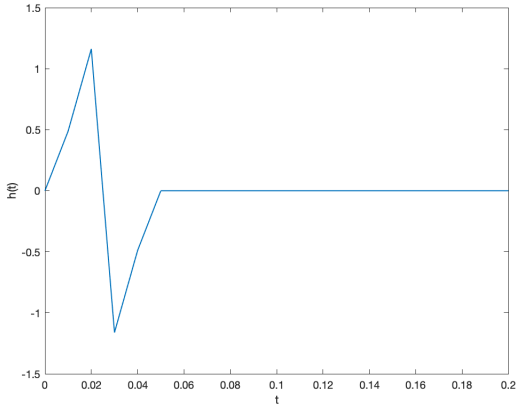

Figure 3.9: Point source load in the acoustic domain, evolving in the time interval $[0, 0.2]$ s

$\boldsymbol{r}(\boldsymbol{x})$ is moreover defined as:

$$\boldsymbol{r}(x, y) = \begin{cases} 1, & \text{if } x_0 - r \leq x \leq x_0 + r \text{ and } y_0 - r \leq y \leq y_0 + r \\ 0, & \text{otherwise,} \end{cases}$$

where $x_0 = 100$, $y_0 = 200$ and $r = 50$. Eventually, function $\boldsymbol{r}(\boldsymbol{x})$ has been plotted on the mesh as shown in Figure 3.10. Simulations have been thus carried out by considering

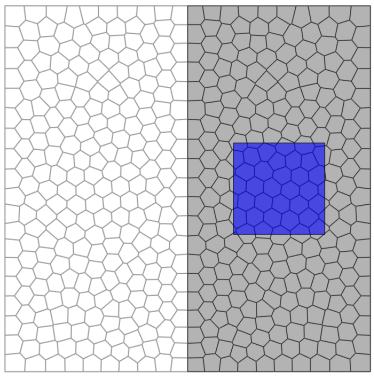

Figure 3.10: Test 1: straight interface. $\boldsymbol{r}(x, y)$ function over polygonal mesh

a polygonal mesh consisting in $N = 500$ polygons. In order to reduce the computational time, it has been chosen to adopt a Newmark scheme for time discretization, as introduced in Subsection 2.7.2. Indeed, Newmark parameters have been set equal to $\beta_N = 1/4$ and $\gamma_N = 1/2$, so that the method is unconditionally stable (see [34]). This fact ensures not to have stability issues by taking $\Delta t = 10^{-2}$ s, in a time interval $[0, 1]$ s.
Solutions at four time instants are shown in Figure 3.11. As it could be noticed by

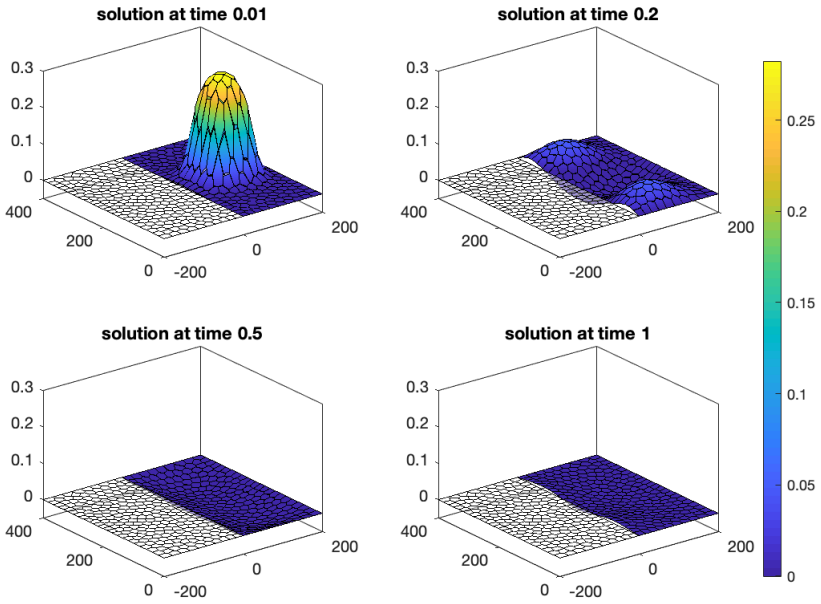

Figure 3.11: Test 1: straight interface. Dissipated solution in the acoustic domain at four time istants

the latter plot, after initial oscillations imposed by the forcing term, the solution starts dampening to zero. This is mainly related to a numerical dissipation caused by considering a Newmark scheme with a too large timestep ($\Delta t = 10^{-2}$ s). In fact, no damping parameters have been taken into account in the considered model. At the physical level the only factor which could affect the natural oscillations initially imposed are interface conditions, that in general cause a loss of energy by transporting it. In order to fix this problem it has been set $\Delta t = 10^{-4}$ s, again with a Newmark scheme. The potential solution is shown, in the acoustic domain, in Figure 3.12. As it could be pointed out, at final time $T = 1$ the solution reaches values comparable with previous ones, ensuring a non-dissipation effect.

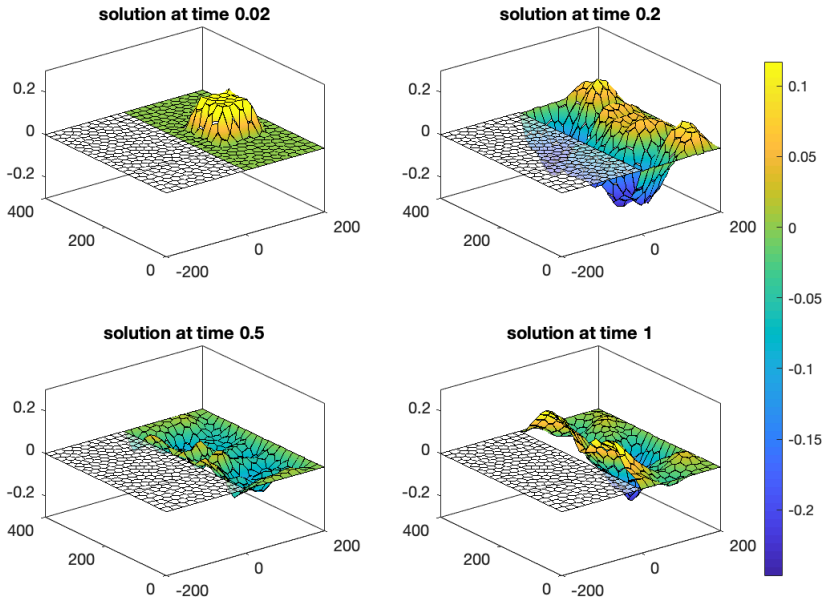

Figure 3.12: Test 1: straight interface. Non-dissipated solution in the acoustic domain at four time istants

Test 2: Transversal interface

The analysis has carried on by considering a different interface. In particular, a plane interface with slope 60° has been considered in the domain $\Omega = \Omega_a \cup \Omega_p = [0, 400]^2$ m^2. Parameters has been set as in Test 1 (Table 3.2). The forcing term f_a has been set equal in time as in Test 1 (equation 3.3), while $\boldsymbol{r}(x, y)$ has been accordingly defined:

$$\boldsymbol{r}(x,y) = \begin{cases} 1, & \text{if } y \leq \frac{40}{23}x - 348 \text{ and } y \geq \frac{40}{23}x - 435 \\ 0, & \text{otherwise.} \end{cases}$$

In Figure 3.13 it has been shown function $\boldsymbol{r}(x, y)$ over the mesh. $\boldsymbol{f}_p$ and $\boldsymbol{g}_p$ has been

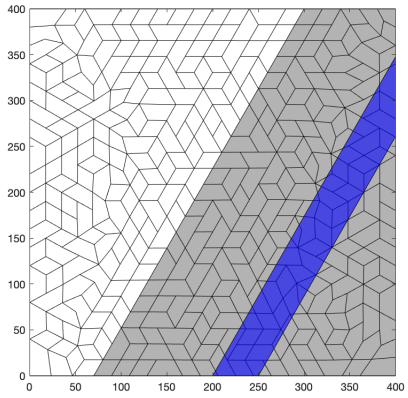

Figure 3.13: Test 2: oblique interface. $\boldsymbol{r}(x, y)$ function over the mesh

again set equal to zero. As time discretization scheme has been chosen again Newmark, with parameters as in Test 1, timestep $\Delta t = 10^{-4}$ s and final time $T = 1$ s. It has been carried out a simulation with $N = 393$ polygons, subdivided into $N_a = 211$ and $N_p = 182$ polygons for the acoustic and poroelastic domain respectively.
In Figure 3.14 it has been shown again the potential in the acoustic domain.

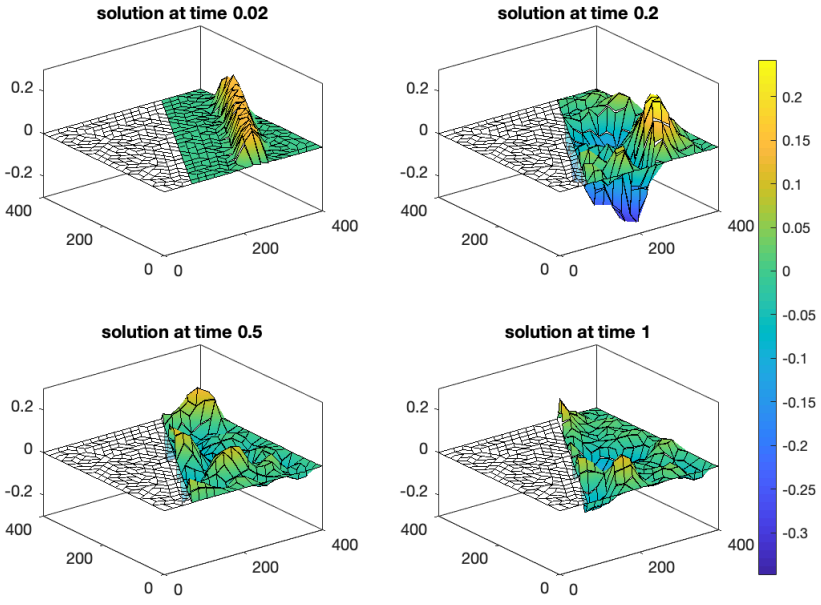

Figure 3.14: Test 2: oblique interface. Potential solution in the acoustic domain at four time istants

Test 3: Circular interface

In this test a square domain $\Omega = [-600, 600]$ m^2 has been considered, with a hole of radius 100 m centered in $(0, 0)$, representing the acoustic domain Ω_a. The interface

Γ_I is therefore nothing but $\partial\Omega_a$, separating Ω_a from the remaining poroelastic domain Ω_p. Again, f_a has been set in time as in Test 1, while $\boldsymbol{r}(x, y)$ has been considered as follows:

$$\boldsymbol{r}(x,y) = \begin{cases} 1, & \text{if } x^2 + y^2 \leq 50^2 \\ 0, & \text{otherwise,} \end{cases}$$

that is considering a cylinder as initial condition. The frequency f_0 has been here set equal to $f_0 = 10$ Hz, in order to impose initial condition in a larger time interval ($[0, 0.1]$ s). In Figure 3.15, we plot the function $\boldsymbol{r}(x, y)$ over an $N = 1324$ polygons mesh, subdivided into $N_a = 25$ and $N_p = 1299$ polygons respectively in the acoustic and poroelastic domains. Time discretization settings (final time, timestep, Newmark

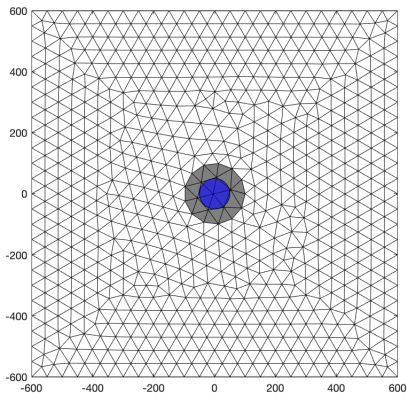

Figure 3.15: Test 3: circular interface. $\boldsymbol{r}(x, y)$ function over the mesh

coefficients) have been chosen as in Test 1. Moreover, in Figure 3.16, it has been chosen to represent both acoustic (pressure) and poroelastic (pressure) solutions in the same plot. In order to show the same physical variables in both the domains, it has been decided to compute the acoustic pressure in terms of a first time derivative of the acoustic potential, namely: $p_a = \rho_a \dot{\varphi}$. The derivative of the potential has been taken directly from the Newmark scheme, as basically the numerical scheme involves as unknowns $\boldsymbol{u}$, $\boldsymbol{w}$ and φ and their first time derivatives. Pressure has been instead calculated through equation (1.5). As it could be noticed, the initial condition imposed in the acoustic domain, propagates through the poroelastic one, reflecting then on the boundary, in which null Dirichlet conditions have been imposed. Note that pressure solutions on both domains have been rescaled by a factor 1000, to better visualize results.

Test 4: Sinusoidal interface

Eventually, with the same data structure of Test 3, it has been considered a square domain $\Omega = [-1500, 1500]^2 \text{m}^2$. A sinusoidal interface has been taken into account by defining it through the relation $y = 40 \sin\left(\frac{\pi}{100} x\right)$. The number of polygons here

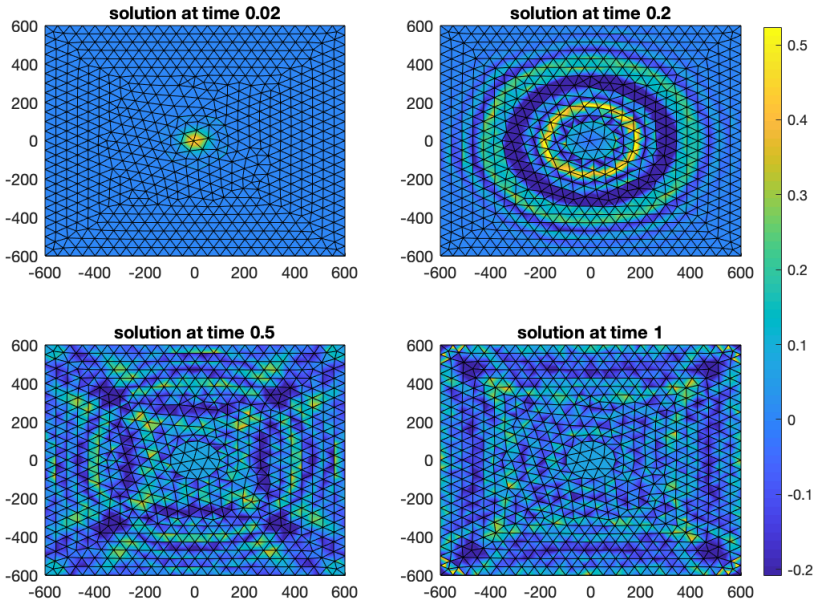

Figure 3.16: Test 3: circular interface. Pressure solutions at four time istants

considered is $N = 3664$, subdivided into $N_a = 1827$ and $N_p = 1837$ polygons. Moreover, as shown in Figure 3.17, it has been again set initial conditions on acoustic domain, by considering $h(t)$ as before and $\boldsymbol{r}(x, y)$ as follows:

$$\boldsymbol{r}(x,y) = \begin{cases} 1, & \text{if } -500 \leq x \leq 500 \text{ and } 500 \leq y \leq 1000 \\ 0, & \text{otherwise.} \end{cases}$$

In Figure 3.18 it has been shown the propagation of pressure at four time instants.

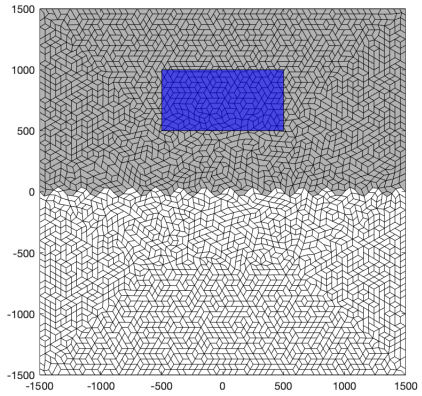

Figure 3.17: Test 4: sinusoidal interface. $\boldsymbol{r}(x, y)$ function over the mesh

Observe how the sinusoidal interface contributes to the dispersion of the acoustic wave in the poroelastic domain. Moreover, at time instant $t = 1$ s, it can be noticed that the

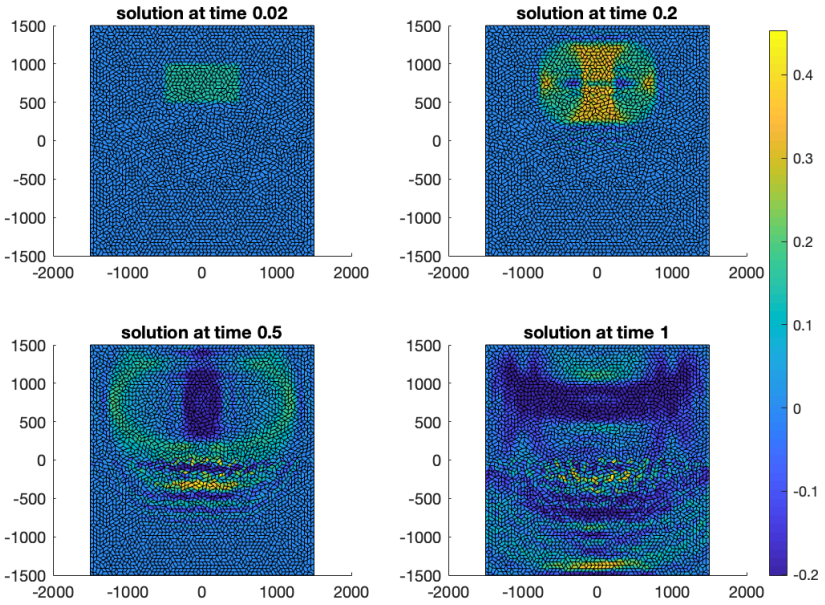

Figure 3.18: Test 4: sinusoidal interface. Pressure solutions at four time istants

wavefront has reached the boundary of the poroelastic domain.

Conclusions

In this work we have presented a discontinuous Galerkin approximation to the coupled poro-elasto-acoustic problem. Existence and uniqueness of the (strong) solution to the continuous problem have been proven. It has been stated a proof of the stability of the continuous and semi-discrete problem (discretized in space). Moreover a priori error estimates in a suitable mesh dependent energy norm have been presented and discussed. Finally, through the software Matlab, numerical simulations have been carried out. Firstly, verification tests have been addressed to validate the theoretical error bounds, and then a number of physically interesting test cases, where different scenarios have been treated.

As a further development opt to drastically reduce the computational time, it would be of great advantage to consider a quadrature free algorithm, recently proposed in literature [7]. By the physical point of view, no conditions on boundary have been considered, other than homogeneous Dirichlet ones. In order to deal with constraints imposed by physical test cases, non reflecting boundary conditions must be considered into the implementation. A further development will also consist in implementing the proposed scheme in the computational code SPEED (http://speed.mox.polimi.it/) to deal with three-dimensional numerical tests in physically relevant scenarios.

Bibliography

[1] M. H. Al-Taie, A. H. Ali, and A. F. Al-Attar. Study the Physical Properties and Thermal Conductivity of Light Weight Refractories Bricks Produced by Adding porcelanite to Kaolinite. *Engineering and Technology Journal*, 33(1 Part (A) Engineering):51–60, 2015.

[2] I. Ambartsumyan, E. Khattatov, I. Yotov, and P. Zunino. A Lagrange multiplier method for a Stokes–Biot fluid–poroelastic structure interaction model. *Numerische Mathematik*, 140(2):513–553, 2018.

[3] P. F. Antonietti, N. Bigoni, and M. Verani. Mimetic discretizations of elliptic control problems. *Journal of Scientific Computing*, 56(1):14–27, 2013.

[4] P. F. Antonietti, A. Cangiani, J. Collis, Z. Dong, E. H. Georgoulis, S. Giani, and P. Houston. Review of discontinuous Galerkin finite element methods for partial differential equations on complicated domains. In *Building bridges: connections and challenges in modern approaches to numerical partial differential equations*, pages 281–310. Springer, 2016.

[5] P. F. Antonietti, P. Houston, X. Hu, M. Sarti, and M. Verani. Multigrid algorithms for hp-version interior penalty discontinuous Galerkin methods on polygonal and polyhedral meshes. *Calcolo*, 54(4):1169–1198, 2017.

[6] P. F. Antonietti, F. Bonaldi, and I. Mazzieri. A high-order discontinuous Galerkin approach to the elasto-acoustic problem. *Computer Methods in Applied Mechanics and Engineering*, 358:112634, 29, 2020. ISSN 0045-7825.

[7] P. F. Antonietti, Facciolà, P. Houston, I. Mazzieri, G. Pennesi, and M. Verani. High-order discontinuous Galerkin methods on polyhedral grids for geophysical applications: seismic wave propagation and fractured reservoir simulations. 2020.

[8] D. N. Arnold. An interior penalty finite element method with discontinuous elements. *SIAM Journal on Numerical Analysis*, 19(4):742–760, 1982.

[9] D. N. Arnold, F. Brezzi, B. Cockburn, and L. D. Marini. Unified analysis of discontinuous Galerkin methods for elliptic problems. *SIAM Journal on Numerical Analysis*, 39(5):1749–1779, 2001/02. ISSN 0036-1429.

[10] D. N. Arnold, F. Brezzi, R. S. Falk, and L. D. Marini. Locking-free Reissner-Mindlin elements without reduced integration. *Computer Methods in Applied Mechanics and Engineering*, 196(37-40):3660–3671, 2007. ISSN 0045-7825.

[11] D. Baraff. Linear-time dynamics using Lagrange multipliers. In *Proceedings of the 23rd annual conference on Computer graphics and interactive techniques*, pages 137–146, 1996.

[12] L. Beirão da Veiga, F. Dassi, and A. Russo. High-order virtual element method on polyhedral meshes. *Computers & Mathematics with Applications*, 74(5):1110–1122, 2017. ISSN 0898-1221.

[13] L. Beirão da Veiga, D. Mora, and G. Vacca. The Stokes complex for virtual elements with application to Navier-Stokes flows. *Journal of Scientific Computing*, 81(2):990–1018, 2019. ISSN 0885-7474.

[14] L. Beirão da Veiga, A. Russo, and G. Vacca. The virtual element method with curved edges. *ESAIM Mathematical Modelling and Numerical Analysis*, 53(2): 375–404, 2019. ISSN 0764-583X.

[15] R. L. Berge, I. Berre, E. Keilegavlen, J. M. Nordbotten, and B. Wohlmuth. Finite volume discretization for poroelastic media with fractures modeled by contact mechanics. *International Journal for Numerical Methods in Engineering*, 2019.

[16] M. A. Biot. General theory of three-dimensional consolidation. *Journal of applied physics*, 12(2):155–164, 1941.

[17] M. A. Biot. Theory of elasticity and consolidation for a porous anisotropic solid. *Journal of applied physics*, 26(2):182–185, 1955.

[18] M. A. Biot. Theory of Propagation of Elastic Waves in a Fluid-Saturated Porous Solid. I. Low-Frequency Range. *The Journal of the Acoustical Society of America*, 28:168–178, 1956.

[19] M. A. Biot. Theory of deformation of a porous viscoelastic anisotropic solid. *Journal of Applied physics*, 27(5):459–467, 1956.

[20] M. A. Biot. Theory of Propagation of Elastic Waves in a Fluid-Saturated Porous Solid. II. Higher Frequency Range. *The Journal of the Acoustical Society of America*, 28:179–191, 1956.

[21] M. A. Biot. Mechanics of deformation and acoustic propagation in porous media. *Journal of applied physics*, 33(4):1482–1498, 1962.

[22] T. Bourbié, O. Coussy, B. Zinszner, and M. C. Junger. Acoustics of porous media, 1992.

[23] F. Brezzi, A. Buffa, and K. Lipnikov. Mimetic finite differences for elliptic problems. *ESAIM: Mathematical Modelling and Numerical Analysis*, 43(2):277–295, 2009.

[24] A. Cangiani, E. H. Georgoulis, and P. Houston. hp-version discontinuous Galerkin methods on polygonal and polyhedral meshes. *Mathematical Models and Methods in Applied Sciences*, 24(10):2009–2041, 2014.

[25] A. Cangiani, Z. Dong, E. H. Georgoulis, and P. Houston. *hp-version discontinuous Galerkin methods on polytopic meshes.* SpringerBriefs in Mathematics. Springer International Publishing, 2017.

[26] B. Castagnede, A. Aknine, M. Melon, and C. Depollier. Ultrasonic characterization of the anisotropic behavior of air-saturated porous materials. *Ultrasonics*, 36(1-5): 323–341, 1998.

[27] G. Chiavassa and B. Lombard. Time domain numerical modeling of wave propagation in 2d acoustic / porous media. *Journal of Computational Physics*, 230(13): 5288–5309, 2011.

[28] N. Chotiros. *Acoustics of the Seabed as a Poroelastic Medium.* 01 2017.

[29] C. Dawson, S. Sun, and M. F. Wheeler. Compatible algorithms for coupled flow and transport. *Computer Methods in Applied Mechanics and Engineering*, 193 (23-26):2565–2580, 2004.

[30] C. A. De Moura and C. S. Kubrusly. The Courant-Friedrichs-Lewy (CFL) condition. *Applied Mathematics and Computation*, 10:12, 2013.

[31] D. A. Di Pietro and J. Droniou. A Hybrid High-Order method for Leray–Lions elliptic equations on general meshes. *Mathematics of Computation*, 86(307):2159–2191, 2017.

[32] D. A. Di Pietro and A. Ern. A Hybrid High-Order locking-free method for linear elasticity on general meshes. *Computer Methods in Applied Mechanics and Engineering*, 283:1–21, 2015.

[33] D. A. Di Pietro and R. Tittarelli. An introduction to Hybrid High-Order methods. 2017.

[34] M. Dokainish and K. Subbaraj. A survey of direct time-integration methods in computational structural dynamics. Explicit methods. *Computers & Structures*, 32(6):1371–1386, 1989.

[35] S. Erlicher, L. Bonaventura, and O. S. Bursi. The analysis of the generalized-α method for non-linear dynamic problems. *Computational Mechanics*, 28(2):83–104, 2002.

[36] Z. Fellah, A. Berbiche, M. Fellah, E. Ogam, and C. Depollier. Acoustic characterization of air-saturated porous materials by solving the inverse problem. 08 2016.

[37] Z. Fellah, M. Fellah, C. Depollier, E. Ogam, and F. Mitri. *Wave Propagation in Porous Materials*, pages 99–119. 01 2018. ISBN 978-953-51-3715-3.

[38] Z. E. A. Fellah, S. Berger, W. Lauriks, C. Depollier, and J.-Y. Chapelon. Inverse problem in air-saturated porous media via reflected waves. *Review of scientific instruments*, 74(5):2871–2879, 2003.

[39] S. Feng and D. L. Johnson. High-frequency acoustic properties of a fluid/porous solid interface. I. New surface mode. *The Journal of the Acoustical Society of America*, 74(3):906–914, 1983.

[40] P. Gauzellino, F. Zyserman, and J. Santos. A study of ultrasonic wave propagation in bones. *Latin American applied research*, 38, 10 2008.

[41] P. Göransson. A 3-D, symmetric, finite element formulation of the Biot equations with application to acoustic wave propagation through an elastic porous medium. *International journal for numerical methods in engineering*, 41(1):167–192, 1998.

[42] B. Gurevich and M. Schoenberg. Interface conditions for Biot's equations of poroelasticity. *The Journal of the Acoustical Society of America*, 105(5):2585–2589, 1999.

[43] B. Gurevich, M. Brajanovski, R. J. Galvin, T. M. Müller, and J. Toms-Stewart. P-wave dispersion and attenuation in fractured and porous reservoirs–poroelasticity approach. *Geophysical Prospecting*, 57(2):225–237, 2009.

[44] M. Hodaei, V. Rabbani, and P. Maghoul. Transient acoustic wave propagation in bone-like porous materials using the theory of poroelasticity and fractional derivative: a sensitivity analysis. *Acta Mechanica*, 231(1):179–203, 2020.

[45] L.-H. Huang and C. Song. Dynamic response of poroelastic bed to water waves. *Journal of Hydraulic Engineering*, 119(9):1003–1020, 1993.

[46] J. M. Huyghe, D. H. van Campen, T. Arts, and R. M. Heethaar. A two-phase finite element model of the diastolic left ventricle. *Journal of biomechanics*, 24(7): 527–538, 1991.

[47] A. V. Idesman. A new high-order accurate continuous Galerkin method for linear elastodynamics problems. *Computational Mechanics*, 40(2):261–279, 2007.

[48] G. Jayaraman. Water transport in the arterial wall—a theoretical study. *Journal of biomechanics*, 16(10):833–840, 1983.

[49] D.-S. Jeng and Y.-S. Lin. Poroelastic analysis of the wave–seabed interaction problem. *Computers and Geotechnics*, 26(1):43–64, 2000.

[50] D. E. Kenyon. A mathematical model of water flux through aortic tissue. *Bulletin of mathematical biology*, 41(1):79–90, 1979.

[51] B. Krishnan, D. M., S. Raja, and K. Venkataramana. Structural and Vibroacoustic Analysis of Aircraft Fuselage Section with Passive Noise Reducing Materials: A Material Performance Study. 03 2015.

[52] A. Kudarova. *Effective models for seismic wave propagation in porous media.* PhD thesis, Delft University of Technology, 2016.

[53] P. Lade and R. De Boer. The concept of effective stress for soil, concrete and rock. *Geotechnique*, 47(1):61–78, 1997.

[54] P. J. Matuszyk and L. F. Demkowicz. Solution of coupled poroelastic/acoustic/elastic wave propagation problems using automatic hp-adaptivity. *Computer Methods in Applied Mechanics and Engineering*, 281:54–80, 2014.

[55] D. Mikhailov. Difference between the longitudinal frenkel-biot waves in water-and gas-saturated porous media. *Fluid dynamics*, 41(1):112, 2006.

[56] L. Mountassir, B. Touriya, and H. Nounah. Elastic characterization of porous bone by ultrasonic method through lamb waves. 5:61–74, 01 2017.

[57] N. M. Newmark. A method of computation for structural dynamics. *Journal of the engineering mechanics division*, 85(3):67–94, 1959.

[58] V.-H. Nguyen and S. Naili. Simulation of wave propagation in anisotropic poroelastic bone plate immersed in fluid. 04 2012.

[59] C. Oomens, D. Van Campen, and H. Grootenboer. A mixture approach to the mechanics of skin. *Journal of biomechanics*, 20(9):877–885, 1987.

[60] A. Pereira, I. F. Menezes, C. Talischi, and G. H. Paulino. An efficient and compact Matlab implementation of topology optimization: application to compliant mechanism. In *Proceedings of the 32nd Iberian latin American congress on computational methods in engineering, Ouro Preto*, 2011.

[61] P. J. Phillips and M. F. Wheeler. A coupling of mixed and discontinuous Galerkin finite-element methods for poroelasticity. *Computational Geosciences*, 12(4):417–435, 2008.

[62] B. Riviere. *Discontinuous Galerkin methods for solving elliptic and parabolic equations: theory and implementation.* SIAM Journal on Applied Mathematics, 2008.

[63] B. Rivière, M. F. Wheeler, and V. Girault. Improved energy estimates for interior penalty, constrained and discontinuous galerkin methods for elliptic problems. part i. *Computational Geosciences*, 3(3-4):337–360, 1999.

[64] R. T. Rockafellar. Lagrange multipliers and optimality. *SIAM review*, 35(2):183–238, 1993.

[65] G. Rosi, V.-H. Nguyen, and S. Naili. Numerical investigations of ultrasound wave propagating in long bones using a poroelastic model. *Mathematics and Mechanics of Solids*, 21, 05 2015.

[66] S. Salsa. *Equazioni a derivate parziali: Metodi, modelli e applicazioni*, volume 98. Springer, 2016.

[67] M. Seppi. *Numerical and analytical vibro-acoustic modelling of porous materials: the Cell Method for poroelasticity and the case of inclusions.* PhD thesis, Alma, 2009.

[68] M. Shojaeefard, R. Talebitooti, R. Ahmadi, and B. Ranjbar. A study on acoustic behavior of poroelastic media bonded between laminated composite panels. *Latin American Journal of Solids and Structures*, 11:2379–2407, 01 2014.

[69] D. M. J. Smeulders. *On wave propagation in saturated and partially saturated porous media.* PhD thesis, Citeseer, 1992.

[70] M. Souzanchi, L. Cardoso, and S. Cowin. Tortuosity and the averaging of microvelocity fields in poroelasticity. *Journal of applied mechanics*, 80(2), 2013.

[71] N. Sukumar and A. Tabarraei. Conforming polygonal finite elements. *International Journal for Numerical Methods in Engineering*, 61(12):2045–2066, 2004.

[72] A. Tabarraei and N. Sukumar. Application of polygonal finite elements in linear elasticity. *International Journal of Computational Methods*, 3(04):503–520, 2006.

[73] C. Talischi, G. H. Paulino, A. Pereira, and I. F. Menezes. Polymesher: a general-purpose mesh generator for polygonal elements written in Matlab. *Structural and Multidisciplinary Optimization*, 45(3):309–328, 2012.

[74] K. Terzaghi. Theoretical soil mechanics. *New York*, 1943.

[75] K. Tuncay and M. Y. Corapcioglu. Effective stress principle for saturated fractured porous media. *Water Resources Research*, 31(12):3103–3106, 1995.

[76] M. F. Wheeler. An elliptic collocation-finite element method with interior penalties. *SIAM Journal on Numerical Analysis*, 15(1):152–161, 1978.

[77] F. Wuttke, P. Dineva, and I. K. Fontara. Influence of Poroelasticity on the 3D Seismic Response of Complex Geological Media. *Journal of Theoretical and Applied Mechanics*, 47, 01 2017.

[78] M. Yang and L. A. Taber. The possible role of poroelasticity in the apparent viscoelastic behavior of passive cardiac muscle. *Journal of biomechanics*, 24(7): 587–597, 1991.

[79] Z. Yingbo. Biot theory in application to seismic prospecting. *Geophysical Prospecting For Petrole*, 4, 1994.

Appendix A

List of symbols

Variable	Description	SI unit
$\boldsymbol{u}$	solid displacement	m
$\boldsymbol{u}_f$	fluid displacement	m
$\boldsymbol{w}$	filtration displacement	m
φ	acoustic potential	m^2/s
p	pressure	N/m^2
ρ_s	solid density	kg/m^3
$\rho_f,\ \rho_a$	(saturating) fluid density	kg/m^3
c	acoustic wave velocity	m^2/s
$\rho_w,\ \rho$	other densities	kg/m^3
ϕ	porosity	-
a	tortuosity	-
k	permeability	m^2
$\mathcal{K}$	hydraulic permeability	m/(Pa s)
η	dynamic viscosity	Pa s
$\lambda,\ \mu$	Lamé coefficients	Pa
λ_f	Lamé coefficients of saturated matrix	Pa
m	Biot's coefficient	Pa
β	Biot's coefficient	-
$\tilde{\boldsymbol{\sigma}}$	total stress	Pa/m^2
$\boldsymbol{\sigma}$	effective stress	Pa/m^2
$\mathbb{C}$	isotropic stress tensor	Pa

Appendix B

Computed numerical errors

Error	N	$p = 2$	order
$\|\boldsymbol{u} - \boldsymbol{u}_h\|_\Omega$	80	0.0012	-
	320	2.3422e-04	**3.4378**
	1280	2.5954e-05	**3.2959**
	5120	7.3874e-06	**3.3237**
$\|\nabla\boldsymbol{u} - \nabla\boldsymbol{u}_h\|_\Omega$	80	0.0289	-
	320	0.0089	**1.9282**
	1280	0.0021	**1.9441**
	5120	4.9442e-04	**1.9595**
$\|\boldsymbol{u} - \boldsymbol{u}_h\|_{1,\Omega}$	80	0.0289	-
	320	0.0089	**1.9277**
	1280	0.0021	**1.9440**
	5120	4.9448e-04	**1.9595**

Table B.1: Monodomain test: computed errors

Interface condition	N	$p = 1$	order	$p = 2$	order	$p = 3$	order
sealed pores ($k = 0$)	50	0.0122	-	0.0045	-	2.5193e-04	-
	100	0.0113	**2.8842**	0.0013	**2.7094**	5.2435e-05	**3.5975**
	200	0.0075	**2.1100**	2.9302e-04	**2.5266**	1.2382e-05	**4.2361**
	400	0.0043	**1.9749**	1.2708e-04	**3.0098**	3.0863e-06	**3.7892**
open pores ($k = 1$)	50	0.0124	-	0.0023	-	1.9780e-04	-
	100	0.0115	**2.9782**	9.1133e-04	**2.8735**	4.8808e-05	**3.8345**
	200	0.0062	**2.0523**	3.6750e-04	**2.6647**	1.0364e-05	**3.7263**
	400	0.0038	**1.8866**	1.2947e-04	**2.9182**	2.6972e-06	**3.9513**

Table B.2: Coupled domains tests: $\|\boldsymbol{u} - \boldsymbol{u}_h\|_{\Omega_p}$ for various interface conditions and polynomial degree

Interface condition	N	$p=1$	order	$p=2$	order	$p=3$	order
sealed pores ($k=0$)	50	0.1581	-	0.0804	-	0.0083	-
	100	0.1326	**1.4998**	0.0297	**1.4030**	0.0027	**2.1905**
	200	0.0978	**1.2759**	0.0130	**1.5010**	8.8210e-04	**2.6452**
	400	0.0656	**1.1770**	0.0071	**1.7753**	3.2378e-04	**2.4498**
open pores ($k=1$)	50	0.1641	-	0.0531	-	0.0066	-
	100	0.1353	**1.5016**	0.0241	**1.5444**	0.0024	**2.3848**
	200	0.0858	**1.1790**	0.0135	**1.6087**	7.5924e-04	**2.3430**
	400	0.0606	**1.1527**	0.0073	**1.7798**	2.8673e-04	**2.5688**

Table B.3: Coupled domains tests: $\|\nabla \boldsymbol{u} - \nabla \boldsymbol{u}_h\|_{\Omega_p}$ for various interface conditions and polynomial degree

Interface condition	N	$p=1$	order	$p=2$	order	$p=3$	order
sealed pores ($k=0$)	50	0.1586	-	0.0805	-	0.0083	-
	100	0.1331	**1.5001**	0.0298	**1.4022**	0.0027	**2.1903**
	200	0.0981	**1.2737**	0.0130	**1.5004**	8.8219e-04	**2.6451**
	400	0.0658	**1.1755**	0.0071	**1.7752**	3.2379e-04	**2.4497**
open pores ($k=1$)	50	0.1646	-	0.0531	-	0.0066	-
	100	0.1358	**1.5020**	0.0242	**1.5439**	0.0024	**2.3845**
	200	0.0860	**1.1769**	0.0135	**1.6083**	7.5931e-04	**2.3429**
	400	0.0607	**1.1514**	0.0073	**1.7796**	2.8674e-04	**2.5688**

Table B.4: Coupled domains tests: $\|\boldsymbol{u} - \boldsymbol{u}_h\|_{1,\Omega_p}$ for various interface conditions and polynomial degree

Interface condition	N	$p=1$	order	$p=2$	order	$p=3$	order
sealed pores ($k=0$)	50	0.0127	-	0.0040	-	2.3235e-04	-
	100	0.0093	**2.3338**	0.0010	**2.7329**	5.0072e-05	**3.6356**
	200	0.0056	**2.1199**	2.5237e-04	**2.6377**	1.1152e-05	**4.2481**
	400	0.0032	**2.0680**	1.0043e-04	**3.0403**	2.7000e-06	**3.8203**
open pores ($k=1$)	50	0.0130	-	0.0019	-	2.0529e-04	-
	100	0.0096	**2.4081**	6.6660e-04	**2.9143**	4.5315e-05	**3.8036**
	200	0.0048	**2.0928**	2.7293e-04	**2.7793**	9.2244e-06	**3.7495**
	400	0.0029	**2.9590**	1.0392e-04	**3.0379**	2.3563e-06	**3.9882**

Table B.5: Coupled domains tests: $\|\boldsymbol{w} - \boldsymbol{w}_h\|_{\Omega_p}$ for various interface conditions and polynomial degree

Interface condition	N	$p=1$	order	$p=2$	order	$p=3$	order
sealed pores ($k=0$)	50	0.1802	-	0.0761	-	0.0074	-
	100	0.1281	**1.2092**	0.0260	**1.4086**	0.0025	**2.2394**
	200	0.0968	**1.3154**	0.0120	**1.5663**	7.8601e-04	**2.6743**
	400	0.0634	**1.1645**	0.0062	**1.7812**	2.8481e-04	**2.4851**
open pores ($k=1$)	50	0.1851	-	0.0494	-	0.0064	-
	100	0.1254	**1.1934**	0.0217	**1.5620**	0.0022	**2.3857**
	200	0.0831	**1.2413**	0.0117	**1.6326**	6.7758e-04	**2.3724**
	400	0.0580	**1.1547**	0.0066	**1.8502**	2.5026e-04	**2.6025**

Table B.6: Coupled domains tests: $\|\nabla \boldsymbol{w} - \nabla \boldsymbol{w}_h\|_{\Omega_p}$ for various interface conditions and polynomial degree

Interface condition	N	$p=1$	order	$p=2$	order	$p=3$	order
sealed pores ($k=0$)	50	0.1806	-	0.0762	-	0.0074	-
	100	0.1285	**1.2084**	0.0260	**1.4078**	0.0025	**2.2392**
	200	0.0970	**1.3132**	0.0120	**1.5658**	7.8609e-04	**2.6742**
	400	0.0635	**1.1637**	0.0062	**1.7811**	2.8482e-04	**2.4850**
open pores ($k=1$)	50	0.1855	-	0.0495	-	0.0064	-
	100	0.1257	**1.1927**	0.0217	**1.5616**	0.0022	**2.3854**
	200	0.0833	**1.2392**	0.0117	**1.6323**	6.7764e-04	**2.3723**
	400	0.0581	**1.1538**	0.0066	**1.8501**	2.5027e-04	**2.6025**

Table B.7: Coupled domains tests: $\|\boldsymbol{w} - \boldsymbol{w}_h\|_{1,\Omega_p}$ for various interface conditions and polynomial degree

Interface condition	N	$p=1$	order	$p=2$	order	$p=3$	order
sealed pores ($k=0$)	50	0.0294	-	0.0053	-	2.8343e-04	-
	100	0.0172	**1.8037**	0.0014	**2.6134**	6.9525e-05	**3.5681**
	200	0.0094	**1.8406**	3.9309e-04	**2.5173**	1.5790e-05	**4.1132**
	400	0.0047	**1.8411**	1.3063e-04	**2.8513**	3.5691e-06	**3.6997**
open pores ($k=1$)	50	0.0297	-	0.0045	-	3.2627e-04	-
	100	0.0157	**1.8069**	0.0013	**2.5050**	7.1933e-05	**3.6018**
	200	0.0101	**2.0355**	3.7244e-04	**2.4775**	1.7916e-05	**3.6017**
	400	0.0045	**1.6230**	1.3814e-04	**2.9237**	3.7768e-06	**3.7460**

Table B.8: Coupled domains tests: $\|\varphi - \varphi_h\|_{\Omega_a}$ for various interface conditions and polynomial degree

Interface condition	N	$p=1$	order	$p=2$	order	$p=3$	order
sealed pores ($k=0$)	50	0.3570	-	0.1029	-	0.0103	-
	100	0.2557	**0.9368**	0.0441	**1.3327**	0.0034	**2.0970**
	200	0.1773	**0.9666**	0.0192	**1.3557**	0.0012	**2.5610**
	400	0.1214	**0.9881**	0.0093	**1.5965**	3.7052e-04	**2.3317**
open pores ($k=1$)	50	0.3525	-	0.0921	-	0.0113	-
	100	0.2483	**0.9574**	0.0421	**1.3053**	0.0035	**2.1135**
	200	0.1817	**1.0623**	0.0184	**1.3266**	0.0012	**2.2306**
	400	0.1177	**0.8612**	0.0098	**1.6614**	3.9264e-04	**2.3747**

Table B.9: Coupled domains tests: $\|\nabla\varphi - \nabla\varphi_h\|_{\Omega_a}$ for various interface conditions and polynomial degree

Interface condition	N	$p=1$	order	$p=2$	order	$p=3$	order
sealed pores ($k=0$)	50	0.3582	-	0.1031	-	0.0103	-
	100	0.2563	**0.9343**	0.0441	**1.3318**	0.0034	**2.0968**
	200	0.1776	**0.9650**	0.0192	**1.3555**	0.0012	**2.5609**
	400	0.1215	**0.9871**	0.0093	**1.5964**	3.7054e-04	**2.3316**
open pores ($k=1$)	50	0.3538	-	0.0922	-	0.0113	-
	100	0.2488	**0.9543**	0.0421	**1.3045**	0.0035	**2.1132**
	200	0.1819	**1.0610**	0.0184	**1.3263**	0.0012	**2.2305**
	400	0.1177	**0.8602**	0.0098	**1.6613**	3.9266e-04	**2.3747**

Table B.10: Coupled domains tests: $\|\varphi - \varphi_h\|_{1,\Omega_a}$ for various interface conditions and polynomial degree

Ringraziamenti

"Quando ero piccolo, m'innamoravo di tutto, correvo dietro ai cani..."

Poi mi sono trovato catapultato in una realtà completamente nuova, senza boschi da esplorare, diversa, che forse non mi è mai andata troppo a genio, ma che è entrata inevitabilmente dentro me: Milano. Le mie piccole Bibbiena e Firenze le attraverso, in confronto, nello stesso tempo in cui percorro via Pacini da Piola a Lambrate. Una via come tante a Milano, che mi ha visto però protagonista di cinque magnifici anni di cambiamenti, scoperte e continui piacevoli salti nel vuoto. Anni iniziati come infiniti, che pian piano mi sono accorto essere in un istante volati rapidissimi. Anni di amicizie interminabili, profonde e vere, di amori, di arpeggi su una chitarra che ne ha viste di ogni. Di inesorabili e intramontabili piatti da lavare e di pochi, ma costruttivi, litigi. Anni di vacanze in tenda, di traghetti, di panini sempre uguali, ma sempre diversi, di ritiri studio, che di studio avevano solo il pretesto. Anni di Baby Luigi in preda al panico sulla pista arcobaleno, anni ad aspettare che la luce del BikeMi smettesse di lampeggiare, anni di insaziabili mandarini. Anni di caffè e brioches da Scaringi, di pizze alla Cuccuma e di nuove conoscenze al Birri, mai consuete. Insomma, anni senza rimorsi. E come per magia mi trovo qui, a scrivere ringraziamenti che segnano un po' il raggiungimento di un traguardo, del quale a una certa mi dovrò anche rendere conto, magari.

Incomincio col ringraziare la professoressa Antonietti per avermi dato la possibilità di addentrarmi in un problema affascinante, quale si è rivelato, incoraggiandomi sempre e trasmettendomi dedizione e interesse verso la materia. Un ringraziamento va senza dubbio anche al professor Mazzieri, disponibile fino all'ultimo momento per chiarire pazientemente ogni minimo dubbio e rassicurarmi sul fatto che avrei trovato gli errori nel codice, che credo oramai conosciate tutti.

Procedo ringraziando chi c'è sempre stato, ben prima dell'università, chi mi ha cresciuto, permettendomi di arrivare a scrivere questo stesso pensiero: la famiglia. Mamma, grazie per avermi insegnato a non odiare mai, a cercare il buono ovunque, anche laddove è realmente difficile da vedere. Per avermi insegnato ad amare e guardare sempre le cose dal lato giusto. Babbo, per l'educazione e rispetto verso la Natura e i consigli sempre azzeccati. Per avermi mostrato come stare al mondo e non avermi mai fatto mancare niente (e io pago). Lori, per la generosità e la semplicità che abbiamo imparato insieme, ridendo, litigando e condividendo tutto. Febo, compagno di

eterne avventure.

Grazie zie, zii, nonne, nonni e cugini, per il supporto e l'affetto naturale manifestato ogni giorno.

Grazie coinquilini, Pacini22, poi divenuti Poggi14. Dipa, se avessimo registrato tutte le canzoni improvvisate insieme, una decina di album li avremmo incisi. Grazie per avermi sempre strappato un sorriso, in qualsiasi situazione, a qualsiasi ora. Ale, per tutte le tisane bevute sdrammatizzando sulla giornata appena trascorsa, guardando improbabili video del nido del cuculo. Michi, per aver condiviso sempre tutto con me: dalla MotoGP alle cinque del mattino, alla Fiorentina che non vince neanche per sbaglio, dai Queen, agli spaghetti allo scoglio. Grazie anche ad Ada e Albertone, colonne sonore di ogni giornata che poteva sembrare monotona.

Grazie GLS, un gruppo immenso, un'altra famiglia. GioPog, grazie per le nottate a parlare del nulla, per i tuoi giudizi senza peli sulla lingua, per esserci sempre e credere in me, anche dall'altra parte delle Alpi. Luke, per la tua generosità, condivisione e umiltà, per tutte le cene insieme e i gelati dell'Aloha. Nene, per i tuoi sorrisi sempre veri che trasmettono tranquillità, per le serate ad ascoltare ogni mio singolo turbamento, per essere Nene. Teo, per le tue lombardate, per il tuo ingenuo modo di essere un po' tra le nuvole, per il nostro De Gregori cantato non proprio all'unisono. Leti, per farmi costantemente viaggiare col pensiero e spingerti sempre un po' più in là con quegli occhioni, per non scadere mai nel banale e non rispondere mai al cellulare. Jimmy, grazie per i tuoi saggi consigli sempre sul pezzo, per le tue storie di avventure stravaganti e per non avermi fatto passare per quello scarso che al giro stava in fondo. Ruff, per i tuoi infiniti racconti e le tue perle da scriverci intere saghe; vedrai che il tuo incessante sogno del teletrasporto un giorno si realizzerà. Giodaz, per tenermi sempre sulle spine, per costringermi a scavare dentro te avvenimenti letteralmente inenarrabili, degni di un Pino D'Angiò. Andre, per le infinite chiacchierate sulla vita, per quei maledettissimi esercizi di economia insieme, che poi ti sei stancato di fare (io no e ho continuato qualche altro anno), per esserci in ogni momento. Albi, per tutte le poesie condivise e per vedere la bellezza in ogni angolo. Grazie Abba per i vinelli che ci scappano quando si riesce, Lollo per la buona persona che sei, Lux per l'affettuosità che mi regali di fronte a tutto, Bea per il cammino percorso insieme, Tina, Nderep, Buch, Cami, Angelì, Eug, Apotz, Tower. Grazie anche alla S di GLS.

Grazie Inamers, una seconda casa per me. Angie, per psicanalizzarmi in tutto, essere sempre energica, solare e attaccarmi su quelli che credi siano i miei punti deboli: tu hai ventiquattro anni e non sai cucinare. Bina, per le interminabili divagazioni su esistenzialismo e libri, anche se all'inizio non mi eri troppo simpatica: sei una gestionale, lo sai. So, per aver ascoltato e condiviso con me ogni respiro dal primo momento che ci siamo conosciuti, per la tua determinazione e per i tuoi ori olimpici. Grazie anche a te Giuli e ai tuoi aggeggi anticalcare nelle bottiglie di via Inama, che ci siamo bevuti un po' tutti. Grazie Marilù, per sempre.

Grazie ai casentinesi, capibugi e non, pochi ma eterni. Grazie Ari, per le nostre

infinite passeggiate con quelle bestiacce (grazie Ivy!), per i tuoi consigli ben pesati e mai scontati, per il tuo esserci sempre stata, anche non vedendoci per mesi. Jack, per tutto il tuo gusto musicale con me condiviso, per i nostri Elliott Smith e Tim Buckley, per le risate senza sosta e le digressioni filosofiche. Ale Borghi, per essere cresciuti senza pensieri, non curandoci degli innumerevoli rischi che correvamo. Grazie Cenni, Giammo, Ale Romano, King.

Grazie ai fiorentini. Lidia, per le nostre camminate per Firenze, per esortarmi costantemente a riscoprire la mia stessa città, dalle statue del loggiato degli Uffizi, a quella sconosciuta città di là d'Arno, per i caffè in piazza della Passera a parlare veramente di tutto. Caro, per i tuoi fedeli consigli, sempre caduti dove dovevano e per aver ringraziato me e la Lidia nella tua tesi. Diego, per la tua filosofia condivisa con me, per le lettere, che più che lettere erano forse trattati. Tommi e Ila, per averne combinate una dietro l'altra insieme.

Grazie agli zii e cugine di Milano, per avermi fatto sentire a casa tutti i lunedì. Per le melanzane inimitabili della zia, per le risate a crepapelle, per gli infiniti racconti di vita e di esperienze che ho fatto mie.

Grazie Co, per continuare ad allungare quell'unica settimana in cui ci siamo conosciuti a Porto. Grazie Dave per le trasferte che non ci vanno mai bene e per avermi sempre regalato un po' di Firenze a Milano. Grazie Franco, Noe, Giulio Perin, Mazza, Jonathan. Grazie compagni di Curvefever nelle sere di quarantena.

E niente, sono qui, laureato, maturo solo in qualche capello bianco, pronto per un altro, sorprendente, tuffo nel vuoto.

"... e a un Dio senza fiato, non credere mai".